Genesis of Iron Ore in the Snelgrove Lake Area, Labrador Trough, Western Labrador

by

© Nicolas Lachance

A Thesis, submitted to the

School of Graduate Studies

in partial fulfillment of the requirements for the degree of

M.Sc. in Earth Sciences (Geology)

Department of Earth Sciences

Memorial University of Newfoundland

March 2015

St. John's Newfoundland

ABSTRACT

The Snelgrove Lake property, located in western Labrador, is underlain by the late Proterozoic Sokoman Formation, the same geological formation that hosts economically significant iron ore deposits elsewhere in Labrador and Quebec. This project aims to better understand the origin of the iron formation, the controls on grade of the iron ore including whether or not there is secondary iron enrichment, and the ambient marine environment in the late Paleoproterozoic, including ocean redox conditions present during the primary deposition of the iron formation.

Iron formations in the Snelgrove Lake area consist of chemically precipitated jasper and Fe-rich sedimentary rocks that contain hard, metallic bluish-grey iron oxides, with total Fe_2O_3 ranging from 22 – 64 wt%. On the basis of petrography, iron minerals occur predominantly as: 1) syngenetically deposited (primary) iron oxides and iron silicates; 2) microplaty hematite (secondary and remobilized); and 3) euhedral magnetite (secondary). Despite textural features suggesting that microplaty hematite occurrences are due to secondary Fe-mobilization, the lack of coarse-grained textures and structurally controlled mineralization argues against hydrothermal enrichment as the cause. Furthermore, the general absence of hydrous ores, the lack of light rare earth element (LREE) enrichment within the iron formation, and the preservation of most primary sedimentary textures argues against pre- or post-metamorphic supergene enrichment. Evidence within suggests that iron was locally remobilized by post-depositional diagenetic fluids, which resulted in the alteration, modification and enrichment of original bedding with Fe-minerals. The current physical assemblage of iron-bearing minerals, and

the local iron grades, were also significantly affected by the early diagenetic appearance of silica cements. Those samples that received silica cement during early diagenesis contain lower Fe grades, and show signs of having been less affected by compaction than those that had no silica cement.

The geochemistry of the iron formation suggests various inputs from hydrothermal, detrital, and hydrogenous sources. Immobile element contents indicate the Snelgrove Lake iron formation has minimal detrital input, but that which is present was likely derived from a mafic detrital source. Flat to weakly positive Eu/Eu* anomalies are common and suggest precipitation of iron minerals in the ocean from low temperature fluids (< 250°C). The iron formations also have REE-Y signatures comparable to other late Paleoproterozoic iron formations and have flat post-Archean average shale (PAAS)-normalized patterns, and Y/Ho ratios ranging from 20-50. The Y/Ho ratios of late Paleoproterozoic iron formations have wider ranges and are generally lower in comparison to early Paleoproterozoic iron formations and is interpreted to reflect the appearance of oxygen in the oceans at that time, and more precisely, the appearance of a redox-stratified ocean. The paleoredox-conditions present during the deposition of iron formation in Snelgrove Lake, as deduced from Ce/Ce* anomalies and other redox-sensitive elements, are generally indicative of an anoxic environment, while its bounding units record signatures that reflect deposition in a more oxic environment, thus suggesting deposition in a redox-stratified basin with iron precipitation near a redox-boundary.

ACKNOWLEDGEMENTS

I extend my sincere gratitude to Altius Resources Inc. for providing the logistical and financial support needed to make this research project possible. I am truly grateful to have been under the guidance of my supervisor, Dr. Stephen Piercey, whose unlimited dedication and passion for science have been a source of inspiration. Thank you Steve for teaching me the importance and impact of communication in science and for passing on your wisdom so selflessly.

I would like to thank my thesis committee members, Drs. Winter and Wilton for carefully reviewing my thesis and providing the valuable comments needed to improve it. Thanks to Drs. James Conliffe of the Geological Survey of Newfoundland and Labrador, George Hudak of the University of Minnesota in Duluth, and Toby Rivers of Memorial University for providing invaluable comments and discussion. Special thanks to Carol Seymour for her support, knowledge and experience in the field, and to Mike Piller and Jon Oliver for helping to carry my heavy rocks.

Finally I would like to thank my family and friends for their patience and support during the course of my study. Evangeline, your love and belief in me have provided the fuel to make this endeavor possible: all my love.

Table of Contents

List of Figures

List of Appendices

Chapter 1- An Introduction to Lake Superior Type Iron Formations of the Labrador Trough.

1.1 Introduction

The Labrador Trough is the informal name given to an 1100-kilometer long belt of sedimentary and volcanic rocks in northeastern Quebec and western Labrador, also known as the Kaniapiskau Supergroup, and previously interpreted as a geosyncline (Dimroth et al., 1972) during the pre-plate tectonic era. The Snelgrove Lake area in northwestern Labrador contains abundant chert and jasper-bearing iron formations of the Sokoman Formation, host of the iron mines of the Labrador Trough (Fig. 1.1). Mining of iron ore occurs in two main areas located approximately 200 km from each other: 1) the Schefferville district (Fig. 1.1), where mining began in 1954; and 2) the Labrador City−Wabush−Fermont district where mining began in 1961 (Neal, 2000). The type of ore currently mined within the Labrador Trough is of three types: 1) taconite; 2) metataconite; and 3) high grade direct shipping ore (DSO). Taconite is defined as low-grade oxide facies ore that is generally magnetite-dominant, weakly metamorphosed and suitable for concentration by fine grinding and magnetic separation and flotation separation (Gross, 1965). Metataconite refers to the metamorphosed equivalent of taconite; it contains high amounts of recrystallized specular hematite relative to magnetite and is coarser grained, characteristics appreciated for the concentration of ore at low costs as well as enhanced recovery (Gross, 1968). High grade direct shipping ore (DSO) contains Fe concentrations generally greater than 60%, sufficient enough that it can be sent directly to market (Stubbins et al., 1961). DSO is recognized as having been

upgraded by secondary enrichment processes, and is separated into two end-members: soft ore and hard ore. The first refers to soft and friable ore consisting of hematite, martite and goethite that has brecciated textures. The genetic model attributed to this type of ore in the Labrador Trough is supergene leaching, a process that dissolves and removes silica through the circulation of low-temperature meteroic fluids, leaving behind Fe-minerals, the creation of voids and subsequent breccias (Stubbins et al., 1961). Hard ore, in contrast, is more massive and has a metallic gray-blue appearance, is locally brecciated, and contains hematite, martite and goethite minerals; hematite is generally found in greater abundance compared to soft ore. The model associated with hard ore is related to late stage, post-diagenetic oxidation and migration of iron minerals (Beukes, et al., 2003).

The Schefferville district is dominated by high grade DSO soft ore in rocks that have low metamorphic grade, whereas the dominant ore type currently mined in Labrador City−Wabush-Fermont is metataconite. The Labrador City−Wabush-Fermont district contains greater mineral resources and is more economically significant in comparison to the Schefferville district. This district has been affected by two separate stages of deformation from the New Quebec and Grenvillian orogenies, which resulted in folding, structural thickening and the recrystallization of iron oxide minerals into coarser grains.

Snelgrove Lake is located approximately 60 km southeast of the Schefferville district, in an area known to have contained DSO-type, high-grade ore since the discovery of the Sawyer Lake Deposit in 1937. The ore at Sawyer Lake is in the form of an irregular shaped, hard blue hematite deposit, and has been recognized as a distinct and different type of ore compared to both Schefferville and Labrador City−Wabush-Fermont (Conliffe, 2014). Despite much exploration effort in and around the Sawyer Lake deposit

area (including Snelgrove Lake) since its discovery, no other deposit were recognized proximal to this deposit, and the general focus of mining companies shifted to the Schefferville and Labrador City−Fermont areas. The rise in iron ore prices in recent years, however, has brought renewed interest and exploration efforts in the Sawyer Lake−Snelgrove Lake area, and the area of study has been staked and owned since 2008 by Altius Resources Inc. in partnership with the junior exploration company Mamba Minerals.

Iron formations within the Snelgrove Lake area are taconites, and are recognized for their relative hardness, metallic steel blue color, higher proportions of hematite relative to magnetite, and locally high Fe-concentrations compared to other taconites in the region. For these reasons they have been regarded, similarly to Sawyer Lake ore, distinct and different from ore mined in Schefferville and Labrador City−Fermont.

Although efforts were made to understand the genetic models associated with different types of ore in the Labrador Trough during the 1950s and 1960s, little critical evaluation has occurred since. This study aims at obtaining a greater understanding and improved characterization of the Snelgrove Lake iron formations, including depositional setting, controls on Fe-grade, and potential upgrading processes (if any) by comparing it to other iron formations/deposits located in the region, and globally through the use of mapping, and mineralogical, lithogeochemical and petrological work.

1.2 Regional and Tectonic Setting of the Labrador Trough

The term Labrador "Trough" is used throughout this work as the name of a belt rather than for its tectonic meaning. The rocks within it are part of a passive continental-

margin sequence deposited on a rifted margin (Wardle et al., 1996), as opposed to a continental rift as the name would suggest.

The rocks of the Labrador Trough (Fig. 1.1) were initially created when rifting of the Superior Craton occurred from ~2.2 Ga (Wardle et al., 2002). They were then subject to the 1.82-1.77 Ga (James and Dunning, 2000) New Quebec collisional orogeny (NQO), the name given to the late Paleoproterozoic Trans-Hudson Orogen (THO) in this part of the Southeastern Churchill Province (Fig. 1.2). The southern part of the Labrador Trough was further deformed during the Grenvillian Orogeny between 1.19-0.98 Ga (Rivers, 1997). Part of the Labrador Trough is included within the Grenville Province, however, the Snelgrove Lake area was not affected by it.

The NQO is divided into three components, from west to east they consist of: 1) the Melezes and Schefferville zones, a mostly autochthonous low-grade metasedimentary and volcanic sequence; 2) the Baby-Howse zone consisting of thick sequences of basalt and co-magmatic gabbro; and 3) the Rachel-Laporte zone composed of metasedimentary sequences but at higher metamorphic grade (Figs. 1.2–1.3). Structurally, the NQO forms a west verging fold and thrust belt that unconformably overlies the Archean gneisses of the Superior Province (Wardle and Van Kranendonk, 1996).

1.3 Attributes of the Labrador Trough Iron Deposits

The broad lithological definition of iron formation is (Gross, 1965): “all stratigraphic units of layered, bedded, or laminated rocks that contain 15 percent iron or more, in which the iron minerals are commonly interbanded with quartz, chert, or

carbonate, and where the banded structure of the ferruginous rocks conforms in pattern and attitude with the banded structure of the adjacent sedimentary, volcanic or metasedimentary rocks." Iron formations are classified into four facies based on the dominant source of Fe in the iron formation: oxide, silicate, carbonate and sulphide. Gross (1965, 1973, 1983a) has used the facies type along with tectonic setting and depositional environment to further classify them into two principal types: Lake Superior-type and Algoma-type, where Lake Superior-type refers to those formed in a continental shelf environment, whereas Algoma-type formed associated with volcanic sequences either at spreading ridges or associated with arc magmatism.

The Sokoman Formation forms part of a band of ferruginous rocks that extends along the eastern margins of the Superior Craton, and is known as one of the most extensive examples of Lake Superior-type iron formation (Gross, 1968b; Gross and Zajac, 1983). The predominant iron facies-type within the Labrador Trough is oxide, but carbonate and silicate facies are also common; sulphide facies are rare (Neal, 2000). Hematite and magnetite are dominant in oxide facies, whereas silicate facies tend to be mineralogically more complex and contain many types of iron-bearing silicate minerals. Silicate facies iron formations have higher SiO_2 contents and occur as jasper-bearing and cherty units. Depositional environments are inferred from well-preserved textures within the iron lithofacies: oolitic textures are predominant in shallow water environments, whereas laminations are predominant in deeper water environments (Gross, 2009).

1.4 Previous Work

The area of study has been previously mapped by geologists of the Labrador Mining and Exploration Company (LME) through the 1930s and 1940s, more specifically, at a scale of 1:12 000 by Dufresne (1950). Subsequent 1:100 000 scale mapping was undertaken in the 1970s by the Geological Survey of Newfoundland (Wardle, 1979). Exploration interest in the area has been generally low since the late 1960s and early 1980s. Since 2005, work from Altius Resources Inc. has included mapping, airborne magnetic and radiometric geophysics, prospecting and geochemistry.

1.5 Objectives

The aim of this M.Sc. research project is twofold: 1) to characterize the mineralogy, stratigraphy and structure of the iron formation and iron ore mineralization, in order to understand the processes involved in their genesis; and 2) to gain an understanding of the depositional setting, including ocean redox conditions and temperature, during the primary deposition of the iron formations. Fieldwork included mapping and sampling of iron formation; an emphasis was placed on detailing the mineralogy and primary depositional features of the iron formation, as well as post-depositional structures. Lab-based work included petrography, scanning electron microscopy, and lithogeochemistry. The following are the major foci for the project:

1. characterization of lithological facies and Fe-mineralization through surface mapping to identify lithological units and utilization of field relationships combined with existing geological maps and magnetic surveys to create a compilation map of the area;

2. determine the role of primary and secondary enrichment processes in the formation of iron ore and testing the relative importance (if any) of sedimentation, diagenesis, structure and metamorphism, and supergene enrichment may have had in controlling iron ore grade;
3. determine how the Snelgrove Lake deposit compares with other iron ore deposits within the Labrador Trough and globally; and
4. use major, trace, and rare earth element geochemistry and petrography to understand:
    - iron concentrations and distribution within stratigraphic units;
    - major and trace element geochemistry associated with both host rocks and the ores;
    - the facies for stratigraphically bounding units;
    - the dominant ore types and mineralogy;
    - redox and temperature conditions of basin fluids and the nature of the ambient environment during sedimentation and iron ore deposition; and
    - the provenance of the sediments in relation to the Labrador Trough.

1.6 Methodology

FIELDWORK

Mapping was carried out in June of 2011 and in July of 2012. Access to the area was provided by helicopter from Schefferville. Most of the Snelgrove Lake iron formations are found in positive relief as hills and mountains (≈ 50-250 m above local

lakes) and have good exposure with abundant outcrop. Sampling and mapping was carried out along a number of planned transects that are perpendicular to strike in order to map changes within stratigraphic units. In total, 80 samples were collected in every unit and/or whenever a change in facies occurred. Unit boundary locations were determined by the combination of our mapping, and compiled information from existing maps and airborne geophysical data. A digitized geological map was compiled and synthesized using MapInfo software from data collected during the 2011 and 2012 field season, aerial photography, and supplemented by airborne magnetic survey maps, and previous geological maps of the area.

SAMPLING

Following the 2011 field season, all samples were prepared for analysis in the Department of Earth Sciences at Memorial University. They were pre-cut to remove weathered surfaces using a water-lubricated saw. Duplicate samples were also created, and a slab was cut for polished thin sections. Rocks were carefully prepared in separate batches based on lithology and Fe concentrations prior to cutting as to avoid contamination during sawing. Samples were quickly described and photographed during the field season at the time of their collection; detailed pictures, and a more thorough macroscopic description of each lithology was performed subsequently at Memorial University.

MAJOR AND TRACE ELEMENT LITHOGEOCHEMISRTY

Samples collected during the 2011 field season were sent to Actlabs, Ancaster, Ontario where they were crushed and pulverized in a mild steel pulverizer. Whole rock

analysis was performed for major elements by X-ray fluorescence, and for trace elements by inductively coupled plasma mass spectrometer (ICP-MS).

PETROGRAPHY

Polished thin sections were prepared for samples collected in the 2011 and 2012 field seasons by Vancouver Petrographics. They were studied and described by the author using transmitted and reflected light. Together with macroscopic descriptions, petrographic studies helped to understand mineralizations by identifying mineral assemblages and facies type (silicate, carbonate, oxide), iron oxides (hematite, magnetite, goethite-limonite), as well as mineral replacement and overgrowth. A selection of petrographic samples were further analyzed and described using scanning electron microscopy (SEM).

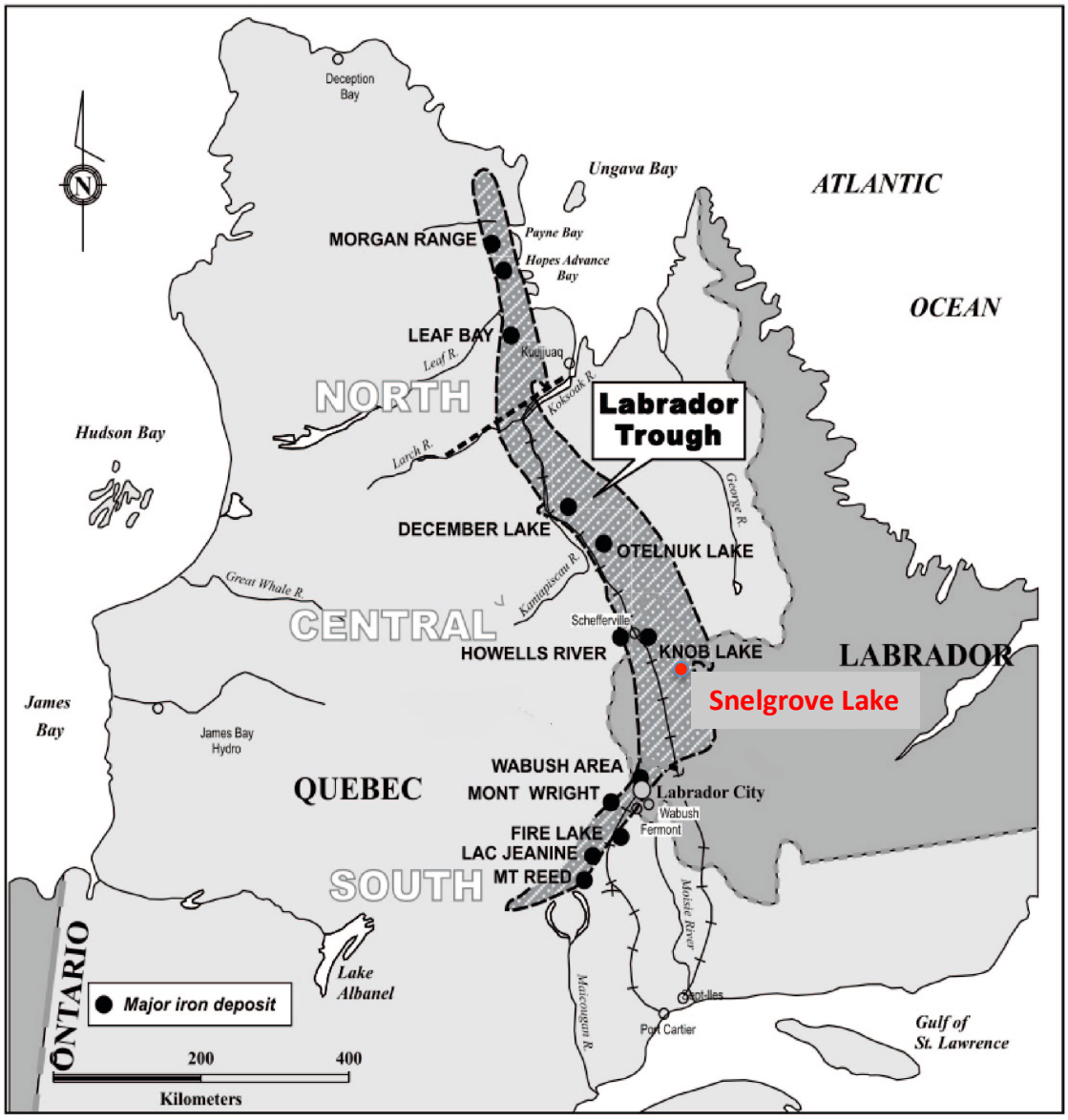

Figure 1.1. Labrador Trough showing the locations of major iron ore deposits in Quebec and Labrador (modified from Neal, 2000).

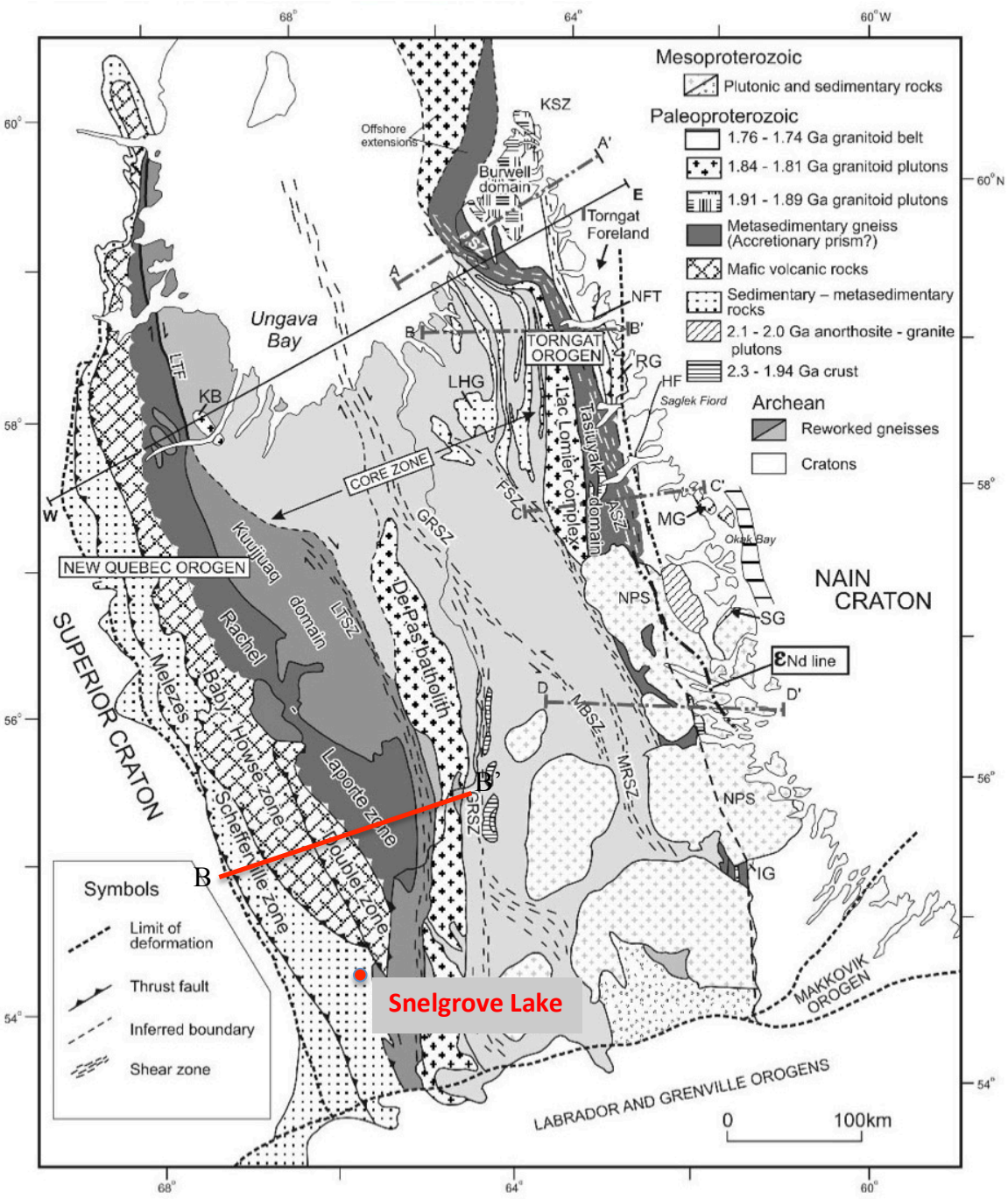

Figure 1.2. Simplified geological map of the Southeastern Churchill Province including lithotectonic divisions of the New Quebec Orogen (modified from Wardle et al., 2002).

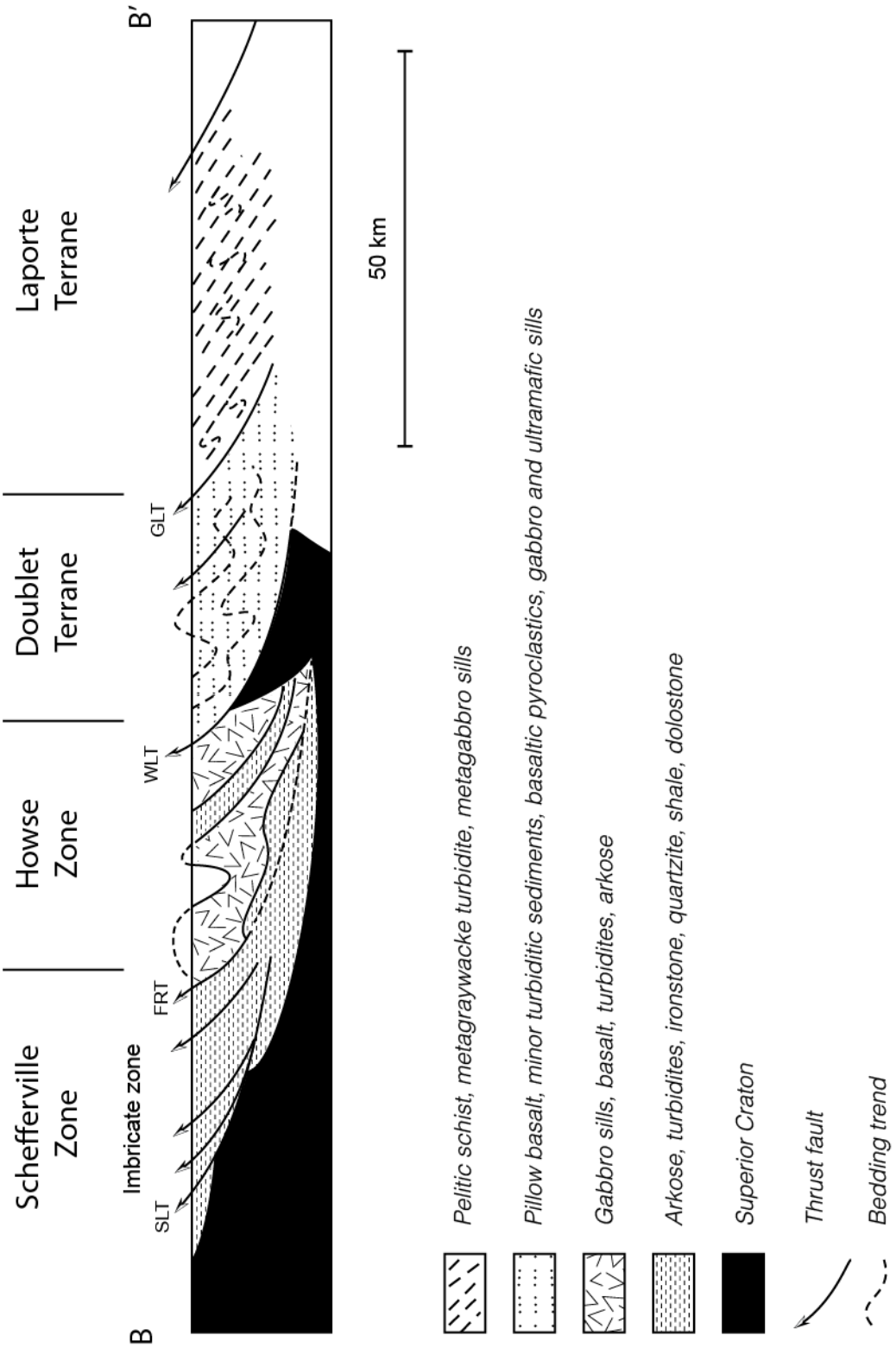

Figure 1.3. Structural cross-section of the New Quebec Orogen (modified from Wardle et al. 1995).

Chapter 2- Geology and Mineralogy of Iron Mineralization in the Snelgrove Lake Area

2.1 Regional Stratigraphy and Structural Geology

Little recent work has been undertaken in the Labrador Trough, with the last published regional mapping undertaken by Wardle (1979)(Figs. 2.1-2.2), and current research carried on the Sawyer Lake deposit by Conliffe (2014); most of the following paragraphs are summarized from Wardle (1979). The Labrador Trough is dominated by Paleoproterozoic sedimentary and volcanic rocks (≥1.85 Ga) of the Kaniapiskau Supergroup (1.6 − 2.2 Ga)(Fig. 2.1). On the western side, these rocks lie unconformably over the Archean gneisses of the Ashuanipi Complex, whereas on the eastern side they are in fault contact with the tonalitic and granodioritic gneisses of the Archean Eastern Basement Complex (EBC). The latter are the oldest rocks in the region and occur immediately to the east of Snelgrove Lake. The lower part of the Kaniapiskau Supergroup is composed of the Knob Lake Group; it is divided into western and eastern successions that contain two cycles of sedimentary rocks. The first cycle consists of the Seward, Attikamagen, Denault and Dolly formations. The latter formations are composed of arkose, shale-siltstone, dolomite-calcareous siltstone, and shale-siltstone, respectively, and represent the transition from initial rifting to shallow shelf environment. The second cycle of sedimentary rocks unconformably overlies the first cycle and contains the rocks that locally occur in Snelgrove Lake. It consists of the basal quartzites of the Wishart Formation, the Sokoman Iron Formation in the middle, and a thick sequence (>1000 m) of black (euxinic) and gray shale-siltstone known as the Menihek Formation at the top

(Hoffman, 1987; Wardle, 1979). Mafic volcanic rocks occur stratigraphically above (Astray Lake Formation) and below (Petitsikapau Lake Formation) the Sokoman Formation. Both formations and associated sills are known as the Nimish Subgroup (Evans, 1978), and consist of pillow lavas, sills, volcanogenic conglomerates and tuffaceous siltstones. The volcanic rocks in the Nimish Subgroup have an approximate age of 1877.8 ± 1.6 Ma (U-Pb zircon; Findlay et al., 1995).

The Knob Lake Group is directly overlain by the Paleoproterozoic Doublet Group, which forms the upper portion of the Kaniapiskau Supergroup. This portion is dominated by a thick sequence of mafic volcanic and intrusive rocks interpreted to have formed as high-volume magmatism during continental rifting, and deposited over the shales of the Menihek Formation. The Kaniapiskau Supergroup was also intruded by peridotite, gabbro and diabase of the Paleoproterozoic Montagnais Intrusive Suite, and by gabbro and diabase from the Mesoproterozoic Shabogamo Group. The sequence of facies present within the stratigraphy of the Knob Lake Group, from basal quartzite, to the thick overlying black (euxinic) and gray shales of the Menihek Formation, provide the basis to suggest it is a foredeep sequence deposited within a foreland basin (Hoffman 1987).

Structurally, the rocks of the area were folded and metamorphosed during the NQO (1.82-1.77 Ga; James and Dunning, 2000). Major structures have been recognized that control the distribution of the Knob Lake Group (Wardle, 1979). Two major anticlinal structures are present: the Snelgrove Lake Anticline is located in the central part of the map (Fig. 2.2); the gneisses of the EBC are present at the core of the anticline and form a reentrant into the Knob Lake Group. The Hollinger Lake Anticline, located to the north, possibly formed as the continuity of the Snelgrove Lake Anticline; however, much

of the original symmetry of the Hollinger Lake Anticline has been destroyed and the intervening fold axis has been removed by overthrusting (Wardle, 1979). The Snelgrove Lake deposit is located to the west of the major anticlines within the Petitsikapau Lake Synclinorium, a broad and complex northwest trending structure formed as tightly shaped F1 folds. At the location of the deposit, the F1 folds have sub-vertical fold axes, but further west of Snelgrove Lake, the fold axes are sub-horizontal, where they are interpreted to be in their original orientation. The sub-horizontal position of the fold axes in the Snelgrove Lake area, and along the Mina Lake Fault are interpreted to be the result of the reverse angle motion of the Mina Lake Fault (Wardle, 1979). Where sub-vertical, the fold axes generally plunge steeply to the west, but occasionally plunge steeply to the east when the axes are overturned. They have a northwest-southeast trend towards the south of the Petitsikapau Lake Synclinorium, but have an east-west trend towards the north. The rotation of the fold axes is interpreted to result from a later period of sinistral strike-slip motion occurring within the Mina Lake Fault (Wardle, 1979)(Fig. 2.2). Throughout the Snelgrove Lake area, bedding is mostly sub-vertical, and metamorphism is generally greenschist facies.

2.2 Mapping and Local Stratigraphy

Local stratigraphy of the Snelgrove Lake area (Fig. 2.3) was determined through a combination of field mapping undertaken in 2011 and 2012, and a compilation from previous studies. Some geological information was inferred from magnetic susceptibility aerial geophysics from Altius Resources (Fig. 2.4), as well as mapping from Wardle (1979) and Dufresne (1950). The stratigraphy from Wardle (1979) and Dufresne (1950)

of the local area were used as a template to develop the stratigraphy of the Snelgrove Lake property. Additionally, the stratigraphy of Klein et al. (1976) developed for the western part of the Labrador Trough was used in defining some of the lithologies.

Mapping, stratigraphic reconstruction, and sampling (Table A1) was undertaken in traverses perpendicular to stratigraphy in order to map out any changes in facies; however, poor exposure in some key areas made it difficult to achieve a high degree of precision. Nevertheless, sufficient exposure allowed definition of stratigraphy and various facies within.

Although present within the mapped area (Fig. 2.3), the lowermost stratigraphic units, the Denault and Dolly Formation, were not covered by detailed mapping, which was initiated within the overlying quartzite of the Wishart Formation. The Wishart Formation is overlain by the Ruth Formation shales, followed by the Sokoman Iron Formation. The Ruth Formation is rich in iron, and because of its intimate chemical and genetic relationship with the overlying Lower Sokoman Formation, it was debated in past literature whether it be part of it or not (Zajac 1974; Klein and Fink 1976). The Sokoman Formation, is traditionally subdivided into a Lower, Middle and Upper Sokoman Formation towards the western succession of the Knob Lake Group (Wardle, 1979). However, the Upper Sokoman, characterized by its high content in iron silicate minerals, was noted by Wardle (1979) to be missing in most of Snelgrove Lake, where the Middle Sokomon Formation is directly overlain by the shales of the Menihek Formation. Because of lack of exposure, the Ruth, Lower Sokoman, and Middle Sokoman formation's stratigraphic contacts are difficult to map, and thus the three formations are undifferentiated on the Snelgrove Lake map (Fig. 2.3). Because of their similarities, the

Ruth and Lower Sokoman Formation samples were grouped together for petrological descriptions, whereas the Middle Sokomon Formation is iron-rich and described as a separate entity. A small area in the southern part of the map consists mostly of silicate iron mineral facies, and could potentially represent the Upper Sokoman or the Lower Sokoman Formation. Although this area was not the focus of detailed mapping and stratigraphy, samples collected there are distinct in comparison to samples of the Middle Sokoman Formation, and have been grouped and informally named the *silicate facies group*.

In the Snelgrove Lake area, the Sokoman Formation is intruded for most of its length by a gabbro sill that is less than 50 meters thick and has variable distribution on surface. The intrusive body is mostly conformable to stratigraphy, and together with the units of the area is also deformed into tight F1 folds. The gabbro sill occurs near the base of the iron formation variably above and below the Ruth Formation and has never been dated. Minor faults generally trending east-west occur and cross-cut stratigraphy broadly perpendicular to bedding.

The following sections contain petrographic observations of samples from the four formations subjected to detailed mapping and sampling: 1) the Wishart Formation; 2) Ruth Formation and Lower Sokoman Iron Formation; 3) Middle Sokoman Iron Formation; and 4) silicate facies.

2.3 Petrography of the Wishart Formation

The Wishart Formation is estimated to range from 40 to 250 m in thickness (Wardle, 1979). Eight samples representing micro-laminated siltstone and sandstone were

collected within this formation (Figs. 2.5 a-c). Detrital grains present within are predominantly quartz with lesser feldspar, are well sorted with most being less than 1mm, and cemented with variable amounts of microcrystalline quartz. The finer grained siltstone samples have bimodal grain sizes with well-sorted detrital grains that are matrix supported in a mixture of micro to cryptocrystalline chert and clay-rich material (Fig. 2.5 b). Very fine siltstones are composed of up to 90% minnesotaite and stilpnomelane, with lesser sub-angular, matrix-supported quartz grains (30-150μm). Iron-rich silicate minerals generally occur in greater abundances towards the upper part of the Wishart Formation near the contact with overlying iron formation.

Roundness of quartz detrital grains is variable, ranging from sub-angular to well rounded; rounding is greatest in samples with visible matrix minerals. Pressure dissolution at grain boundaries is common in coarser samples with some grains having sutured contacts that interlock (Fig. 2.5 c). Feldspar grains are most often rounded and show concave to convex boundaries with surrounding quartz grains highlighting preferential dissolution of quartz over feldspar (Tucker, 2001).

2.4 Petrography of the Ruth, and Lower Sokoman Iron Formations

Macroscopically, the Ruth Formation shales (RS) and the Lower Sokoman Iron Formation (LSIF) are very similar and commonly indistinguishable (Figs. 2.5 d-e). They both consist of thinly bedded and laminated black ferruginous shale/mudstone composed of iron oxides, iron silicates, quartz and felsic detritus, and they locally weather to a dark brown color, a feature that distinguishes these units from the Middle Sokoman Iron

Formation. The thickness of the two combined formations is poorly constrained; however, field relationships suggest that together they are less than 100 meters thick.

Microscopic observation of sedimentary textures reveal differences between the RS and LSIF: the RS is slightly richer in clay minerals and felsic detritus; iron oxides are present exclusively as magnetite in the RS, whereas magnetite with minor amounts of fine microplaty hematite are present in the LSIF; and shallow water features (peloids) form a minor component in the LSIF but rarely occur in the RS. Riebeckite also occurs in one of the LSIF samples.

Iron-rich facies in both RS and LSIF contain microscopic laminations defined by alternating iron oxides (15%), carbonaceous matter, iron carbonates (siderite and/or ankerite) and iron-manganese oxide (jacobsite and/or bixbyite) minerals. Iron carbonates and iron-manganese oxide minerals are exclusively found in these formations within the Snelgrove Lake area. The iron carbonates occur as euhedral crystals similar in form to magnetite, and are commonly devoid of a central core (Fig. 2.5 e). Magnetite crystals are 5-150 μm with many of the larger grains having ilmenite cores. Locally, some magnetite crystals are partly oxidized to martite. Minor chalcopyrite is present in some samples in both formations.

2.5 Petrography of the Middle Sokoman Iron Formation

2.5.1 Sedimentary Features and Facies of the Middle Sokoman Iron Formation

The Middle Sokoman Iron Formation in Snelgrove Lake contains the most iron-rich rocks. Previous studies noted that the Sokoman Formation has similar textures to

limestone (Dimroth et al., 1973), allowing the use of Folk's (1959) limestone classification for describing the iron formations.

The iron formation consists of chemically precipitated sedimentary rocks with minor detrital material. They occur as bands (5-10cm) of ferruginous chert and quartz-rich material (Fig. 2.5 f) alternating with bands (5-10cm) of hematite and/or magnetite and quartz. Transitions between bands vary from gradual to abrupt; the bands are locally discontinuous, appearing as a series of boudins instead of continuous units. Iron-rich layers vary from massive and devoid of internal structure to peloid-bearing, whereas silica-rich layers are commonly peloidal. Both oolitic and non-oolitic particles (peloids) occur; oolitic particles are rarer and are distinguished by single to multiple concentric rings of jasper or iron oxide representing shallow water facies (Figs. 2.5 h; 2.6 b), whereas non-oolitic particles are rounded to shard-like (Fig. 2.5 g), and composed partially to completely of iron oxide with variable amounts of quartz and jasper. Some particles have a flat or elongated form; however, many are spastoliths, meaning they have been flattened by compaction of the sediment (Fig. 2.6 a; Simonson, 1987). Allochthonous facies are common within the iron formation and consist of locally transported conglomerates (intraformational breccias) that contain intraclasts of penecontemporaneous facies.

2.5.2 Quartz in the Middle Sokoman Iron Formation

Quartz content in the iron formations occurs mainly as 4 components: 1) microquartz/chert; 2) megaquartz; 3) patchy quartz, and 4) quartz-filled cracks (Figs. 2.6-2.7; 2.9- paragenetic sequence of minerals). Features of these quartz types include:

1. microquartz/chert (< 35 μm ; Folk, 1957) forms irregularly shaped subhedral crystals within the cores of ooliths and peloids (Fig. 2.6 b);
2. megaquartz (35-150 μm; Folk, 1957) most commonly occurs as the matrix in pore spaces between ooliths and peloids and consists of euhedral crystals of constant grain size in any sample (Fig. 2.6 c);
3. patchy quartz occurs as randomly distributed patches of larger subhedral crystals (> 1mm) that are irregular in shape and size (Fig. 2.6 d), crystals almost always interpenetrate each other with boundaries that commonly overlap those of ooliths. Patchy quartz is commonly associated with areas rich in iron oxides (Fig 2.7 g);
4. quartz-filled cracks that occur as radial 10-50 μm cracks within ooliths and peloids and as larger mm-size cracks that cross-cut synsedimentary textures. Both types of cracks consist of micro- and/or megaquartz with patchy quartz occurring most commonly in larger cracks (Fig. 2.6 e). There is a gradational change in crystal size from fine-grained quartz at crack boundaries (50 μm), to coarse-grained quartz towards the center of cracks (1 mm), especially in larger cracks.

2.5.3 Iron Minerals in the Middle Sokoman Iron Formation

Iron within the Middle Sokomon Iron Formation occurs mainly in 3 forms: 1) syngenetic iron oxide and silicates; 2) coarse microplaty hematite; and 3) euhedral magnetite (Figs 2.6-2.9).

Syngenetic iron occurs as hematite, magnetite and iron silicates tracing fine sedimentary textures in various forms, including: 1) fine-grained dusty hematite within and intergrown with chert (jasperoidal)(Fig 2.6 f); 2) anhedral, spongy hematite found in solitary form (Fig. 2.6 g); 3) fine microplaty subhedral crystals of hematite (~10 μm) (Fig 2.7 a); 4) hematite, and more rarely, magnetite in peloids and ooliths (Figs. 2.6 h; 2.7 b); and 5) semi-massive to massive magnetite-hematite forming bands and intergrown with stilpnomelane and minnesotaite.

Coarse microplaty hematite occurs as euhedral crystals 20-200μm in size (Figs. 2.7 c-e). It differs from syngenetic, fine microplaty hematite in that it is a replacement texture and frequently overgrows and cross-cuts primary sedimentary textures. It commonly forms iron-rich patches that have sharp boundaries with iron-poor zones in the rock (Fig. 2.7 d). Minor subhedral magnetite is commonly present within hematite-rich patches (Fig. 2.7 f). Coarse microplaty hematite locally occurs as mm-scale straight to sinuous cross-cutting veins (Figs. 2.7 h; 2.8 a). The veins are connected to iron-rich patches of microplaty hematite and intermixed with iron silicate minerals. They vary from conforming to sedimentary textures (sinuous veins) or cross-cutting the sedimentary structures (straight veins).

Euhedral crystals of magnetite (20-200μm) are present in all samples in varying abundances (Figs. 2.6 h; 2.7 a). They commonly overgrow and cross-cut sedimentary textures, and may coalesce to form aggregates and mm-scale patches. Locally, they define fabrics in the rock and occur as linear arrangements of euhedral crystals; riebeckite is associated when a fabric occurs (Fig 2.8 b). Martitisation of magnetite to hematite and

goethite occurs in some magnetite-bearing samples (Fig. 2.7 c, 2.8 e). Commonly, martitised samples exhibit multiple paragenetic stages with the first stage exhibiting hematite pseudomorphing magnetite, and the second exhibiting the transformation of martite (hematite) to goethite.

2.5.4 Petrography of Fault Zone Rocks

Minor faults are present in the Snelgrove Lake area, and occur in small steeped-sided linear valleys (Fig. 2.3). The rocks nearby and within faults are deformed and commonly contain abundant quartz veins. Although deformed, iron formations are still mostly intact and iron-rich beds and laminae are discernible (Fig. 2.8 c). Most of the rocks directly within the faults are strongly silicified and altered, an effect that decreases with distance from the faults. White quartz veins occur and cross-cut bedding in outcrop, and whereas bedding is intact in most cases, dismembered bedding with breccia textures occur locally.

The most altered samples are poor in iron and rich in quartz. The quartz is recrystallized and milky white, whereas iron, when present, is in the form of hydrous oxides and iron silicates. Ooliths are present but are replaced by quartz and are only identifiable by the fine clay matrix still present in their centers (Fig. 2.8 d). Iron formations distal to faults (10-40m) are more similar to unaltered iron formations; however, they differ in containing abundant hydrous iron oxides, including earthy hematite, botryoidal goethite and coarse grained bladed hematite. A pervasive iron oxide cement occurs as matrix between quartz grains in micro-textures, a characteristic only

seen in fault-proximal iron formations (Figs. 2.8 e), and commonly accompanied by the martitisation of magnetite crystals.

2.6 Iron Silicate Facies

Samples containing abundant iron silicate minerals were collected in the southernmost region of the studied area. The silicate minerals consist of minnesotaite, stilpnomelane, and/or chamosite, and occur, in association with magnetite, in greater abundance than quartz. There is a progression in facies from fine-grained stilpnomelane-rich to coarse-grained minnesotaite-rich facies. The stilpnomelane-rich samples are abundant in peloids composed predominantly of fine-grained iron silicates, whereas the matrix is predominantly microquartz and megaquartz. The minnesotaite-rich samples are much coarser; minor coarse-grained quartz and magnetite occur, whereas fine sedimentary textures are absent or have been destroyed/replaced by the growth of crystals of minnesotaite (Figs. 2.8 f). Magnetite occurs as euhedral crystals in all samples.

MESOPROTEROZOIC	
SHABOGAMO GROUP	*Gabbro, diabase*
PALEOPROTEROZOIC	
MONTAGNAIS GROUP **Retty Peridotite-Gabbro**	*Peridotite sills, gabbro, diabase sills*
KANIAPISKAU SUPERGROUP	
DOUBLET GROUP **Willbob Formation** **Thompson Lake Formation** **Murdoch Formation**	*Pillow basalt, pillow breccia* *Chloritic siltstone, black slate* *Chloritic phyllite, siltstone, black slate*
KNOB LAKE GROUP	
WESTERN SUCCESSION	***EASTERN SUCCESSION***
Menihek Formation *Black shale, siltstone*	*Gray shale, siltstone, minor schist and phyllite, minor tuff*
Nimish Astray Lake Formation	*Mafic lava, conglomerate, pyroclastics*
Sokoman Formation *Cherty iron formation*	
Nimish Petitsikapau Lake Formation	*Mafic lava, conglomerate, pyroclastics*
Wishart Formation *Orthoquartzite, gray quartzite, siltstone*	*Gray, black chert; minor iron formation*
UNCONFORMITY	
Dolly Formation *Gray shale, siltstone*	
Denault Formation *Dolomite, calcareous siltstone*	*Stromatolitic dolomite, dolomite, calcareous phyllite, minor mafic tuff*
Attikamagen Formation *Gray shale, siltstone*	*Gray shale, siltstone, pillow lava, tuff, minor schist and phyllite*
Seward Formation **Upper Member:** *Red siltstone, shale orthoquartzite and purple sandstone*	**Upper Member:** *Orthoquartzite, biotite-sericite phyllites*
Middle Member: *Pink feldspathic sandstone, arkose, granule conglomerate*	*not exposed*
Lower Member: *Gray feldspathic sandstone, granule conglomerate*	*not exposed*
ARCHEAN OR PALEOPROTEROZOIC	
Leucogranites and mylonitised equivalents. Large amphibolite, amphibolite gneiss and schist bodies in archean gneiss	
ARCHEAN **EASTERN BASEMENT COMPLEX**	
Tonalite-granodiorite gneisses, minor amphibolite, minor biotite gneiss and schist	

Figure 2.1. Regional stratigraphy of the Labrador Trough. The stratigraphy relevant to the Snelgrove Lake area is highlighted in blue color (modified from Wardle, 1979).

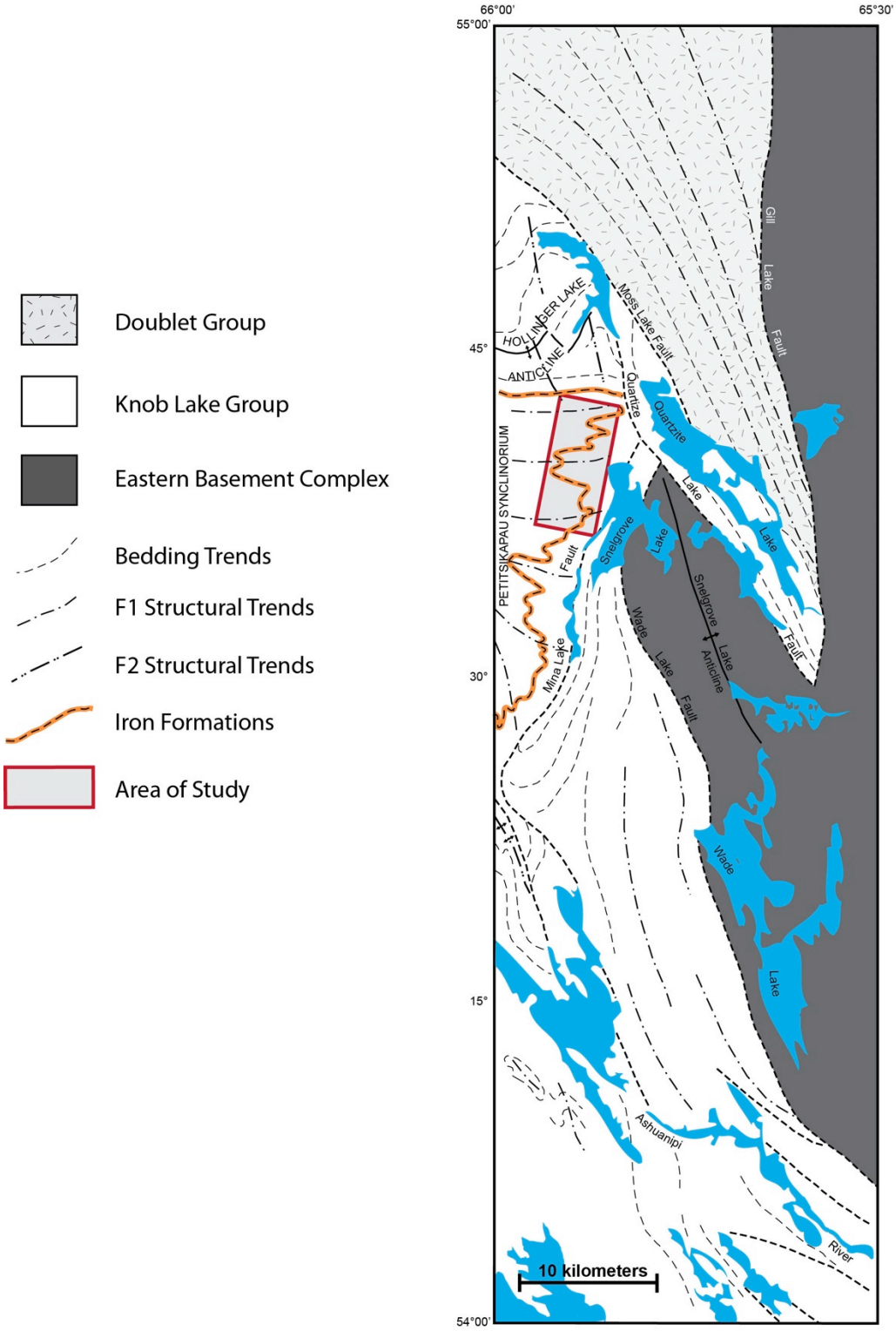

Figure 2.2. Generalized structural trends of the eastern margin of the Labrador Trough showing the Snelgrove Lake area (modified from Wardle, 1979).

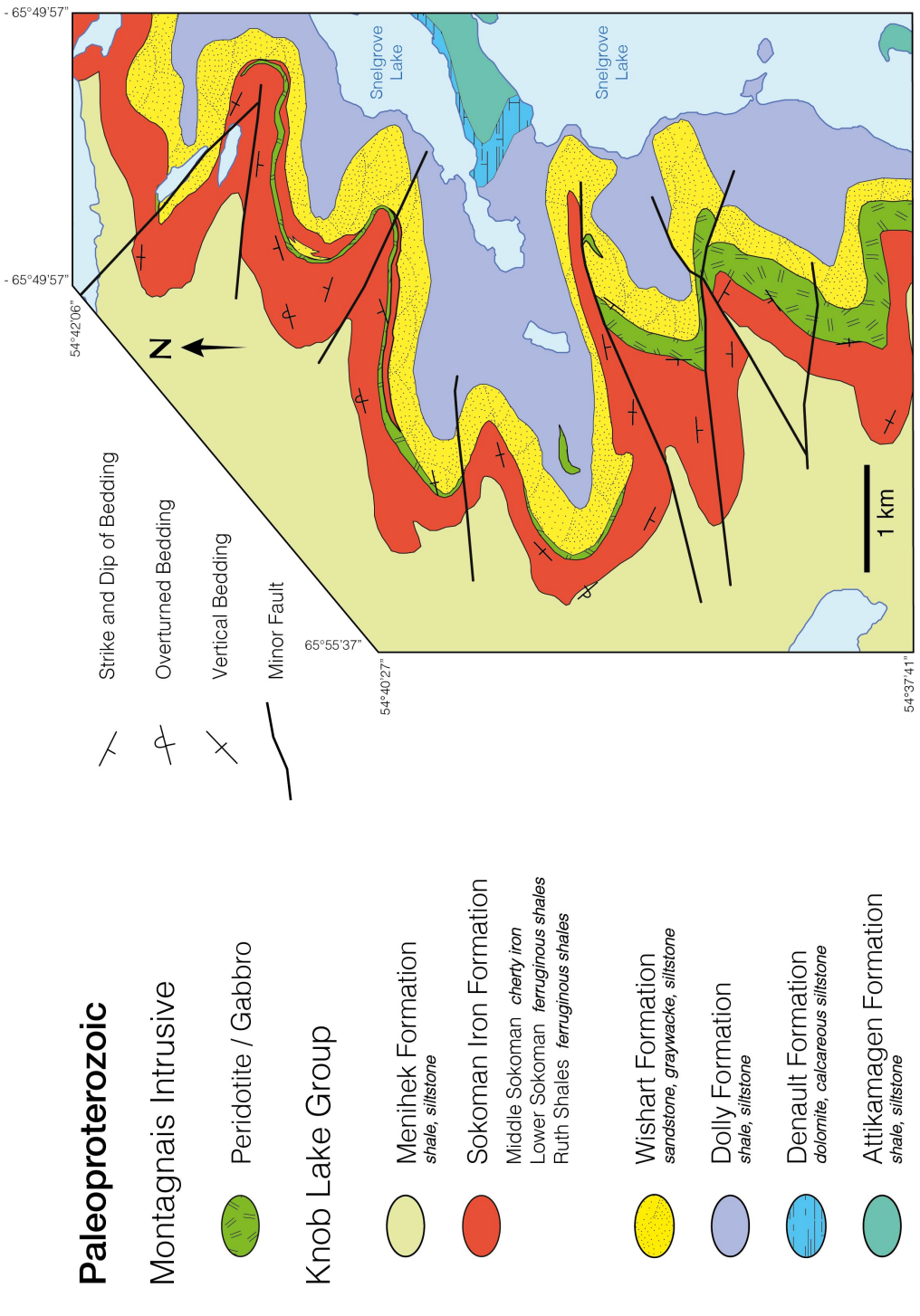

Figure 2.3. Surface geological map and stratigraphy of the Snelgrove Lake area. The Lower Sokoman, Ruth Shale and Middle Sokoman formations are undifferentiated (stratigraphy modified from Wardle, 1979).

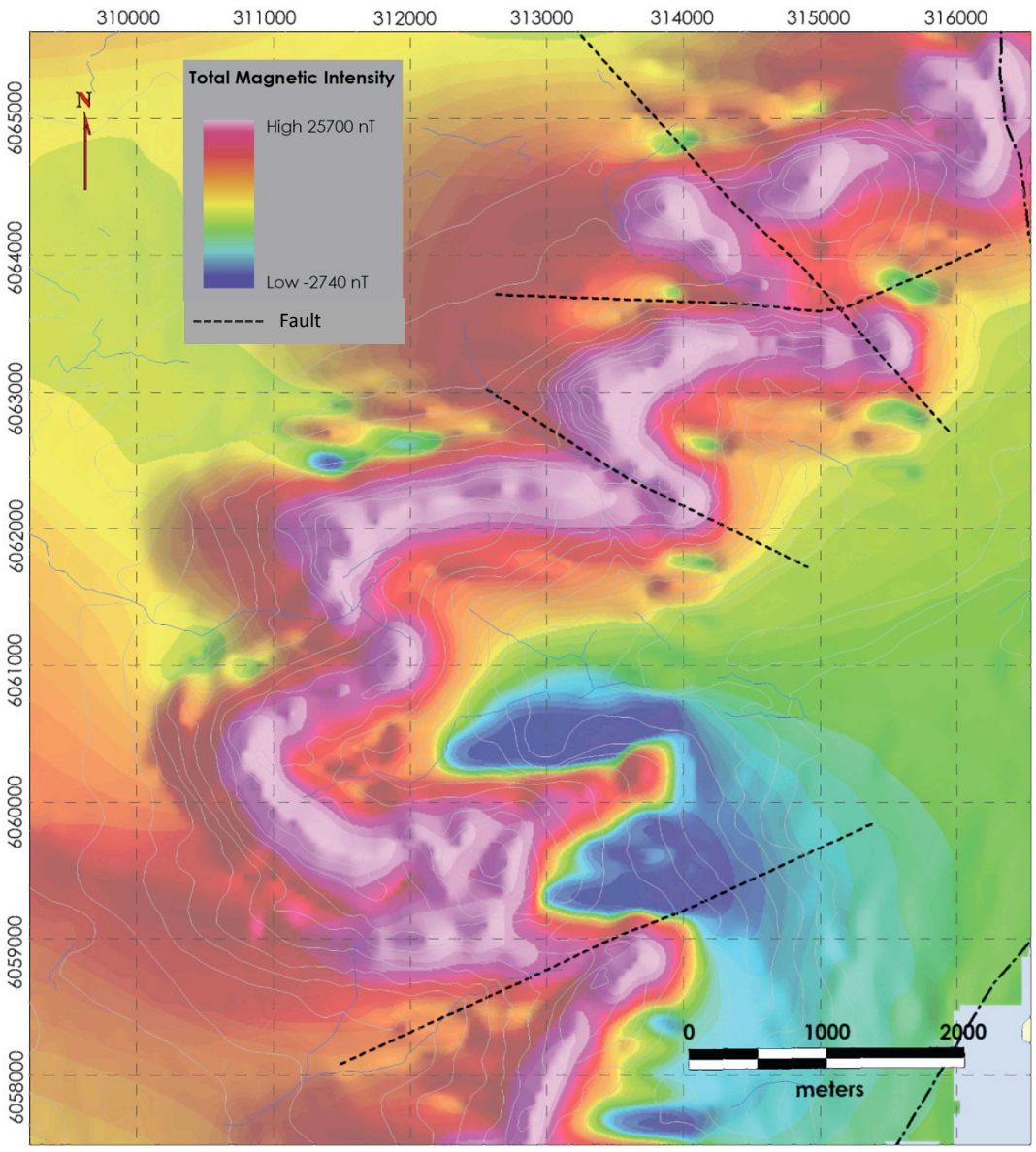

Figure 2.4. Map of total magnetic intensity aerial geophysics of Snelgrove Lake area (Altius Minerals, 2011).

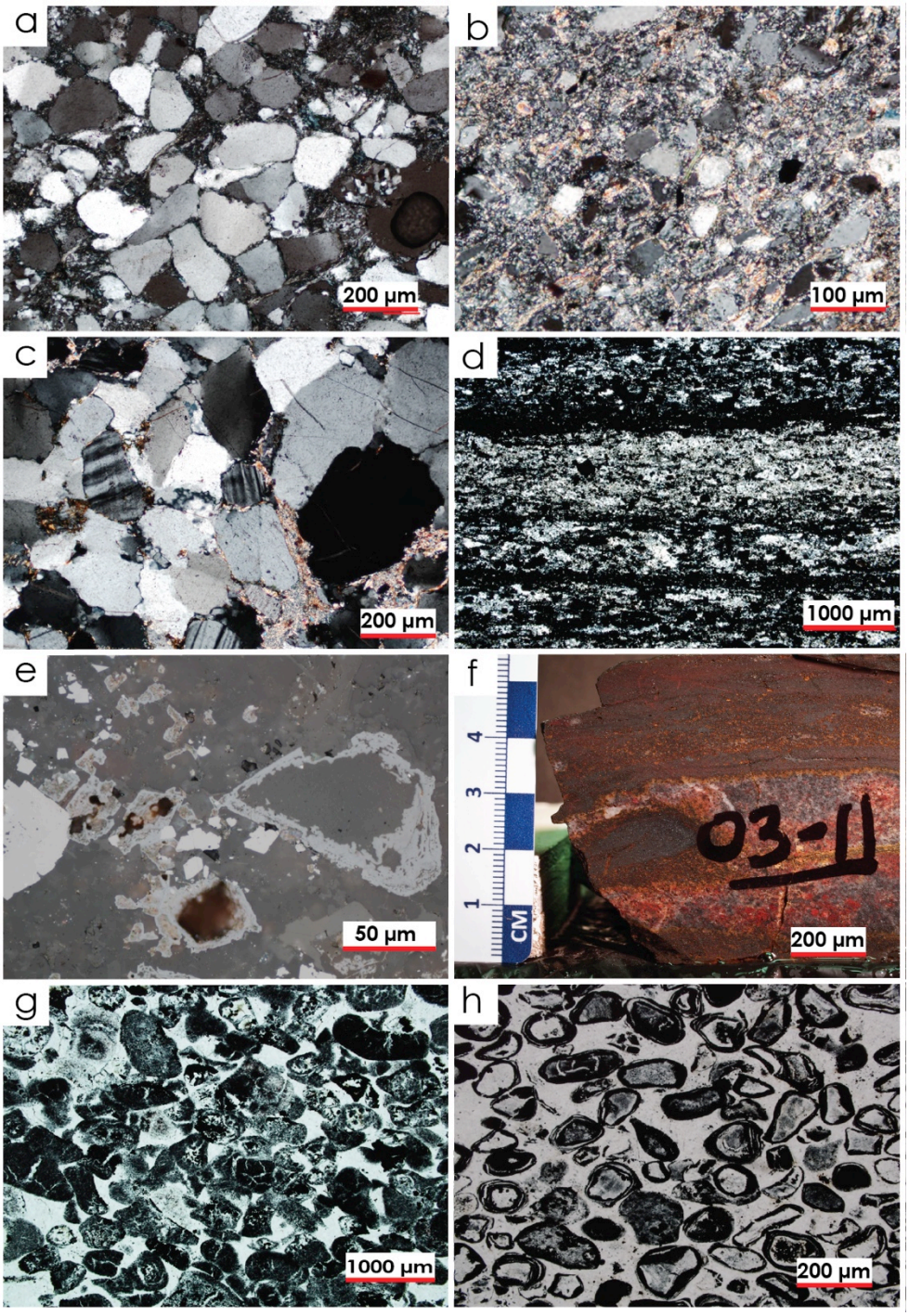

Figure 2.5. Photomicrographs and photographs of the Wishart Formation in cross-polarized light in a-c, Lower Sokoman and Ruth shales formations in d-e, and Middle Sokoman Formation in f-h. (a) Chert cemented sub-rounded quartz grains. (b) Chert and iron silicate matrix supported quartz and feldspar grains. (c) Pressure dissolution with sutured contacts, harder feldspar grains share concavo-convex boundaries with quartz. (d) Iron oxide laminations; plane polarized light. (e) Mn-Fe crystals with missing core; reflected light. (f) Alternating Fe-rich and quartz-jasper-rich bands; hand sample. (g-h) Non-compacted oolith/peloids in syngenetic facies of the Middle Sokoman Formation; plane polarized light.

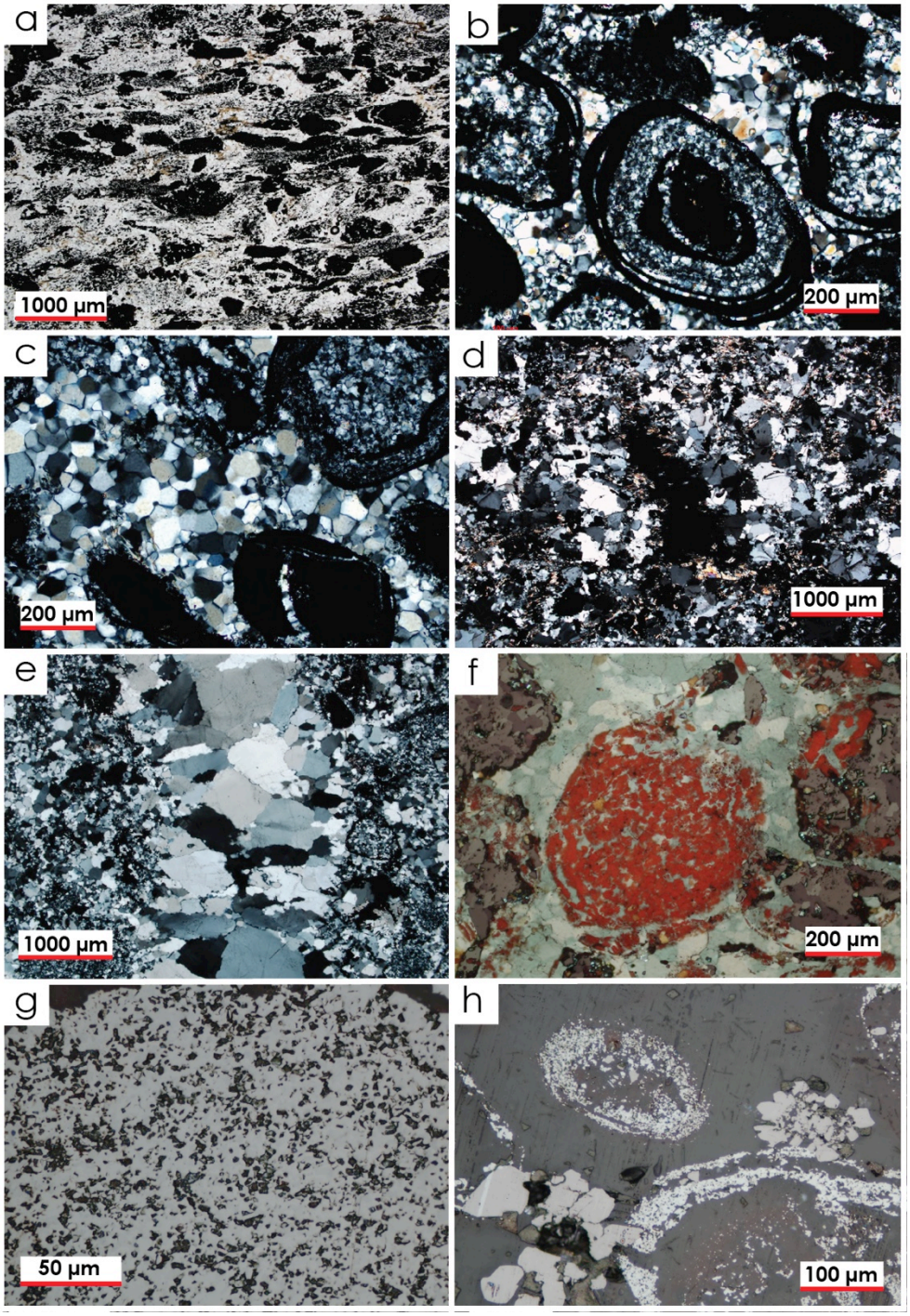

Figure 2.6. Photomicrographs of the Middle Sokoman Formation. (a) Iron oxide Peloids/Ooliths (black) in compacted facies; plane polarized light. (b-c) Microquartz and iron oxide oolith (black) in megaquartz matrix; crossed polarized light. (d) Patchy quartz texture mixed with iron silicate and iron oxide; crossed polarized light. (e) Large cement quartz-filled crack, gradational change in crystal grain-size from crack boundary to center; crossed polarized light. (f) Dusty hematite (red) in peloid; crossed-polarized light. (g) Spongy hematite texture inside peloid; reflected light. (c) Spongy hematite (pale grey) forming rings in oolith, and magnetite crystal aggregates (pinkish grey); reflected light.

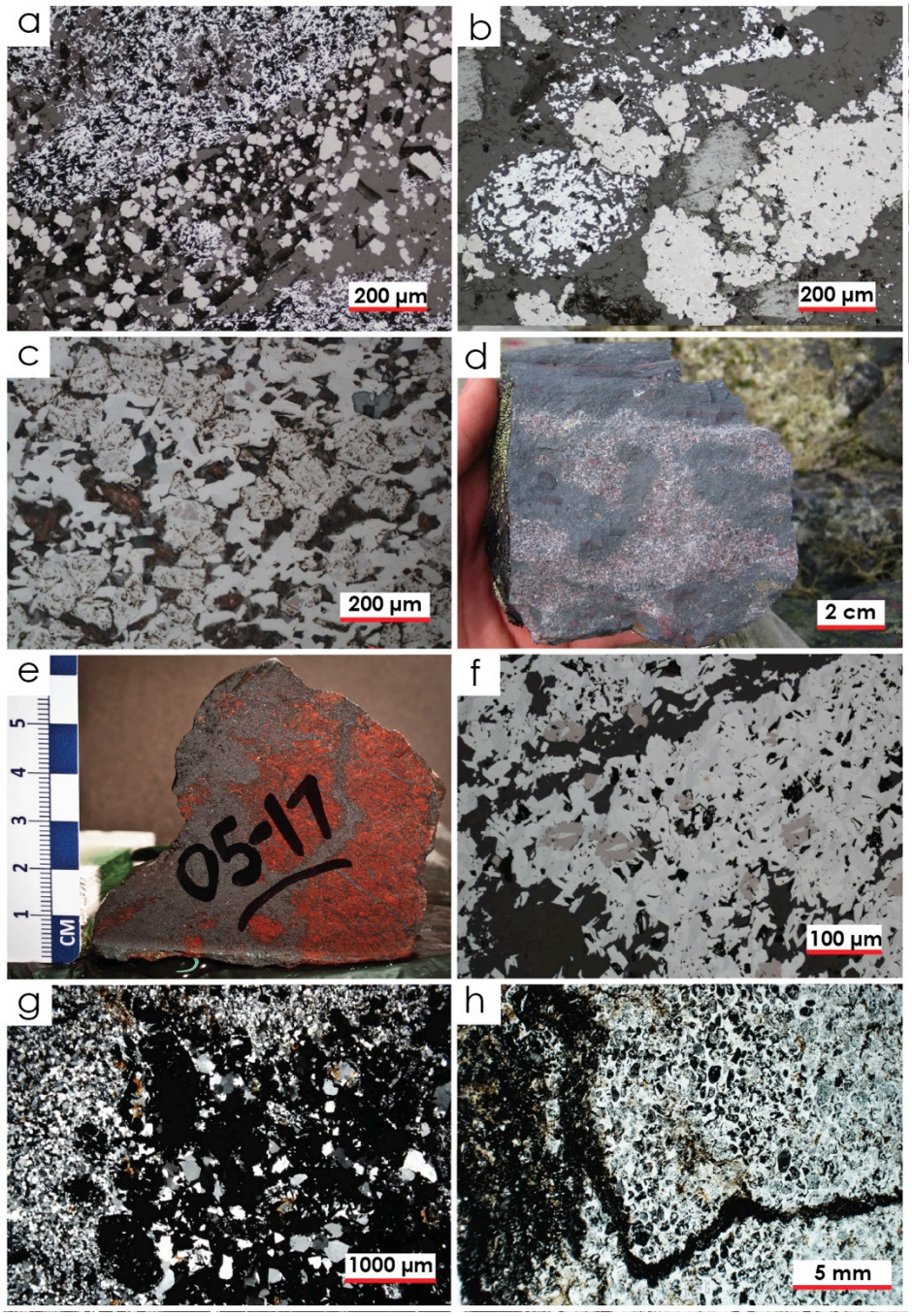

Figure 2.7. Photomicrographs of Middle Sokoman Formation: (a) Syngenetic iron in the form of fine microplaty hematite needles (pale grey) and magnetite crystals inside peloid (pinkish grey), black crystals are stilpnomelane; reflected light. (b) Magnetite (pinkish grey) forming as peloid, with separate fine microplaty hematite peloid (pale grey); reflected light. (c) Magnetite and hematite intergrown with stilpnomelane and minnesotaite with oxidation of magnetite to martite; reflected light. (d) Microplaty hematite formed as mottles, (e) and veins. (f) Magnetite (darker pinkish grey) oxidizing to coarse-grained microplaty hematite; reflected light. (g) Patchy quartz texture inside microplaty hematite (black); plane polarized light. (h) Curvilinear vein of microplaty hematite (black); plane polarized light.

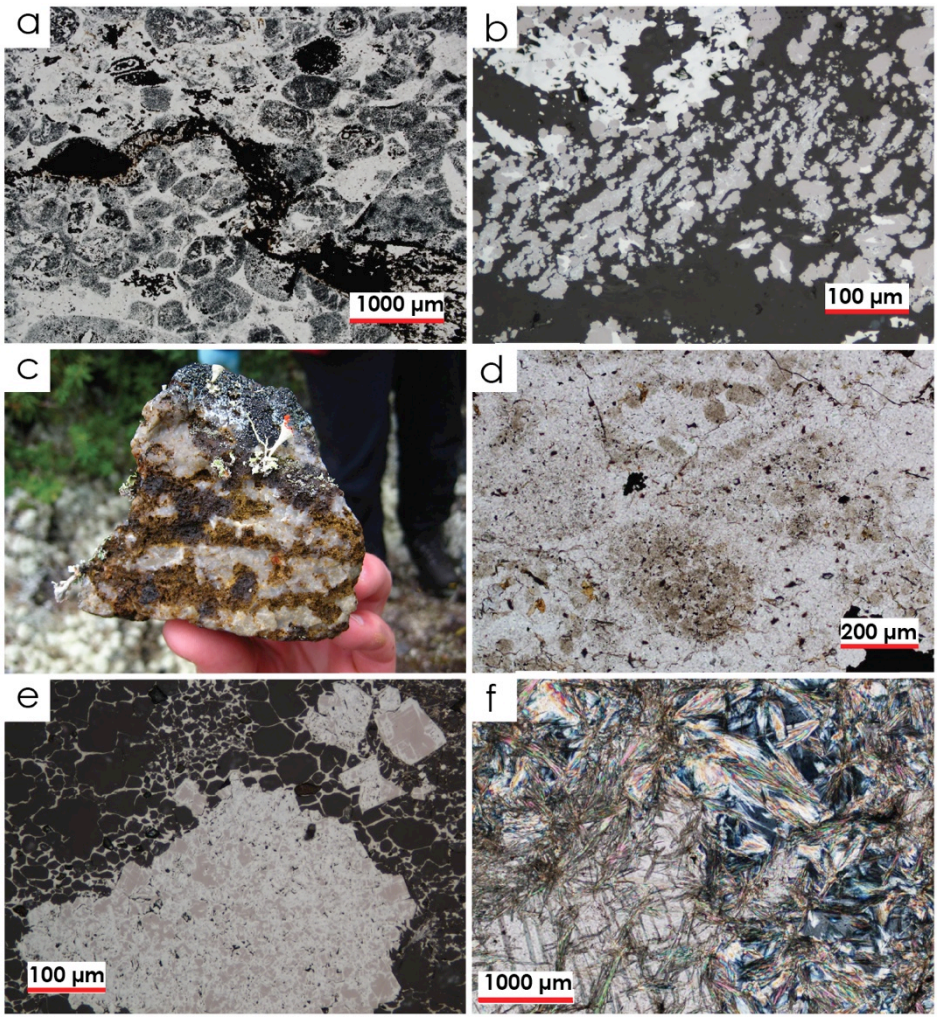

Figure 2.8. (a) Photomicrograph of meandering microplaty hematite vein incorporating peloids; plane polarized light. (b) Deformed magnetite grains within peloid; reflected light. (c) Remnants of goethite and limonite bedding alternating with milky white quartz in fault rock sample. (d) Remnant peloids highlighted by chamosite dust in fault rock; plane-polarized light. (e) Martitisation of magnetite crystal with pervasive iron oxide cement occurring between quartz crystals (dark grey) in fault-proximal sample; reflected light. (f) Stilpnomelane-rich facies with quartz in iron silicate-rich sample; crossed-polarized light.

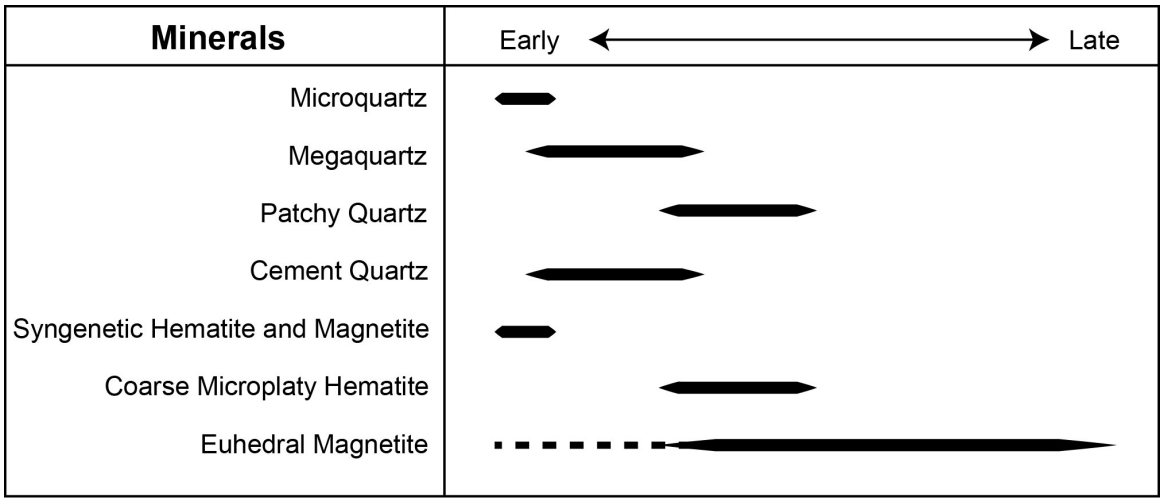

Figure 2.9. Paragenetic sequence of quartz and iron oxide minerals portraying their evolution relative to each other within facies.

Chapter 3- Geochemistry of Snelgrove Lake Area Iron Formations and Associated Rocks

3.1 Introduction

Iron formations in the Snelgrove Lake area were analyzed for major, minor and trace elements (Table A2). The results are utilized to characterize the lithologies, investigate their provenance, the redox conditions of the ocean at time of formation (oxygenation history), and their hydrothermal and post-depositional diagenetic chemical history. In order to highlight any geochemical trends specifically within the iron–rich group of samples, Middle Sokoman Formation samples have been divided into two groups: syngenetic and epigenetic. The first group contains samples in which iron oxide is interpreted to have formed simultaneously with the host rock and has remained mostly unaltered since formation (syngenetic). The second group is composed of samples that contain iron oxides in the form of coarse microplaty hematite (described in chapter 2), and inferred to have originated from iron that was recrystallized and/or remobilized (epigenetic).

3.2 Lithogeochemistry

All samples were crushed and pulverized in a mild steel (low contamination) pulverizer and analyzed at Actlabs of Ancaster, Ontario. Whole rock analysis for major elements was performed by X-ray fluorescence method on fused disks. Loss on ignition (LOI) was obtained by standard weight loss methods. Trace elements were determined by inductively coupled plasma mass spectrometer (ICP-MS) using 2 different digestion

methods. For whole rock analyses, including REE and high field strength elements (HFSE), a fusion pre-preparation and digestion in HF-HNO_3 were undertaken followed by analysis via ICP-MS. To obtain elements associated with ore mineralization (e.g., Zn, Pb, Au, Ag), a partial digestion by aqua regia was undertaken with subsequent analysis by ICP-MS. Trace element data obtained from both aqua regia, and fusion methods were used exclusively for principal component analysis, whereas all other statistical techniques performed in this chapter were used with trace elements obtained from HF-HNO_3 digestion.

Eight reference samples were submitted for analysis for quality control purposes. Precision and accuracy were tested on reference material of known and accepted values, unknown material and analytical duplicates by using the percent relative standard deviation (%RSD) and percent relative difference (%RD). For both minor elements analyzed by ICP-MS and major elements analyzed by X-ray fluorescence method, precision and accuracy are generally less than ±10% for %RSD and %RD. However, they tend towards >±10%RD for elements that have concentrations close to the detection limits of the given elements.

3.3 General Major and Minor Element Variations

Major components of iron formations are dominated by iron and silica (Fig. 3.1)(Table A2). Fe_2O_3 concentrations vary from 21.2 – 63.9 wt.% within the Middle Sokoman Iron Formation (MSIF) and from 29.8 – 49.3 wt.% in the Lower Sokoman Iron Formation (LSIF) and Ruth Formation shales (RS). The Wishart Formation contains much lower concentrations of Fe_2O_3, from 1.3 – 6.1 wt.%. SiO_2 ranges from 29.1– 76.9

wt.% within the MSIF, from 38.5 – 51.1 wt.% within the LSIF and RS combined, and from 61.5 – 89.5 wt.% within the Wishart Formation. The remainder of major element oxides (Al_2O_3, MgO, K_2O, CaO, Na_2O, and TiO_2) are generally <4 wt.% within MSIF samples, whereas in the LSIF and RS combined, and in the Wishart Formation they form <23 wt.% and <31 wt.% respectively. Of these elements, MgO is found in highest concentrations likely due to iron silicate minerals minnesotaite ($\{Fe^{2+}Mg\}_3Si_4O_{10}\{OH\}_2$) and magnesio-riebeckite ($Na_2\{Mg3Fe_2^{2+}\}Si_8O_{22}\{OH\}_2$) along with TiO_2, which is found as ilmenite ($FeTiO_3$) within the core of magnetite crystals. MnO and P_2O_5 concentrations are uniformly low with <0.1 wt.% in the MSIF and Wishart Formation, and <0.6 wt.% in the LSIF and RS. Chalcophile elements Cu, Zn, Pb are found as trace elements (<150 ppm each) in all samples.

Principal component analysis (PCA) is a statistical technique that uses either correlation or the covariance matrix of a multi-element geochemical dataset to identify the least number of variables that will explain major variations in the data (Grunsky, 2010). The measured variables represent the eigenvectors of either the covariance or the correlation matrix. Ultimately, more than one set of variables, the principal components, can exist to explain the variability. The principal components are commonly plotted against one another to provide a graphical means of viewing the relationships among multiple elements from bulk geochemical data and can identify geochemical trends that are the result of geological and geochemical processes (Grunsky, 2010).

This technique was applied to the data of the Snelgrove Lake iron formation samples only. Figure 3.2 is a bivariate plot of the first two principal components, which account for 70% of the dataset variability. Groups of elements within the plot can be

viewed as representing different poles. SiO_2 and Fe_2O_3, which by weight percent form the bulk of all samples, occur at the top and bottom of the plot in opposite directions, and represent quartz and iron-oxides respectively. Rare earth elements cluster together in proximity to K_2O, TiO_2, Al_2O_3, Rb, Ba, V, Ta, Hf, Zr, Ga, Nb, Th and Co, reflecting their association with aluminosilicates (clays) and heavy mineral phases. In addition to clays, REE are proximal to P_2O_5 and Cs, suggesting they are controlled by phosphate minerals (e.g., apatite, monazite). Cu (aqua regia digestion (AR)), Ni(AR), Sn, Zn, Ag, and Tl are related to sulfides, whereas MgO, MnO, Na_2O along with Ge form a group that are likely related to magnesio-riebeckite, manganese oxides and possibly chlorite. The elements As, Sb and W plot together and are possibly adsorbed on organic matter or Fe-oxides (Yuan-Hui, 1991). Zn(AR) and CaO are plot together, potentially reflecting Zn(AR) incorporation in carbonates.

3.4 Mobile Elements and Weathering/Alteration

All samples were plotted in A-CN-K –type diagrams (Fig. 3.3)(Nesbitt and Young,1984; Nesbitt, 2003) to assess the distribution of mobile elements. Low concentrations of Al_2O_3 in most iron formation samples reflect low clay content. Higher concentrations of Al_2O_3 in the Wishart Formation, LSIF and RS compared to MSIF samples are reflected by their higher chemical index of weathering values (CIW = $100*Al_2O_3/(Al_2O_3+Na_2O+K_2O+CaO)$(Nesbitt and Young, 1984; Nesbitt, 2003). Most MSIF samples show values that range from 3 to 60 with 3 samples over 60. A positive correlation exist between the CIW and Zr, higher values in samples of Wishart, Ruth and

Lower Sokoman formations probably indicate greater concentrations of detrital minerals (Fig 3.3 c).

3.5 Sediment Provenance

Studies in modern and ancient marine environments illustrate that the chemistry of iron formations is a function of elements derived from hydrothermal, detrital, and hydrogenous sources (e.g., Peter, 2003). There is a general consensus that Lake Superior-type iron formations have obtained their iron from hydrothermal vents (Klein and Beukes, 1992; Isley and Abbott, 1999; Bekker et al., 2010). In Al-Fe-Mn and Fe/Ti vs. Al/Al+Fe+Mn plots (Figs 3.4 a-b)(after Bostrom, 1973), iron and manganese are usually associated with a hydrothermal source in marine sediments, whereas Al_2O_3 and TiO_2 come from detrital sources. The plots further highlight that iron formations have minimal detrital components and there are no chemical distinctions between syngenetic and epigenetic MSIF samples.

Despite a hydrothermal input, other immobile elements can provide insight into the detrital components present in the samples. The provenance of the detrital component was tested using ratios of elements enriched in continental crust (Th, Zr) and those enriched in mafic or mantle derived material (Co)(Fig. 3.4 c)(McLennan, 1993). Other mafic derived elements (V, Cr, Mg) were also chosen (not shown) and illustrate similar results to those using Co. Wishart Formation samples have signatures reflecting derivation from upper crust-like material; however, they have Zr/Co ratios greater than the upper crust suggesting some potential detrital zircon accumulation in the sandstones. The iron formation samples show a mixing between more mafic detritus and upper crustal

material. Interestingly, the Montagnais gabbros, which intrude the iron formations and shales, have similar ratios to the iron formations. This supports the idea of submarine volcanic activity as a source for iron in Lake Superior-type iron formations (Klein, 2005; Bekker et al., 2010).

3.6 REE-Y Systematics

Rare earth element (REE) and Y (REY) composition of samples were plotted on post-Archean average shale (PAAS)-normalized plots (Figs. 3.5). Results show similar patterns that are generally flat relative to PAAS but with variations in absolute abundances between lithologies. The Wishart Formation has the highest absolute REE content of all the Snelgrove Lake samples with a bimodal distribution that is caused by variations within facies (Fig. 3.5 a). In particular, the samples with the lowest REE also have the lowest Al_2O_3 and highest SiO_2 content (not shown), and are coarser grained and less slaty (i.e. less micaceous) than those that contain higher amounts of REE. The LSIF and RS have broadly similar patterns but with values less than 1, suggesting derivation from sources similar to, but less enriched than PAAS (Fig. 3.5 b-c). Lower Sokoman samples tend towards lower REE values. The MSIF samples tend to have more variable patterns with depletions in absolute REE content relative to PAAS. Syngenetic MSIF contain variable patterns, but most have either flat to HREE-enriched patterns. The epigenetic iron formations contain more systematic patterns with flat to weakly depleted LREE, and flat to enriched HREE (Fig. 3.5 d-e). Fault zone rocks have highly irregular signatures with low absolute REE contents, the significance of their signatures is

uncertain, but these are likely related to potential REE-Y mobility associated with faulting (Fig. 3.5 f).

The samples from Snelgrove Lake exhibit variable Eu and Ce anomalies. The europium anomaly (Eu/Eu*) is known to be a useful parameter for quantitive determination of the temperature of the hydrothermal fluids from which hydrothermal sedimentary rocks precipitate (Klein and Beukes, 1989; Derry and Jacobsen, 1990; Bau and Dulski, 1996; Frei et al., 2008). Specifically, a positive europium anomaly on a shale normalized plot is indicative of deposition from a fluid with a temperature greater than 250°C, whereas a negative anomaly from a fluid with a temperature below 250^{o}C (Sverjensky, 1984). Most iron formation samples from the Snelgrove Lake area have flat to weakly positive Eu/Eu* anomalies (Figs. 3.5 and 3.6 a) suggesting deposition from low temperature fluids, consistent with other Lake Superior-type iron formations (Bau and Dulski, 1996). However, it is also possible that the weakly positive Eu/Eu* anomalies are due to detritus present within the iron formation (e.g., detrital material from a more mafic source?).

Cerium anomalies provide insight into potential redox conditions of sediment formation as Ce is a strongly redox sensitive trace element. In particular, Ce is insoluble in modern oceans and adsorbs onto Mn nodules leading to Ce depletion (negative Ce anomaly) in oxygenated seawater; under anoxic conditions it is highly soluble and therefore enriched in anoxic seawater. (e.g., Elderfield and Greaves,1982; Elderfield et al., 1988). Iron oxides/oxyhydroxides are known to scavenge REE from sea water, and will commonly inherit Ce anomalies characteristic of the ocean at the time of formation (e.g., Bau and Dulski, 1996b; Bau, 1999; Peter et al., 2003). Figure 3.6 b contains data for

the cerium anomalies (Ce/Ce*). Values for MSIF are variable but generally tend towards negative Ce/Ce* anomalies, indicating anoxic depositional conditions (de Baar et al., 1988; German et al., 1991b; Goodfellow et al., 2003b). In particular, the RS and LSIF samples show fewer variations between samples and have values equal to or slightly lower than 1, indicating deposition in a weakly oxic to sub-oxic environment. There are no observable patterns between epigenetic and syngenetic MSIF samples.

Based on their similar chemistry, the geochemical pair Y and Ho is known to have predictable behaviors in rocks of marine environments (e.g. Bau et al., 1995; Bau, 1996; Nozaki et al., 1997). These elements rarely fractionate in rocks and thus are predicted to retain their chondritic Y/Ho ratios of ~ 27. In contrast, in marine environments Y behaves differently with strong fractionation from Ho that results in seawater having Y/Ho ratios of > 44 (Bau, 1996). On this basis, it is predicted that sediments that are composed of particles that have spent considerable amounts of time suspended in the ocean should have high Y/Ho ratios close to that of the seawater (Bau, 1996). Y/Ho ratios of MSIF samples show wide variations between 20 and 37, with a mean of 29 and no distinction between syngenetic and epigenetic samples (Fig. 3.7 a). Samples of the LSIF, RS and Wishart Formation, with the exception of 3 samples from the Wishart Formation, have Y/Ho ratios between 25 and 31, and are generally closer to the average PAAS shale composite (Fig 3.7 a). The lack of correlation between Y/Ho and Zr of all samples indicates that detrital input has no effect on Y systematics. Y/Ho ratios of the Snelgrove Lake iron formations appear to be in line with other late Paleoproterozoic iron formations, which generally have Y/Ho between 20 and 50 (e.g., Planavsky et al., 2010).

3.7 Redox Sensitive Elements as Proxies for Oxygenation

Trace and minor elements, including V, Cr, U, and Mn, are very useful for understanding ancient paleoredox of a sedimentary environment and are presented in figures 3.7 (b) and 3.8 (e.g., Jones and Manning, 1994; Calvert and Pederson, 1993). Manganese values in MSIF are found mostly below 1000 ppm, whereas values for LSIF and RS are mostly above 1000 ppm. A value of 1000 ppm is used and interpreted as a limit between oxygen-rich and oxygen-depleted waters according to Calvert and Pederson (1993, 1996), where values >1000 ppm are indicative of a more oxic environment. U/Th data in comparison (e.g. Jones and Manning, 1994) suggest that the entire sequence of sediments from the RS to the Wishart Formation were deposited within a mostly anoxic environment (Fig. 3.7b). However, the RS and the LSIF tend to plot slightly closer to the oxic field, relative to most of the MSIF samples. In general, data from the Ce/Ce* anomaly, U/Th ratios and Mn values, all coincide to indicate that the LSIF and the RS were deposited in under more oxic conditions relative to the MSIF.

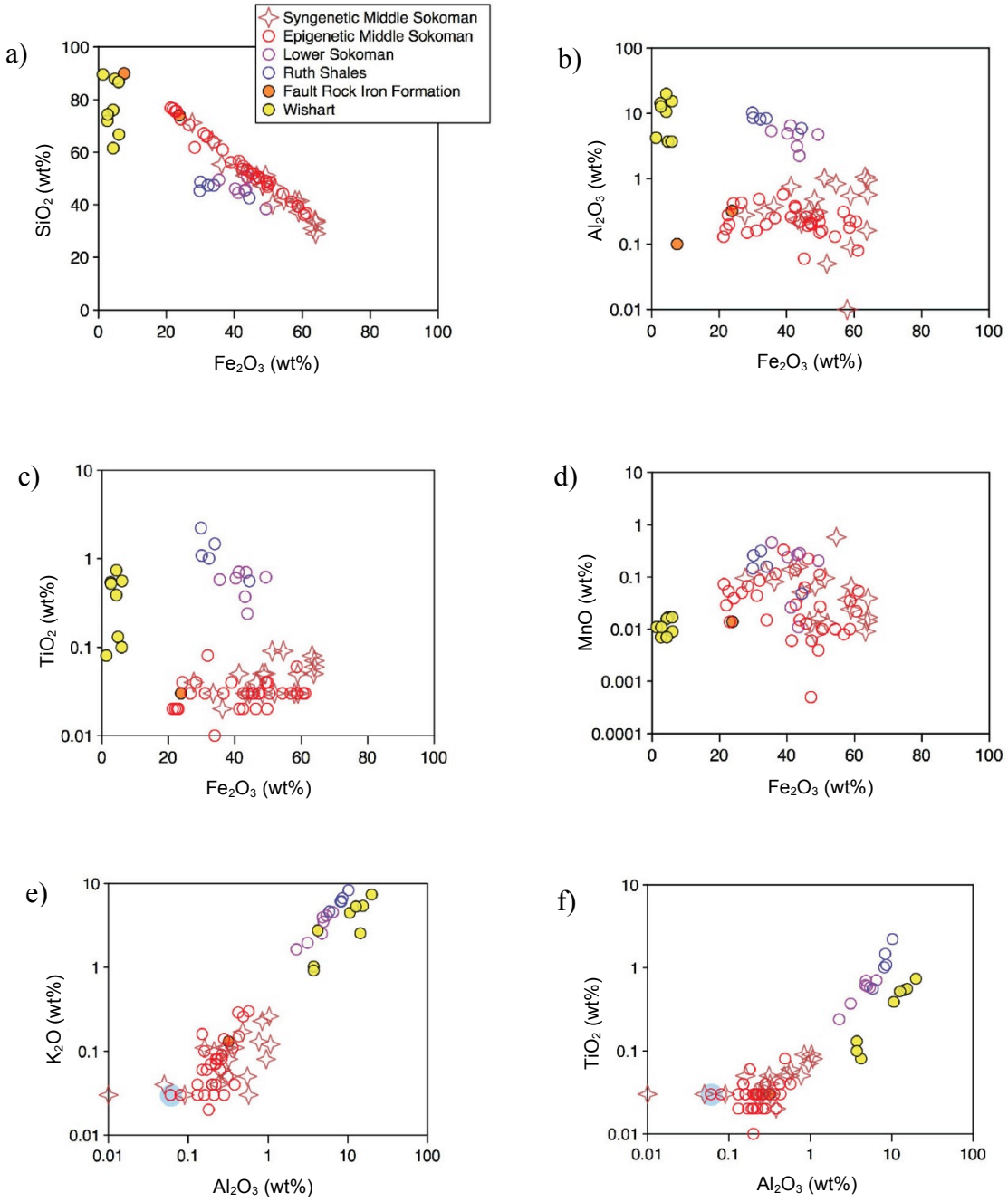

Figure 3.1. Bivariate plots showing relationship of selected major and minor elements. (a) Fe_2O_3 vs. SiO_2, (b) Fe_2O_3 vs. Al_2O_3, (c) Fe_2O_3 vs. TiO_2, (d) Fe_2O_3 vs. MnO, (e) Al_2O_3 vs. K_2O, (f) Al_2O_3 vs. TiO_2.

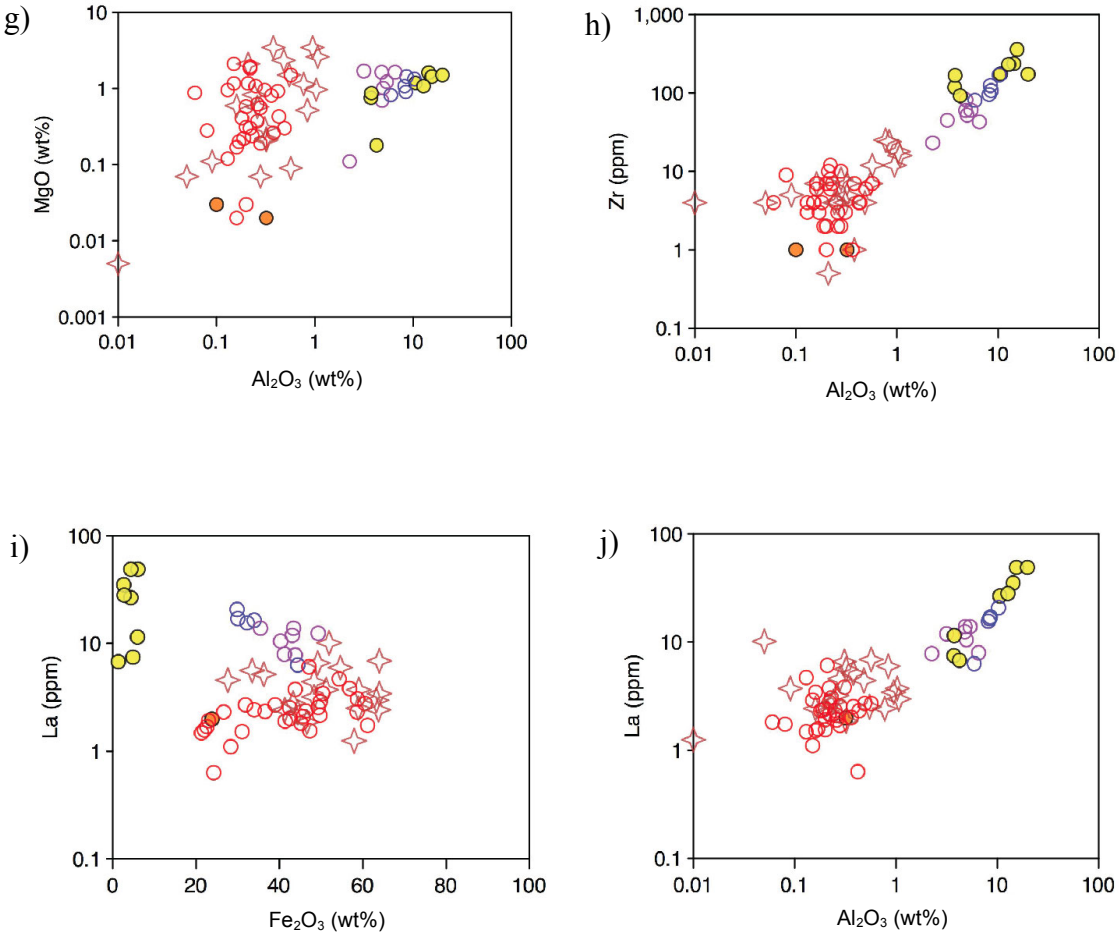

Figure 3.1. continued. Bivariate plots showing relationship of selected major and minor elements. (g) Al_2O_3 vs. MgO, (h) Al_2O_3 vs. Zr, (i) Fe_2O_3 vs. La, (j) Al_2O_3 vs. La.

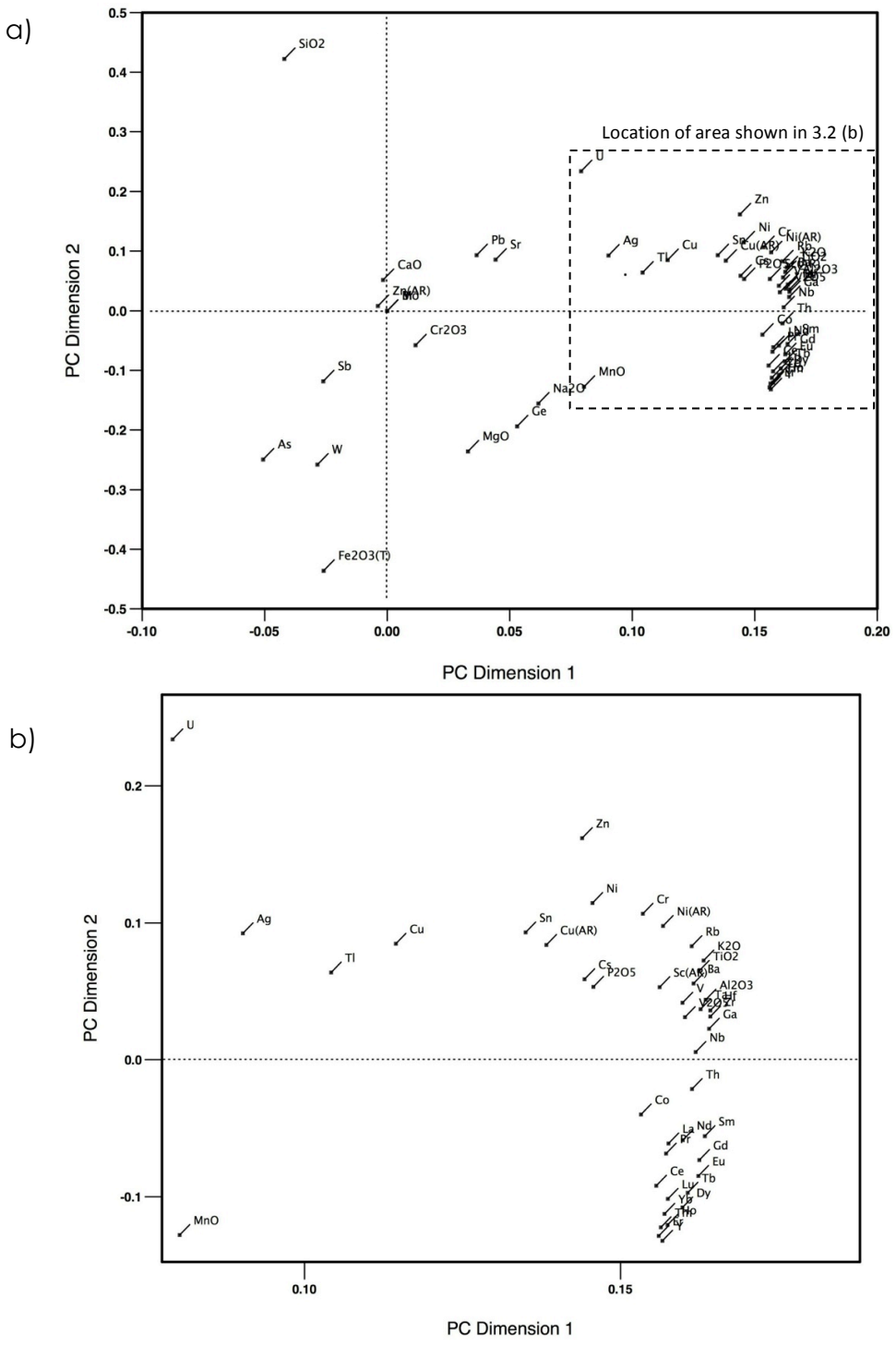

Figure 3.2. (a) Bivariate plot of the first two components of the principal component analysis, which account for 70% of the variability in the dataset. The analysis was performed for the Middle Sokoman, Lower Sokoman and the Ruth formations. (b) Close up of elements in (a) inferred to represent the detrital component.

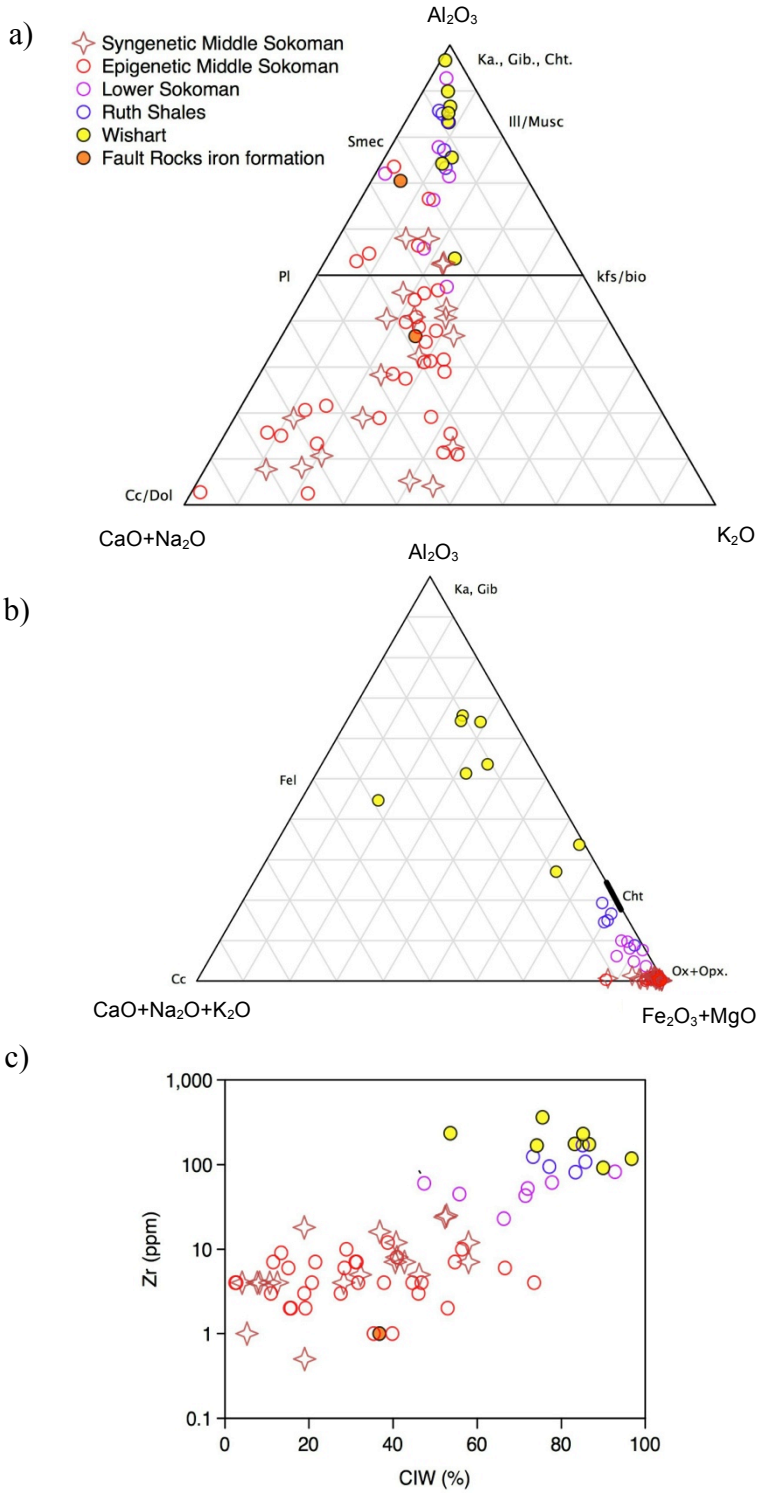

Figure 3.3. (a) $CaO+Na_2O - Al_2O_3 - K_2O$, and (b) $CaO+Na_2O+K_2O - Al_2O_3 - Fe_2O_3+MgO$ plots based on Nesbitt (2003), and Nesbitt and Young (1984). (c) Bivariate plot of chemical index of weathering (CIW) vs. Zr.

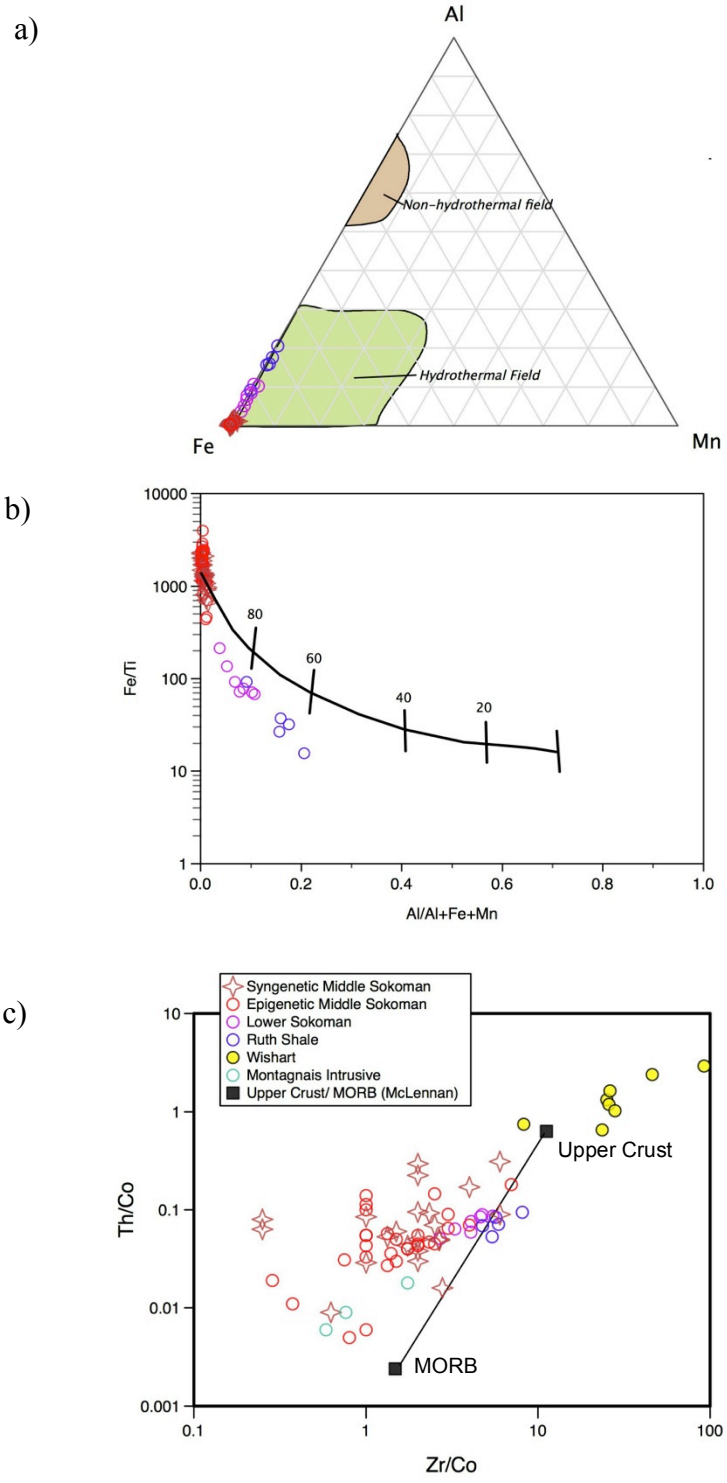

Figure 3.4. (a) Fe-Al-Mn and (b) Fe/Ti vs. Al/Al+Fe+Mn diagrams showing the relative distribution of hydrothermal versus detrital components of a sediment (Boström, 1973). (c) Bivariate plot of Zr/Co vs. Th/Co ratios illustrating provenance (McLennan, 1993).

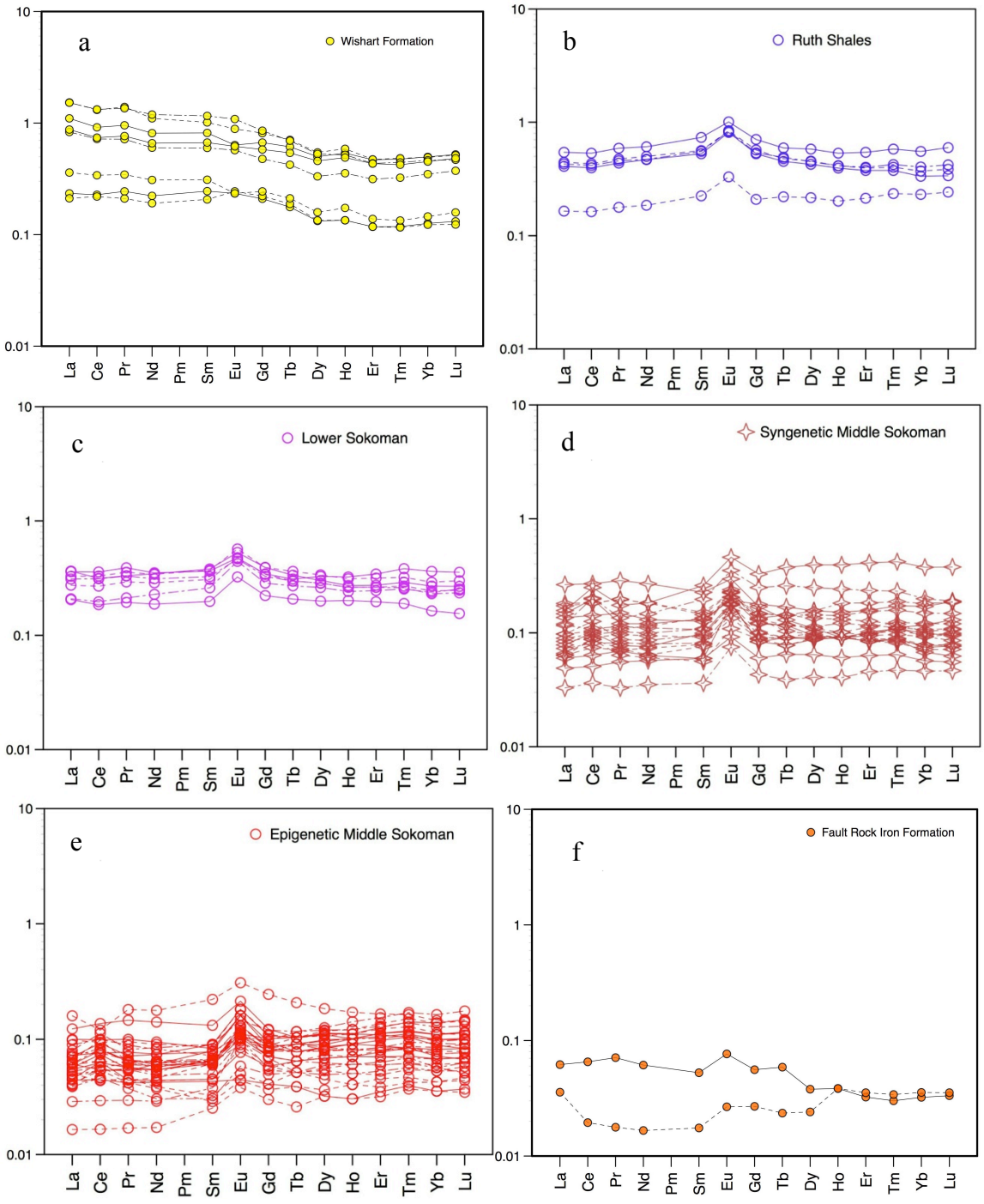

Figure 3.5. Post Archean Shale Normalized (PAAS, McLennan 1989) plots of rare earth elements for (a) Wishart Formation, (b) Ruth Formation shales, (c) Lower Sokoman Formation, (d) syngenetic Middle Sokoman Formation, (e) epigenetic Middle Sokoman Formation, and (f) fault rocks of iron formation.

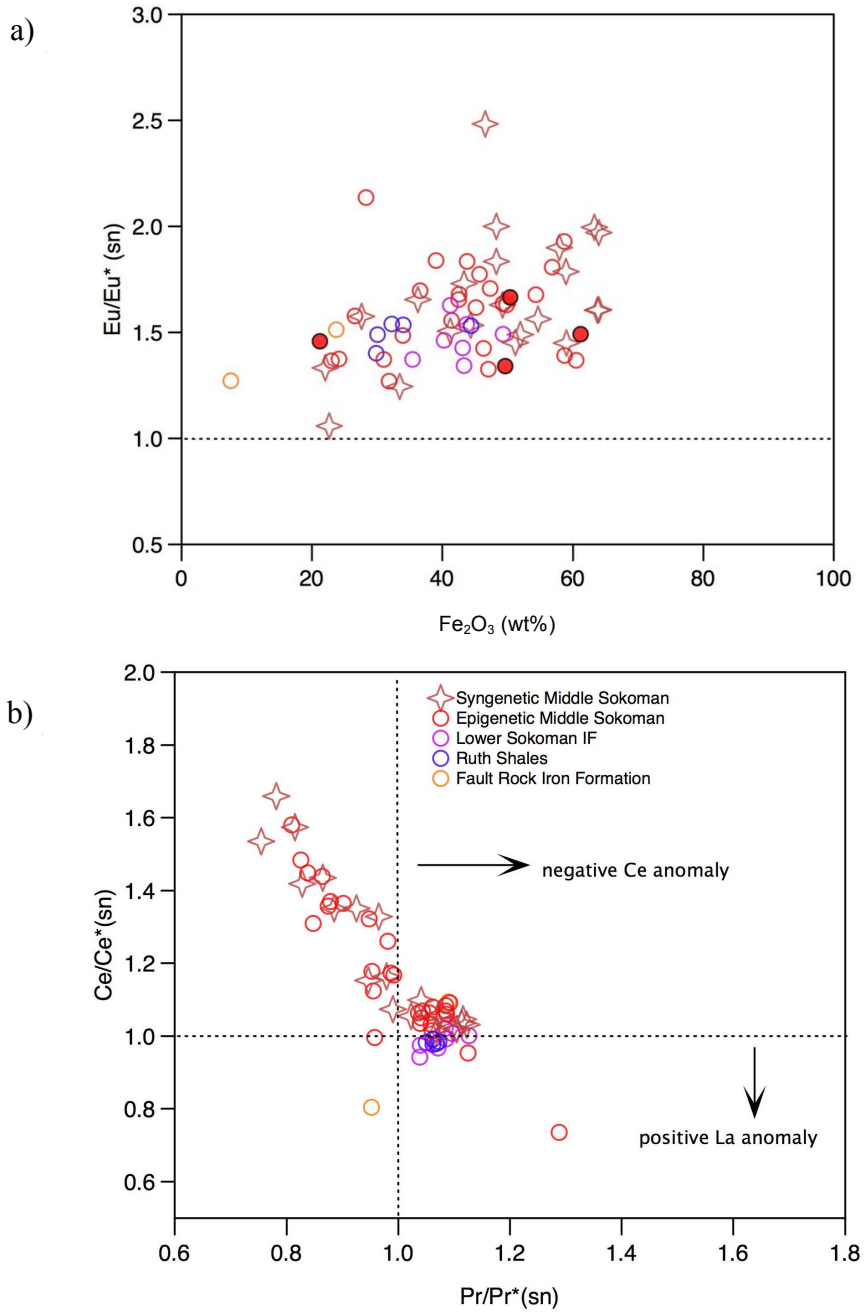

Figure 3.6. (a) Bivariate plot of Eu/Eu* vs. Fe_2O_3. Positive Eu/Eu* anomalies suggest deposition from hydrothermal fluids under 250°C (Bau and Dulski, 1996). Eu/Eu* calculated as $[Eu/(0.5Sm+0.5Gd)]_{SN}$. (b) Bivariate plot of Ce/Ce* vs. Pr/Pr* (Kamber and Webb, 2004). The Ce/Ce* anomaly is used to measure the redox-potential of oceans, and indirectly, the presence of oxygen. A tendency towards depletion is inferred to indicate the presence of oxygen (Elderfield and Greaves, 1982; Elderfield et al., 1988). This diagram is used to discriminate real Ce/Ce* anomalies from those created by the downward pattern of light rare earth elements (LREE). Ce/Ce* calculated as $[Ce/(0.5Pr + 0.5La)]_{SN}$ and Pr/Pr* as $[Pr/(0.5Ce + 0.5Nd)]_{SN}$. SN = shale normalized (McLennan, 1989).

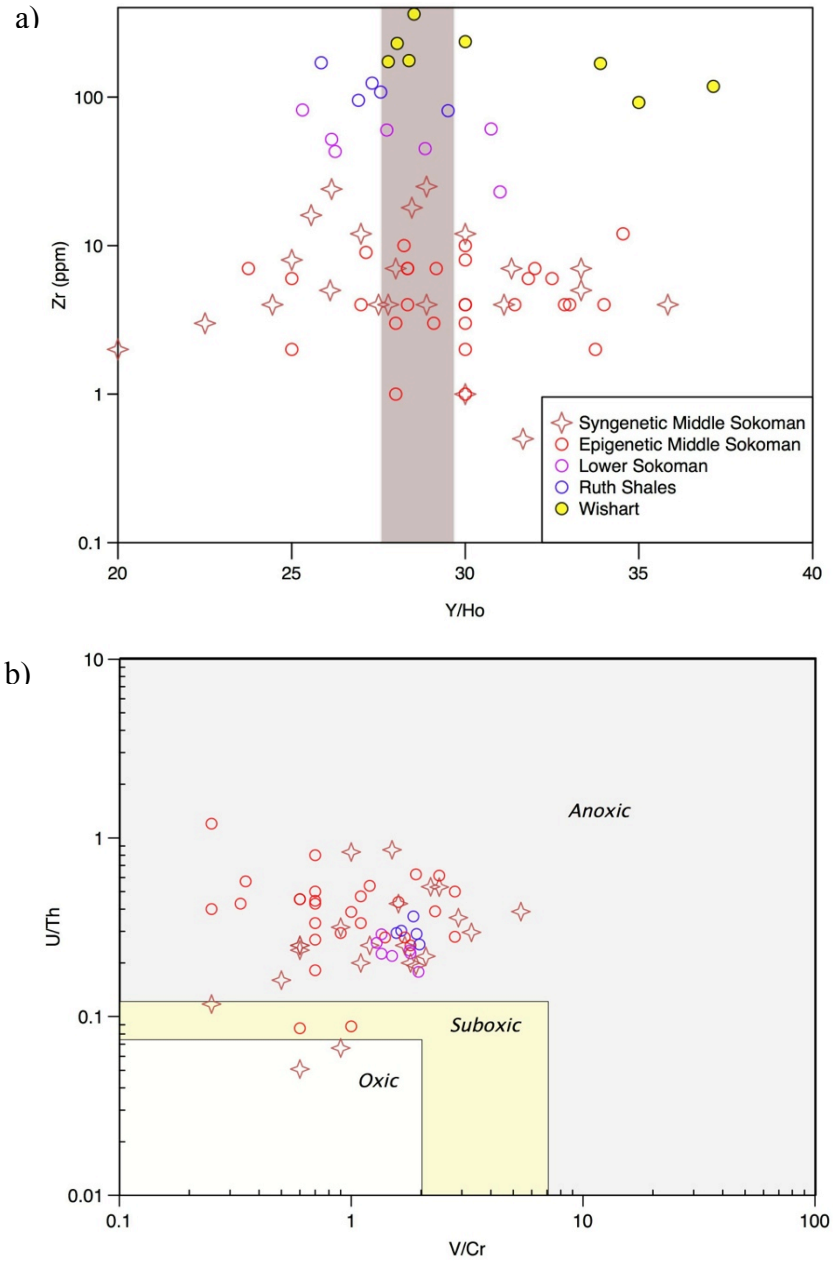

Figure 3.7. (a) Plot of Y/Ho vs. Zr of samples from the Middle Sokoman, Lower Sokoman, Ruth Shale and Wishart Formation. Shaded area indicates PAAS shale composite values. Y/Ho ratios are chosen to determine the amount of element fractionation in oceanic setting. The lack of correlation with Zr illustrates that detrital input has no effect on Y systematics. (b) Plot of U/Th vs. V/Cr ratios (Jones and Manning, 1994) showing the differences between lithologies for the syngenetic Middle Sokoman, epigenetic Middle Sokoman, Lower Sokoman, and Ruth Formation samples. Oxic, suboxic and anoxic limits determined from Tyson and Pearson (1991).

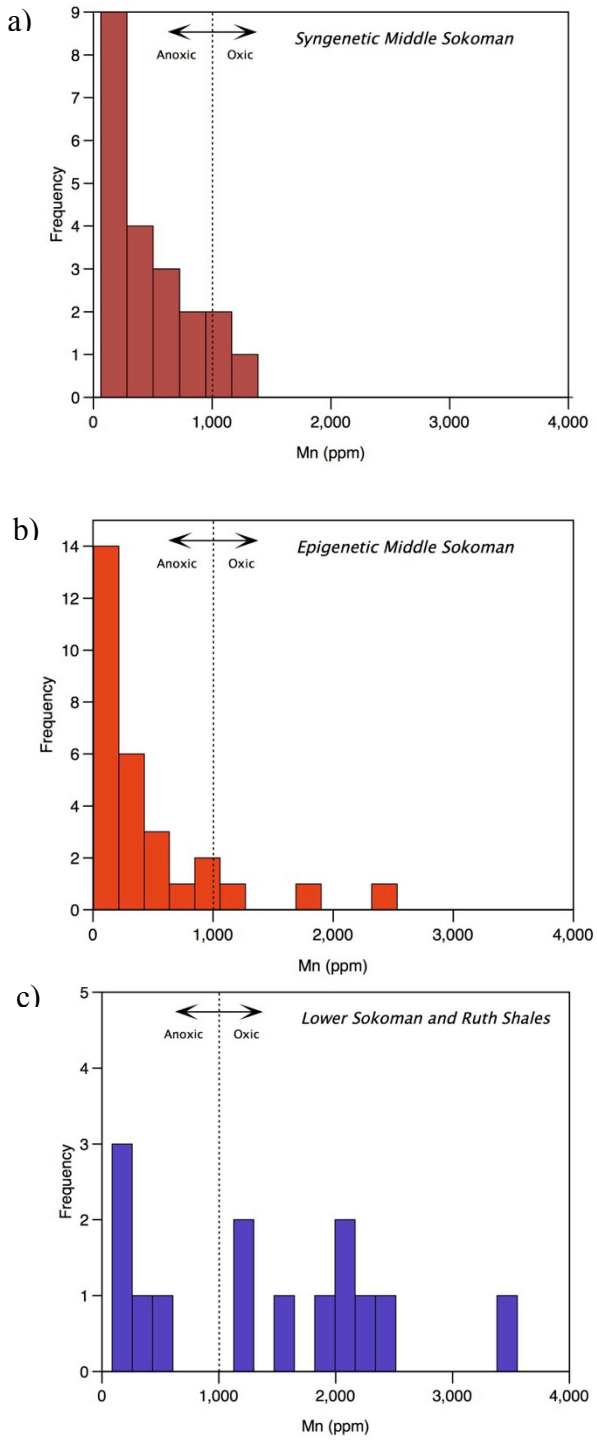

Figure 3.8. Plots of redox sensitive elements. Histograms of Mn for (a) syngenetic Middle Sokoman Formation, (b) epigenetic Middle Sokoman Formation, and (c) Lower Sokoman and Ruth formations. A value of 1000 ppm Mn is inferred as a boundary between oxic and anoxic fields (see Calvert and Pederson, 1993, 1996).

Chapter 4- Discussion

4.1 Textural Evidence for Syngenetic to Diagenetic Iron Remobilization

Textures and facies relationships in the Snelgrove Lake samples suggest multiple stages of iron remobilization (Figs. 4.1-4.2 a). The relationships of iron minerals and quartz suggest that most iron remobilization occurred during diagenesis (Fig. 2.9). Syngenetic iron is prevalent in many samples with iron tracing fine sedimentary textures, indicating that despite minor martitisation and physical remobilization by debris flows, it has remained relatively unmodified since original precipitation.

Fe-rich lithofacies contain abundant coarse-grained microplaty hematite. The microplaty hematite grains coalesce into iron-rich lenticular bodies that exist within Fe-poor syngenetic facies (Fig 4.1 a). The richer iron formations commonly contain veins of microplaty hematite (Figs. 2.7 e, h), suggesting iron remobilization and local enrichment via a diagenetic veinlet network. In some areas original bedding is partially to completely replaced by microplaty hematite (Fig. 2.7 d) and most Fe-rich lithofacies are roughly semi-conformable to conformable to stratigraphy (Fig. 4.2 a). The local enrichment in iron within these beds is strongly influenced by the presence or absence of jasper/quartz. For example, Fe-poor zones contain only syngenetic iron with jasper and fine hematite dust, and the pore spaces between ooliths/peloids are mostly free of iron minerals (Fig. 4.2 b). In contrast, zones enriched in iron are dominated by coarser grained microplaty hematite without abundant quartz/jasper. To explain the existence of Fe-poor and Fe-rich zones separated by such well-defined and sharp borders, it is suggested that partial cementation (heterogeneous cementation) was coincident with mobilization of iron by

diagenetic fluids. Cemented regions would have prevented penetration of iron-rich fluids, focusing them in porous regions without siliceous cement (Fig. 4.1b). Heterogeneous cementation has been documented previously in the Sokoman Formation (Simonson, 1987) and is further discussed below (section 4.2).

These types of stratigraphy-related patterns of iron remobilization, and diagenetic control on iron grades are noted in other lithologies within the Labrador Trough (Fig. 4.2 e)(Fryer, 1977; Gross, 2009) and in iron formations in proximity to the Snelgrove Lake area (Fig. 4.2 f). This suggests that the processes responsible for creating diagenetic Fe-remobilization occurred on a regional scale in this part of the Labrador Trough. For instance, similar patterns are described in iron formations from the central part of the Labrador Trough (Fryer, 1977), where samples are divided into two groups of enriched and non-enriched facies based on their type of iron oxides. Particularly, the enriched group is described as being extensively recrystallized and enriched in iron, with relict textures indicating they were originally identical to others that have suffered minor, or no iron migration (Fryer, 1977). These facies are comparable to the syngenetic (non-enriched) and epigenetic (enriched) samples of Snelgrove Lake.

Euhedral crystals of magnetite overgrow all types of iron mentioned above (Fig. 4.3 c), and reticulated magnetite textures that define fabric (Fig. 2.8b) suggest that euhedral magnetite was the last mineral to crystallize (without iron remobilization), and was likely a result of regional metamorphism (Figs. 2.8 b).

4.2 The Importance of Siliceous Cements in Controlling Iron Remobilization

Silica cements were critical diagenetic features in Snelgrove Lake iron formations

and played an important role in creating the various textures and influencing grade and geometry of iron ore. Textural evidence strongly suggests that cements formed early in the diagenetic history of these rocks. For example, cement-filled cracks (Fig. 2.6 e) occur proximal to ooliths that are locally incorporated within the silica-rich cracks themselves. The inclusion of primary sedimentary components within the contents of the cracks is only possible if the cracks were filled whilst the sediment was unconsolidated (Figs. 4.2 c-d). These relationships argue against these cracks being quartz veins, and suggest they are diagenetic features. Additionally, subtle gradational changes in crystal sizes from finer grained at the crack boundary to coarser grained towards the center of larger cracks are thought to represent remnants of chalcedonic textures (e.g., Simonson, 1987). The pristine chalcedonic textures described by Simonson (1987) contain spherulitic fans with zebraic patterns that radiate inwards towards the center of the crack; these are present in iron formations west of Snelgrove Lake where the metamorphic grade is lower.

Cementation within the Snelgrove Lake iron formation is heterogeneous. For example, flattened ooliths (spastoliths) occur directly next to zones with unflattened ooliths (Fig. 2.5 h-2.6 a), implying that cementation only affected the areas with unflattened ooliths prior to compaction, and indicating that differential compaction occurred. The silica cements played an important role in controlling iron grades by preventing the secondary diagenetic remobilization of iron into pore spaces, resulting in dilution of grade in syngenetic iron formation. Cemented regions, acting as rigid material, would also have prevented compaction and upgrading of iron during compaction due to the reduction of pore space in syngenetic iron formation.

4.3 REE Geochemistry, Redox Sensitive Elements and the Deposition of Iron Formations

The great oxygenation event (GOE; ~2.4-2.2 Ga), is presumed to have led to fundamental changes in the oxygen content of the atmosphere and oceans, and is seen as a critical juncture of the planet's evolution (e.g., Bekker et al., 2010; Planavsky et al., 2010; Holland, 2006). Models that attempt to explain the sudden appearance of Superior-type iron formation during the Paleoproterozoic suggest an intimate link with the cycle of oxygen, and thus, these deposits can be utilized to provide insight into oxygen contents of the ocean at the time of their formation (e.g., Bekker et al., 2010). Iron formations within the Kaniapiskau Supergroup were deposited between 2.4-1.8 Ga, an interval of time that includes and succeeds the GOE. The iron formations in the Snelgrove Lake region specifically were deposited at the later stage (~1.85 Ga) of that time span, and thus offer a chance to study the cycle of oxygen after the GOE. They also record the general paleoceanographic conditions of the ocean, in addition to the cycles of other elements, such as Y and REE (e.g., Bau, 1996, 1999; Bau and Alexander, 2006; Bekker et al., 2010; Planavsky et al., 2010).

The REE and HFSE signatures of the MSIF in Snelgrove Lake have variable signatures broadly consistent with a component from upper continental crustal sources (e.g., Figs. 3.5 c- 3.6); however, they have much lower absolute concentrations than other lithologies in Snelgrove Lake. Furthermore, they have REE-Y systematics that are not entirely consistent with generation solely from crustal sources (e.g., $Ce/Ce^* < 1$ in some cases; $Y/Ho > 27$), indicative of REE-Y scavenging from the seawater at the time of

formation (e.g., Bau, 1999). As a result, the REE-Y systematics, amongst other elements, can provide insight into the ocean redox conditions of iron formation deposition in the Snelgrove Lake area.

The REE-Y signatures of MSIF samples of the Snelgrove Lake area are similar to other global late Paleoproterozoic iron formations. In particular, they have wide ranges of light to heavy REE patterns and mostly positive Ce anomalies; however, Snelgrove Lake iron formations tend to have lower Y/Ho ratios, between 20-37, compared to other Paleoproterozoic iron formations. Planavsky et al. (2010) showed that late Paleoproterozoic iron formations have wide ranges of light to heavy REE ratios and absolute concentrations, compared to early Proterozoic and Archean iron formations, with positive Ce anomalies and Y/Ho ≈ 20-50. In contrast, early Proterozoic and Archean iron formations have higher and more restricted ranges of Y/Ho ratios from 30-50, and no positive Ce anomalies.

Variations in REE-Y signatures (Figs. 3.5, 3.7a) of the MSIF samples, and other Paleoproterozoic iron formations, likely reflect deposition in a redox-stratified ocean in proximity to a chemocline. These variable REE-Y behavior, and temporal variations from Archean through late Paleoproterozoic, reflect a change in Fe-Mn oxyhydroxide behavior in the ocean, particularly the dissolution and reprecipitation of these particles due to the presence of a strong chemocline (oxic-anoxic boundary in the ocean)(Planavsky et al., 2010). The REE-Y concentrations vary as a result of their sensitivity to being adsorbed on Fe-Mn oxyhydroxide. For example, LREE concentrations in ocean water are known to decrease due to preferential removal on Fe-Mn oxides/oxyhydroxides in oxic environments, whereas an increase occurs in anoxic

environments from the reductive dissolution of Fe-Mn particles (German et al., 1991; Byrne and Sholkovitz, 1996). Y/Ho ratios are also affected since Y is less particle-reactive than its geochemical analog Ho, and due to removal of Ho in oxic environments, Y/Ho ratios increase, whereas the opposite occurs in anoxic environments (Bau, 1996). The most parsimonious explanation for the differences in REE-Y trends from Archean to late Paleoproterozoic iron formations is a change in redox conditions of sedimentary basins related to the appearance of atmospheric oxygen after 2.4 Ga (e.g., Bekker et al., 2004; Planavsky et al. 2010).

The assertion that the MSIF were deposited at a redox boundary is further supported by redox-sensitive trace element data. There is very little difference between samples that are syngenetic or diagenetic (e.g., Fig. 3.6-3.8), but given the potential for element changes during diagenesis, the syngenetic iron formations are the best proxies for basin redox conditions. Using primarily U/Th, Mn, and Ce/Ce* values, the bounding units of the MSIF (i.e., the Ruth Shales and Lower Sokomon Formation), have values suggesting deposition under more oxic conditions. In contrast, the syngenetic MSIF samples have values indicating more reducing conditions. The stratigraphic coincidence of both oxic and anoxic signatures in the sedimentary rocks add support to the notion that the MSIF was deposited at a chemocline between anoxic and oxic conditions. Furthermore, if correct, the anoxic signatures of the MSIF questions the validity of traditional models that support non-biological Fe-oxidation by free oxygen (Cloud, 1973), while reinforcing more recent models that invoke a combination of metabolic microbial Fe oxidation (direct biological oxidation) in suboxic and anoxic conditions and non-biological oxidation of Fe at a redox interface (e.g., Planavsky, et al. 2010; Bekker et al.,

2010). However, if the traditional model of oxidation of ferrous iron by free oxygen is invoked, then the redox data might be interpreted otherwise. It is possible that the removal of oxygen by the oxidation of iron might deplete oxygen levels within the ocean enough to produce anoxia and be recorded within the iron formation.

Lastly, oolithic facies present within the MSIF are indicative of deposition within shallow, active waters, whereas clay-rich facies within the bounding units to the MSIF suggest deposition within less energetic waters. In a non-biological Fe-oxidation model requiring free oxygen, the oxic layer within a stratified ocean would be located nearer the surface compared to the anoxic layer (Poulton et al., 2010), making the redox data for these lithologies seem paradoxical since it suggests the bounding units (deeper water) were deposited in more oxic waters relative to the MSIF (shallow water). This could perhaps be explained by the existence of a shifting chemocline within an ocean that varied in depth over time. However, it could also lend support to the hypothesis stated above, that the anoxic signatures of the MISF are a reflection of the lowering of oxygen levels within the surface layer of the ocean, due to the removal of oxygen by the oxidation of iron.

4.4 Current Models of Secondary Enrichment of Iron Formations

A key to the generation of iron ore (>50-70%Fe) is the upgrading of banded iron formation to higher grades via secondary processes. Existing models for the secondary enrichment include two main models: 1) supergene and 2) hydrothermal. Supergene enrichment can be further subdivided into ancient supergene, modern supergene and supergene modified hydrothermal (e.g., Beukes et al., 2003).

Supergene enrichment involves the removal of silica and thus the proportional increase of iron, and has resulted in many of the largest deposits in the world (e.g., Beukes et al., 2003; Gutzmer et al., 2008). Supergene deposits that generally formed via the leaching of abundant silica are accompanied by the creation of voids and breccias and the destruction of fine sedimentary textures, with ores that are dominated by hydrous iron oxides (e.g., goethite and limonite). In ancient deposits, the hydrous iron oxides are commonly metamorphosed to hematite and magnetite (Morris, 1985; e.g., Simonson, 2011; Beukes et al., 2003). Morris and Kneeshaw (2011) have also argued for the existence of additional processes leading to Fe-enrichments via mimetic replacement of chert and silicate minerals by Fe in groundwaters, processes that are characterized by the preservation of primary sedimentary textures and the oxidation of magnetite to martite.

The genesis of hydrothermally enriched Fe deposits is less well understood due to the variability of geology and mineralogy of these deposits (e.g., Beukes et al., 2003; Gutzmer et al., 2008). In general, however, they are interpreted to have been enriched either by silica leaching and/or iron addition via hydrothermal fluids (e.g., Gutzmer et al., 2002). Some deposits are structurally controlled, others occur proximal to intrusive rocks, and some deposits were upgraded by metamorphism, suggesting potential roles for structure, magmatism, and metamorphism in Fe-upgrading.

4.5 Comparison of Snelgrove Lake with other Models

The nature of mineralization and facies relationships in Snelgrove Lake do not support a hydrothermal origin for iron enrichment. In particular, the mineralization does not have diagnostic structural control, a spatial association to intrusive rocks, nor does it

have tabular or pipe-like bodies common to hydrothermally-enriched Fe deposits (Beukes et al., 2003). Additionally, pegmatitic textures, a common feature of hydrothermal deposits (Beukes et al., 2003), are mostly absent except for rare occurrences of large bladed hematite crystals. A comparison of major elements (Conliffe, 2014) of taconites, hydrothermally altered iron formations, and supergene direct shipping ore (DSO) from various regions in the Labrador Through with data from Snelgrove Lake is revealing (Fig. 4.4). The hydrothermally altered iron formations are from the Sawyer Lake deposit, where Conliffe (2014) argues for hydrothermally enriched ore by late stage oxidation and post-diagenetic hematite migration. The comparison shows (Fig. 4.4) that mobile elements Mg, Ca, and Na, are present in greater concentrations in Snelgrove Lake iron formations than in supergene DSO and hydrothermally altered ore, and similar concentrations to the Schefferville taconites. The greater concentrations of mobile elements in these rocks essentially translate into minimal leaching of mobile elements compared to supergene DSO and Sawyer Lake-type ore, and contradicts the supergene enrichment, and possibly hydrothermal enrichment models.

In addition to these data, modern supergene enrichment is also precluded given the lack of hydrous ores, dissolution cavities, and/or lateritic crusts, and unconformities (e.g., Neal, 2000; Beukes et al., 2003). The lack of supergene textures, and the fact that most of the primary sedimentary textures are still preserved also argues against modern supergene enrichment. The only areas where hydrous ores exist are proximal to fault zones; however, grades of ores near faults are very poor, implying faults and fault-related fluids were not responsible for local Fe-enrichment. Interestingly, these rocks are more similar to supergene DSO and hydrothermally altered ore in respect to Mg, Ca, and Na

(Fig. 4.4).

The likelihood of ancient pre-metamorphic supergene enrichment is also unlikely, despite the presence of non-hydrous Fe-oxides as the dominant type of Fe-minerals in the Snelgrove Lake iron formations. In particular, the geochemical systematics, including enrichments in LREE and depleted in HREE, due to differential mobilization within the weathering profile (Gutzmer et al., 2008), are notably absent in the Snelgrove Lake samples.

The samples do, however, contain textural evidence to suggest that iron was subjected to remobilization during diagenesis likely via low temperature fluids. Therefore, during diagenesis, Fe-remobilization and a reorganization of Fe-minerals, rather than Fe-enrichment, is the most likely model to explain locally Fe-rich lithofacies in the Snelgrove Lake area.

4.6 An Integrated Iron Remobilization Model

Any model attempting to explain the genesis of iron lithofacies in Snelgrove Lake must account for the heterogeneous growth of coarse-grained hematite and quartz, accompanied by locally remobilized iron, at both the local to regional scale. Diagenetic fluids are clearly an important part of this process and likely have occurred throughout this part of the Labrador Trough (Simonson, 1987). In this section, a model is proposed with two factors that could potentially provide a mechanism for the displacement of fluids and the heterogeneous remobilization and local enrichment of iron.

The model involves the displacement of fluids through a partially cemented iron formation. Due to differential cementation, heterogeneous porosity was created within the

iron formation, with areas not cemented or lithified being conduits for fluids (Fig. 4.1 b), be they external seawater or more likely diagenetic fluids (e.g., dewatering of nearby shales). Differential compaction features within the iron formation (e.g., Simonson, 1987) are consistent with compaction during the early stages of diagenesis, and imply that compaction was already occurring while the sediment was not completely lithified. Significant compaction during early diagenesis also suggests the rapid burial of iron formation. The setting of the Labrador Trough is interpreted to be a foredeep/foreland basin due to the collision of the Superior Craton, and Rae Province/Nain Craton that led to the development of a fold and thrust belt (Hoffman, 1987). Foreland basins are typically parallel to the thrust belt and are created by flexural subsidence of the crust from the weight of the prograding fold and thrust belt (Hoffman, 1987). The flexural subsidence in the foreland basin lead to crustal bulging and uplift on the continent, and eventually to erosion and infilling of the foredeep with sediments. It is likely that in the Snelgrove Lake area and regionally, loading of the foreland basin with the nearly 1000m thick accumulation of the Menihek Formation shales (Wardle, 1979) within the foredeep was the driving force to move fluids within the underlying iron formation.

In addition to compaction, the presence and texture of coarse-grained microplaty hematite crystals suggests that heat may have been involved in their formation during early diagenesis (Morris, 1980). There are abundant mafic volcanic and intrusive rocks in the area, the question is whether or not these rocks were the direct causes of iron enrichment (e.g., skarn-type upgrading), or are just products of the regional geothermal gradient that led to iron remobilization. Given that there is no direct spatial relationship between iron enrichment and specific volcanic or intrusive phases argues against a direct

magmatic role for iron enrichment. However, it is likely that the elevated geothermal gradient present in the basin associated with magmatism may have enhanced fluid circulation (vis a vis a seafloor hydrothermal system) thereby increasing fluid circulation, iron remobilization, and local iron enrichment.

Chapter 5- Conclusion

5.1 Key Conclusions

1. Petrographic observations show that iron occurs in 3 distinct forms: a) primary syngenetic iron consisting of hematite and magnetite; b) coarse-grained enriched microplaty hematite; and 3) euhedral magnetite. Silicate minerals minnesotaite, stilpnomelane and chamosite also occur in the Snelgrove Lake area but are constrained to a minor area.

2. Interpreted Fe-rich lithofacies, or the secondary remobilization of iron minerals, is represented by coarse-grained microplaty hematite occurrences in Snelgrove Lake. They are concentrated into patches that are generally linear and conformable to stratigraphy, and inferred to be the result of the alteration, modification and local enrichment of original bedding. Remobilization of iron is thought to have occurred, at least locally, in fluids through partially porous sediment during diagenesis.

3. The iron formations contain evidence that support the appearance of silica cements during early diagenesis. Heterogeneous cementation is interpreted as having

played an important role in controlling iron ore grades in enriched and un-enriched facies, in addition to defining textures in the iron formation in general.

4. Faulting shows no direct relation to the secondary enrichment of iron in Snelgrove Lake. Hydrous Fe-oxides are different and distinct, and appear exclusively within and in proximity to fault zones. They are interpreted as the result of the alteration of syngenetic iron by later faulting events.

5. The geochemistry of syngenetic iron formation samples, the Ce/Ce* anomalies, manganese values, and U/Th ratios indicate that the Middle Sokoman Formation recorded signatures reflecting relatively anoxic waters compared to the underlying Lower Sokoman Formation and Ruth Shales. This suggests that the basin was likely redox-stratified and that the deposition of iron particles occurred in proximity to the boundary between anoxic and oxic waters.

6. Higher grades of iron are associated with samples that have evidence for remobilization and local enrichment of iron, likely due to normal diagenesis and compaction. Samples with higher grades did not have early quartz cementation during diagenesis.

5.2 Future Work and Recommendations

This thesis has provided much new information on the nature and textures of iron occurrences in the Snelgrove Lake area, and the controls on their genesis. Relying on geochemistry and textures, a case has been made to show that local enrichments occurred during the early history of the iron formation and are likely related to diagenetic alteration. Supergene enrichment and hydrothermal enrichment, in their classic definition,

have largely been dismissed as suitable models to explain the iron remobilization. Although diagenetic alteration likely affected the ore forming process, the precise cause and nature of these processes is not fully understood. Better knowledge of these processes is key to understanding the nature of iron remobilization in Snelgrove Lake, other areas of the Labrador Trough, and globally.

Since fieldwork for the thesis has been completed, the project has been drilled and further evaluated economically. Future studies of the causes of secondary enrichment of iron in the region could benefit from using drill core, but also using data from a larger area outside of Snelgrove Lake.

The sampling performed for geochemistry purposes during this study was completed before the complete identification of different types iron occurrences. Therefore samples could not be cut according to final sampling, and often included many types of iron occurrences within them. In order to get a better grasp on the geochemical nature of iron remobilization, future sampling should be performed with a focus on comparing enriched (microplaty hematite) vs. non-enriched facies (syngenetic iron). This could potentially be undertaken using microanalytical methods (e.g., microprobe and LA-ICP-MS). Precise sampling should facilitate work related to unresolved questions, notably: what was the nature of the remobilizing fluids; what led to the dissolution of iron at the source, and its precipitation in different locations? Oxygen isotopes and fluid inclusion studies may provide fruitful avenues of research to answer the questions above.

Although considerable effort was spent attempting to understand the processes related to secondary enrichment of iron formations during this project, the reason for the sudden increase in iron precipitation within oceans globally during the late

Paleoproterozoic is important, and key to understanding physico-chemical conditions of the oceans during that time. The Labrador Trough should be a key area for addressing these global questions.

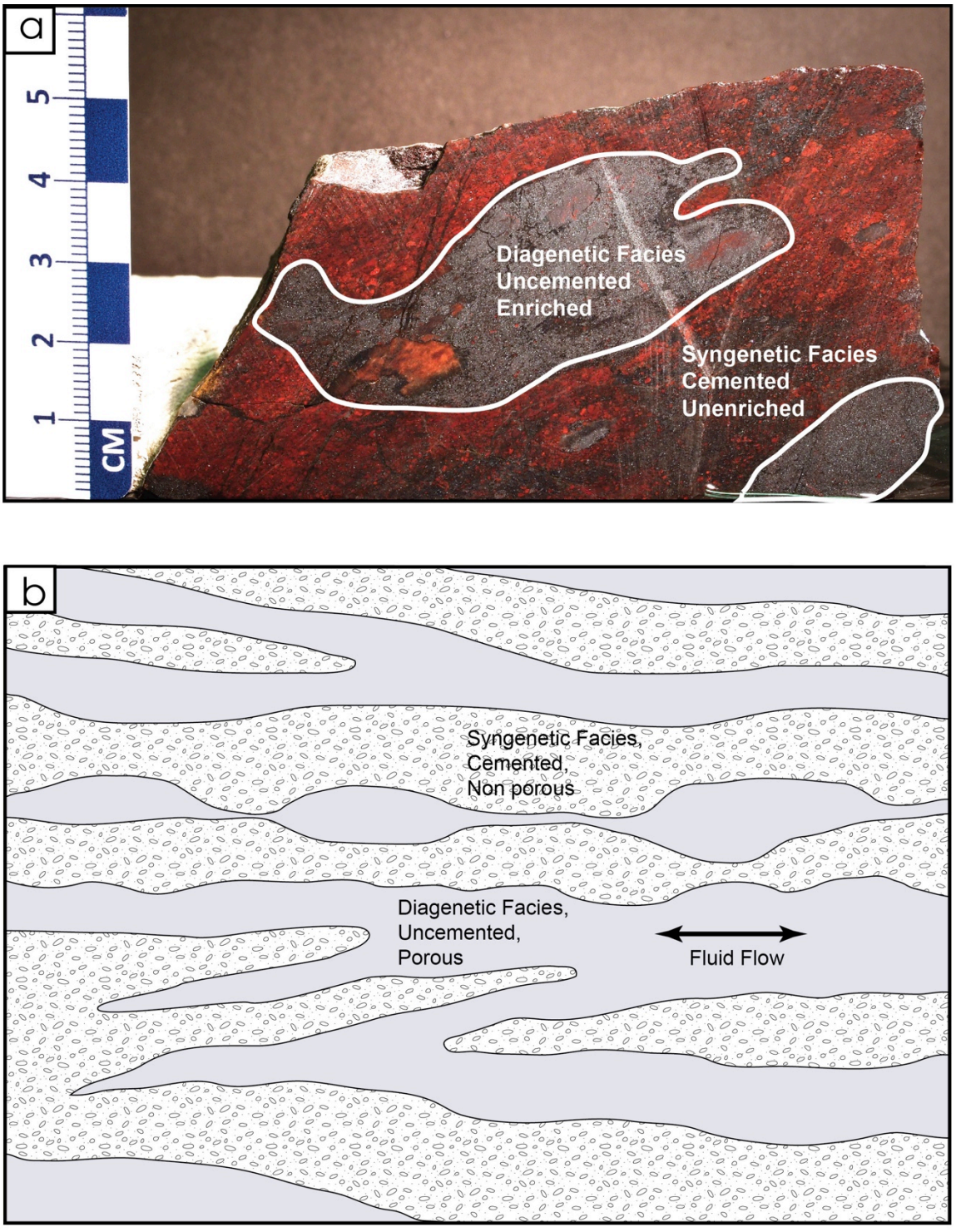

Figure 4.1. Interpretation of diagenetic enrichments of iron by fluids in Snelgrove Lake. (a) Hand sample showing early cemented region of red jaspery syngenetic facies, and uncemented and enriched regions (grey). (b) Facies model of cemented regions of the iron formation preventing fluid flow and the diagenetic enrichment of iron vs. porous, uncemented and diagenetically enriched facies (grey).

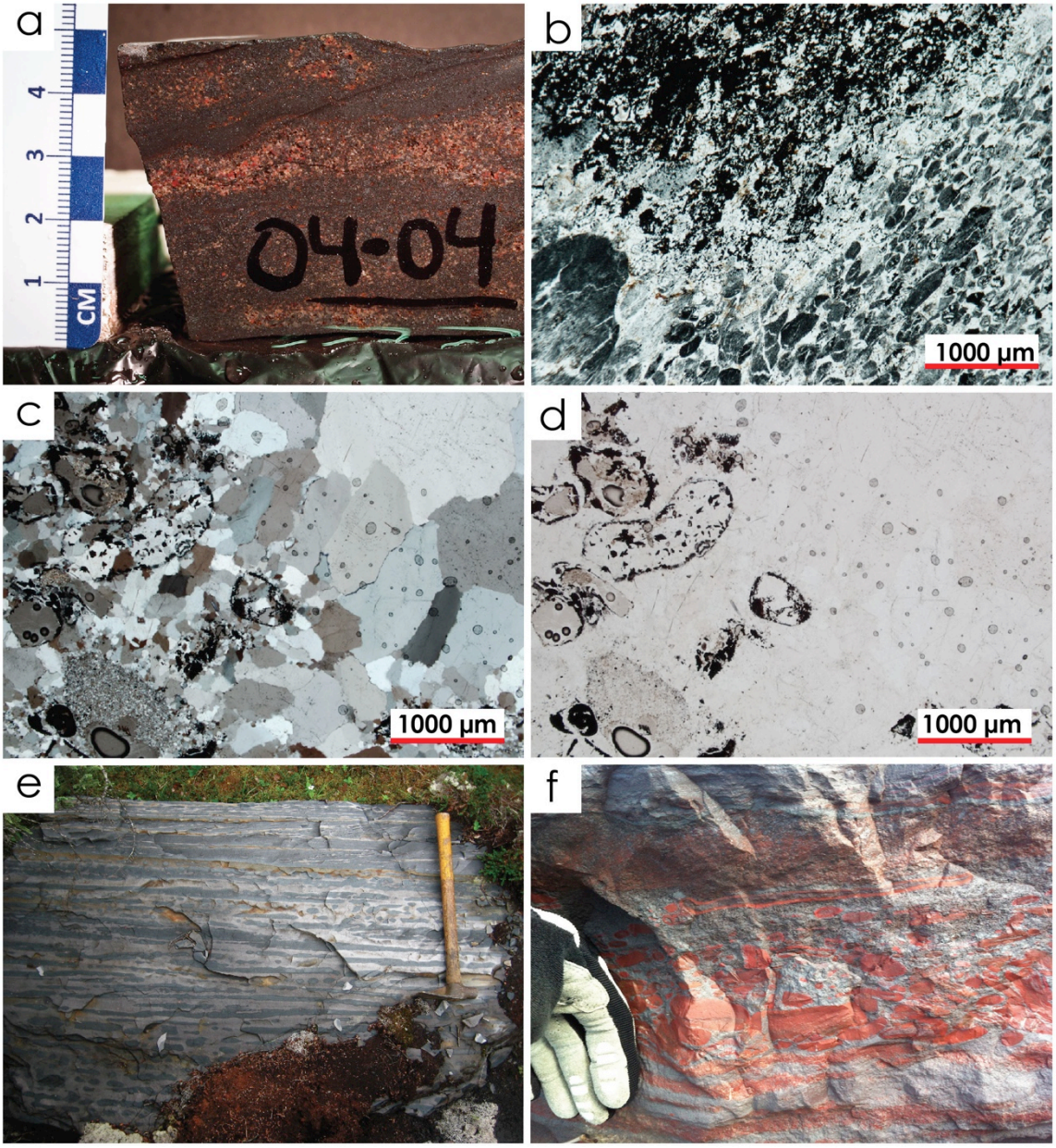

Figure 4.2. (a) Iron oxide rich bands conformable to stratigraphy. (b) Diagenetic microplaty hematite (top) adjacent to syngenetic unenriched facies (bottom). Note the abrupt boundary between the two zones; plane polarized light. (c) Oolith incorporated inside large cement quartz filled crack; crossed-polarized light. (d) Same as (c) in crossed-polarized light. (e) Diagenetic alteration of original bedding in quartzite near Snelgrove Lake. (f) Diagenetic alteration of jasper-hematite bedding from the Schefferville mining district.

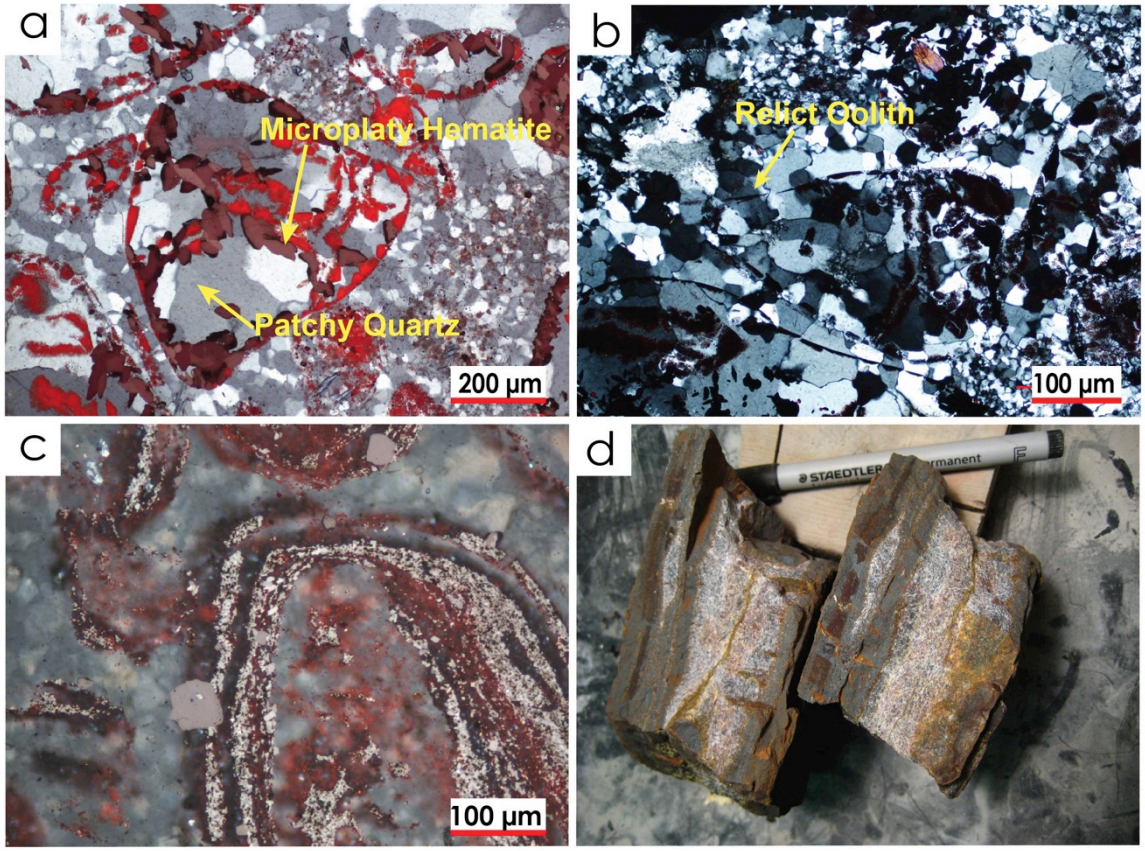

Figure 4.3. (a) Patchy quartz rimmed by microplaty hematite in oolith; crossed-polarized light. (b) Patchy quartz crystals overlapping boundary of relict oolith; crossed-polarized light. (c) Oolith rimmed with syngenetic iron, and crosscut by overgrown magnetite crystals; crossed-polarized light. (d) Fe-rich bands alternating with Fe-poor bands.

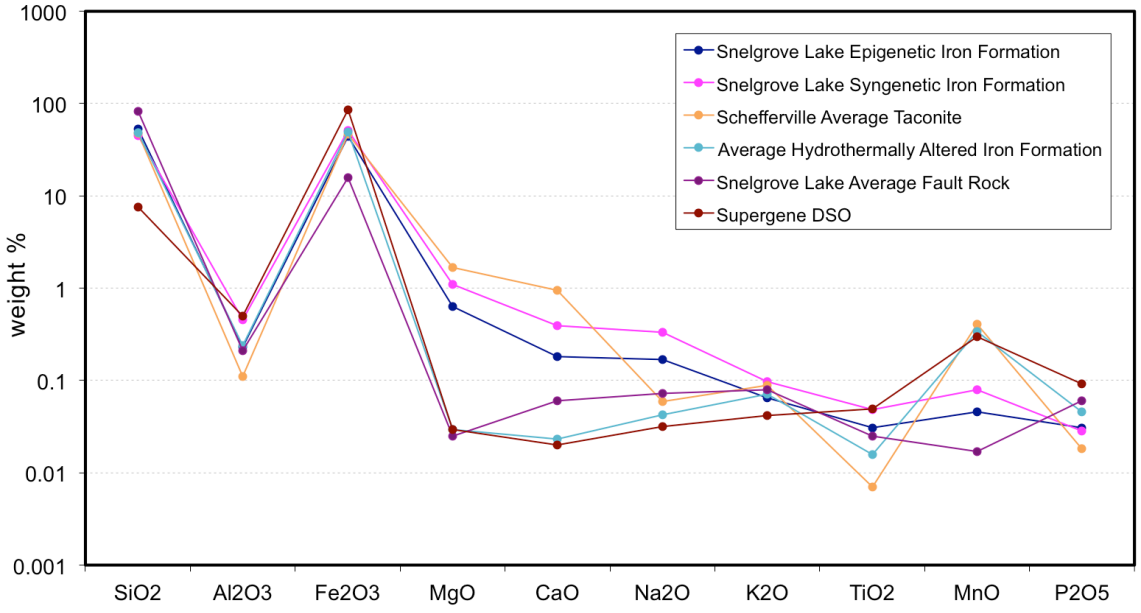

Figure 4.4. Major elements from: Snelgrove Lake epigenetic iron formation, Snelgrove Lake syngenetic iron formation, Schefferville average taconites, average hydrothermally altered iron formation, Snelgrove Lake average fault rock, and supergene DSO (Source: James Conliffe).

Bibliography

Bau, M., Dulski, P. and Möller, P., 1995. Yttrium and holmium in South Pacific seawater: vertical distribution and possible fractionation mechanisms. Chem. Erde, 55: 1-15.

Bau, M., 1996. Controls on the fractionation of isovalent trace elements in magmatic and aqueous systems: evidence from Y/Ho, Zr/Hf, and lanthanide tetrad effect. Contrib. Mineral. Petrol. 123, 323–333.

Bau, M., Dulski, P., 1996b. Distribution of yttrium and rare-earth elements in the Penge and Kuruman iron-formations, Transvaal Supergroup, South Africa. Precambrian Res. 79, 37–55.

Bau M., 1999. Scavenging of dissolved yttrium and rare earths by precipitating Fe oxyhydroxide: experimental evidence for Ce oxidation, Y–Ho fractionation, and lanthanide tetrad effect. Geochim. Cosmochim. Acta 63, 67–77.

Bau M. and Alexander B., 2006. Preservation of primary REE patterns without Ce anomaly during dolomitization of Mid- Paleoproterozoic limestone and the potential re-establishment of marine anoxia immediately after the "Great Oxidation Event". S. Afr. J. Geol. 109, 81–86.

Bekker, A., Holland, H.D., Wang, P. L., Rumble, D., Stein, H.J., Hannah, J.L., Coetzee, L.L., and Beukes, N.J., 2004. Dating the rise of atmospheric oxygen. Nature, v. 427, p. 117−120.

Bekker, A., Slack, J. F., Planavsky, N., Krapež, B., Hofmann, A., Konhauser, K. O., & Rouxel, O. J., 2010. Iron formation: the sedimentary product of a complex interplay among mantle, tectonic, oceanic, and biospheric processes. Economic Geology, 105(3), 467–508.

Beukes, N. J., Gutzmer, J., & Mukhopadhyay, J., 2003. The geology and genesis of high-grade hematite iron ore deposits. Applied Earth Science: IMM Transactions Section B, 112(1), 18–25.

Boström, K., 1973. The origin and fate of ferromanganoan active ridge sediments: Stockholm: Contributions to Geology, v. 27, p. 147–243.

Byrne R. and Sholkovitz E., 1996. Marine chemistry and geochemistry of the lanthanides. In Handbook on the Physics and Chemistry of the Rare Earths (eds. K. A. Gschneider Jr. and L. Eyring). Elsevier, Amsterdam.

Calvert S.E., and Pedersen T.F., 1996. Sedimentary geochemistry of manganese; implications for the environment of formation of manganiferous black shales, Economic Geology, vol. 91, no. 1, pp. 36–47.

Calvert S.E., & Pedersen T.F., 1993. Geochemistry of recent oxic and anoxic sediments: Implications for the geological record: Marine Geology, v. 113, p. 67-88.

Cannon, W.F., 1976. Hard iron ore of the Marquette Range, Michigan. Economic Geology, Vol 71, 1012-1028.

Chauvel, J-J., & Dimroth, E., 1974. Facies types and depositional environment of the Sokoman Iron Formation, Central Labrador Trough, Quebec, Canada: Jour. Sed. Petrology, v. 44, p. 299-327.

de Baar, H.J.W., German, C.R., Elderfield, H., and van Gaans, P., 1988. Rare earth element distributions in anoxic waters of the Cariaco Trench: Geochimica et Cosmochimica Acta, v. 52, p. 1203-1219.

Conliffe, J., 2014. The Sawyer Lake iron-ore deposit, western Labrador: Potential for future high-grade iron-ore deposits in the Labrador Trough. Current Research, Newfoundland and Labrador Department of Natural Resources, Geological Survey, Report 14-1, pages 1-14.

Derry, L.L., and Jacobsen, S.B., 1990. The chemical evolution of Precambrian seawater: Evidence from REEs in banded iron-formations. Geochimica et Cosmochimica Acta, v. 54, p. 2965–2978.

Dimroth, E., 1972. The Labrador geosyncline revisited. American Journal of Science, Vol. 272, p. 487-506.

Dimroth, E., and Chauvel, J-J., 1973. Petrography of the Sokoman Iron Formation in part of the Central Labrador Trough, Quebec, Canada. Geol. Soc. America Bull., v. 84, p. 111-134.

Dufresne, C., 1950. The Sawyer Lake – Snelgrove Lake map area. Unpublished private report, Labrador Mining and Exploration Company Ltd, Montreal.

Elderfield, H., and Greaves, M. J., 1982. The rare earth elements in seawater. Nature (London), v. 296, p. 214-219.

Elderfield, H., Charnock, H., Lovelock, J. E., Liss, P. S., and Whitfield, M., 1988. The oceanic chemistry of the rare-earth elements. Philosophical Transactions of the Royal Society of London, Series A: Mathematical and Physical Sciences, v. 325, p. 105-124.

Evans, J., 1978. Geology and geochemistry of the Nimish Subgroup, Dyke Lake area, Newfoundland and Labrador. Mineral Development Division, Newfoundland Department of Mines and Energy, Report 78-4.

Findlay, J.M., Parrish, R.R., Birkett, T.C. and Watanabe, D.H., 1995. U–Pb ages from the Nimish Formation and Montagnais glomeroporphyritic gabbro of the central New Québec Orogen, Canada. Canadian Journal of Earth Sciences, Volume 32, pages 1208-1220.

Folk, R. L., 1974. Petrology of sedimentary rocks. Austin, Texas, Hemphill Pub. Co., p.182

Frei, R., Dahl, P.S., Duke, E. F., Frei, K. M., Hansen, T. R., Frandsson, M. M. and Jensen, L. A., 2008. Trace element and isotopic characterization of Neoarchean and Paleoproterozoic Fe formations in the Black Hills (South Dakota, USA): assessment of chemical change during 2.9–1.9 Ga deposition bracketing the 2.4–2.2 Ga first rise of atmospheric oxygen. Precambrian Res. 162, 441–474.

Fryer, B. J., 1977. Trace element geochemistry of the Sokoman Iron Formation. Canadian Journal of Earth Sciences, 14(7), 1598–1610.

German C. R., Holliday B. P. and Elderfield H., 1991. Redox cycling of rare earth elements in the suboxic zone of the Black Sea. Geochim. Cosmochim. Acta 55, 3553–3558.

German C. R. and Elderfield H., 1990. Application of the Ce anomaly as a paleoredox indicator: the ground rules. Paleoceanography 5, 823–833.

Goodfellow, W.D., Peter, J.M., Winchester, J.A., and van Staal, C.R., 2003b. Ambient marine environment and sediment provenance during formation of massive sulfide deposits in the Bathurst Mining Camp: Importance of reduced bottom waters to sulfide precipitation and preservation. Economic Geology Monograph 11, p. 129–156.

Gross, G.A., and Zajac, I.S. 1983. Iron-formation in fold belts marginal to the Ungava craton; *in* iron-formation, facts and problems; (ed.) A.F. Trendall and R.C. Morris; Elsevier, Amsterdam-Oxford-New York- Tokyo, p.253-294.

Gross, G.A.:

1965: General geology and evaluation of iron deposits; in Geology of Iron Deposits in Canada, Economic Geology Report 22, Vol. I, Geological Survey of Canada, 181.

1968b: Iron Ranges of the Labrador Geosyncline; in Geology of iron deposits in Canada; Economic Geology Report 22, Vol. I, Geological Survey of Canada, 179p.

1973: The depositional environment of principal types of Precambrian iron-formation; in genesis of Precambrian iron and manganese deposits; Proceedings of Kiev Symposium, 1970, UNESCO Earth Sciences 9, Paris. p.15-21.

1983a: Tectonic systems and the deposition of iron-formation; Precambrian Research, v.20, p.171- 187.

2009: Iron formation in canada, genesis and geochemistry, Geological Survey of Canada, open file 5987.

Grunsky, E. C., 2010. The interpretation of geochemical survey data. Geochemistry-Exploration Environment Analysis, 10 (1), 27–74.

Gutzmer, J., Chisonga, B. C., Beukes, N. J., and Mukhopadhyay, J., 2008. The geochemistry of banded iron formation-hosted high-grade hematite-martite iron ores. Reviews in Economic Geology*,* 15*,* 157–183.

Hoffman, P.F., Early Proterozoic foredeeps, foredeep magmatism, and superior-type iron-formations of the Canadian shield. Precambrian Geology Division, Geological Survey of Canada, Ottawa, Ontario. Proterozoic Lithospheric Evolution, Vol. 17, 85-98.

Holland, H. D., 2005. Sedimentary mineral deposits and the evolution of Earth's near- surface environments. Econ. Geol. 100, 1489–1509.

Holland, H. D., 2006. The oxygenation of the atmosphere and oceans, Philosophical Transactions of the Royal Society B: Biological Sciences, vol. 361, no. 1470, pp. 903–915.

Isley, A.E., and Abbott, D.H., 1999. Plume-related mafic volcanism and the deposition of banded iron formation: Journal of Geophysical Research, v. 104, p. 15,461−15,477.

James, D.T., and Dunning, G.R. 2000. U–Pb geochronological constraints for Paleoproterozoic evolution of the Core Zone, southeastern Churchill Province, northeastern Laurentia. Precambrian Research, 103: 31–54.

Klein, C., 1974. Greenalite, stilpnomelane, minnesotaite, crocidolite and carbonates in a very low-grade metamorphic Precambrian iron formation, Canadian Mineralogist, Vol. 12, 475-498.

Klein, C. and Fink, R.C., 1976. Petrology of the Sokoman Iron Formation in the Howells River area, at the edge of the Labrador Trough. Economic Geology, Vol 71, 453-487.

Klein, C. and Beukes, N.J., 1989. Geochemistry and sedimentology of a facies transition from limestone to iron-formation deposition in the early Proterozoic Transvaal Supergroup, South Africa. Econ. Geol, 84, 1733-1774.

Klein, C., 2005. Some Precambrian banded iron-formations (BIFs) from around the world: Their age, geologic setting, mineralogy, metamorphism, geochemistry, and origins, American Mineralogist, vol. 90, no. 10, pp. 1473–1499, Oct. 2005

Klein, C., Beukes, N.J., 1992. Proterozoic iron-formations. In: Conde, K.C. (Ed.), Proterozoic Crustal Evolution. Developments in Precambrian Geology, vol. 10. Elsevier Science Publishers, Amsterdam, pp. 383–418.

Lesher, C. M., 1978. Mineralogy and petrology of the Sokoman Iron Formation near Ardua Lake, Quebec. Canadian Journal of Earth Science, Vol 15, 480-500.

Louis, A. Derry, and Stein, B. Jacobsen, 1990. The chemical evolution of Precambrian seawater: Evidence from REEs in banded iron formations: Geochimica et Cosmochimica, Acta vol. 54, no. 11, pp. 2965–2977, Jan. 1990.

McLennan, S.M., Hemming, S., McDaniel, D.K., and Hanson, G. N., 1993. Geochemical approaches to sedimentation, provenance, and tectonics: Special Paper Geological Society of America, v. 284, p. 21-40.

McLennan, S.M., Bock, B., Hemming, S.R., Hurowitz, J.A., Lev, S.M., and McDaniel, D.K., 2003. The roles of provenance and sedimentary processes in the geochemistry of sedimentary rocks, *in* Lentz, D. R., ed., Geochemistry of Sediments and Sedimentary Rocks: Evolutionary Considerations to Mineral Deposit-Forming Environments, GEOText 4: St. John's, NL, Canada, Geological Association of Canada, p.7-38.R. C.

Morris, R.C., 1980. A textural and mineralogical study of the relationship of iron ore to banded iron formation in the Hamersley Iron Province of Western Australia. Econ. Geol., 75, 184–209

Morris, R. C., 1985. Genesis of iron ore in banded iron- formation by supergene and supergene-metamorphic processes – a conceptual model'. In (ed. K. H. Wolf) 'Handbook of strata-bound and stratiform ore deposits', Vol. 13, 73–235; 1985, Amsterdam, Elsevier.

Morris, R. C., and Kneeshaw, M., 2011. Genesis modelling for the Hamersley BIF-hosted iron ores of Western Australia: a critical review. Australian Journal of Earth Sciences, 58(5), 417–451.

Morris, R. C., 2012. Microplaty hematite–its varied nature and genesis. Australian Journal of Earth Sciences, 59(3), 411–434.

Neal, H.E., 2000. Iron deposits of the Labrador Trough. Canadian Institute of Mining, 1-9.

Nesbitt, H.W., and Young, G. M., 1984. Prediction of some weathering trends of plutonic and volcanic rocks based on thermodynamic and kinetic considerations: Geochimica et Cosmochimica Acta, v. 48, p. 1523-1534.

Nesbitt, H.W., 2003. Petrogenesis of siliciclastic sediments and sedimentary rocks. In: Lenz, D.R. (ed.), Geochemistry of Sediments and Sedimentary Rocks. Geological Association Canada, Newfoundland, Geotext 4, 39-51.

Nozaki, Y., Zhang, J., Amakawa, H., 1997. The fractionation between Y and Ho in the marine environment. Earth Planet. Sci. Lett. 148, 329–340.

Peter J. M., Kjarsgaard I. M., and Goodfellow W. D., 2003. Hydrothermal sedimentary rocks of the Heath Steele Belt, Bathurst Mining Camp, New Brunswick: Part 1. Mineralogy and mineral chemistry: Geological Survey of Canada, 601 Booth Street, Ottawa, Ontario, Canada, contribution 1999105.

Peter J. M., Kjarsgaard I. M., and Goodfellow W. D., 2003. Hydrothermal sedimentary rocks of the Heath Steele Belt, Bathurst Mining Camp, New Brunswick: Part 2. Bulk and rare earth element geochemistry and implications for origin: Geological Survey of Canada, 601 Booth Street, Ottawa, Ontario, Canada, contribution 1999105.

Peter, J. M., & Goodfellow, W. D., 2003. Hydrothermal sedimentary rocks of the Heath Steele belt, Bathurst mining camp, New Brunswick: part 3. Application of mineralogy and mineral and bulk compositions to massive sulfide exploration. Geological Survey of Canada, contribution 199912.

Planavsky, N., Rouxel, O., Bekker, A., Shapiro, R., Fralick, P., and Knudsen, A., 2009. Iron-oxidizing microbial ecosystems thrived in late Paleoproterozoic redox-stratified oceans: Earth and Planetary Science Letters, v. 286, p. 230−242.

Planavsky, N., Bekker, A., Rouxel, O. J., Kamber, B., Hofmann, A., Knudsen, A., and Lyons, T. W., 2010. Rare Earth Element and yttrium compositions of Archean and Paleoproterozoic Fe formations revisited: New perspectives on the significance and mechanisms of deposition. Geochimica Et Cosmochimica Acta, 74(22), 6387–6405.

Planavsky, N. J., McGoldrick, P., Scott, C. T., Li, C., Reinhard, C. T., Kelly, A. E., et al., 2011. Widespread iron-rich conditions in the mid-Proterozoic ocean. Nature, 1–5.

Poulton, S.W., Fralick, P.W. and Canfield, D.E., 2010. Spatial variability in oceanic redox structure 1.8 billion years ago. Nature Geoscience, 3, 486–490.

Poulton, S.W. and Raiswell, R., 2002. The low- temperature geochemical cycle of iron: From continental fluxes to marine sediment deposition. American Journal of Science 302: 774-805.

Rivers, T., 1997. Lithotectonic elements of the Grenville Province: review and tectonic implications, Precambrian Research 86(3):117.

Seymour, C., Winter, L., O'Driscoll, J., Butler, R., 2009. Renewed exploration in Canada's premier iron ore district – Labrador West. Iron Ore 2009, The Australian Institute of Mining and Metallurgy, Section 2, Chapter 20.

Simonson, B. M., 1987. Early silica cementation and subsequent diagenesis in arenites from four early Proterozoic iron formations of North America. Journal of Sedimentary Research, 57(3).

Slack, J. F., Grenne T., Bekker A., Rouxel O. J., and Lindberg P. A., 2007. Suboxic deep seawater in the late Paleoproterozoic: Evidence from hematitic chert and iron formation related to seafloor-hydrothermal sulfide deposits, central Arizona, USA, Earth and Planetary Science Letters, vol. 255, no. 1, pp. 243–256.

Skulski, T., Robert P. W., and Alan D. S., 1993. Early Proterozoic (1.88–1.87 Ga) tholeiitic magmatism in the New Québec Orogen. Canadian Journal of Earth Sciences, vol. 30, E93-129, 1993.

Stubbins, J.B., Blais, R.A. and Zajac, I.S., 1961. Origin of the soft ores of the Knob Lake Range. Canadian Mining and Metallurgical Bulletin, Volume 585, p. 43-58.

Sverjensky, D.A., 1984. Europium redox equilibria in aqueous solution: Earth and Planetary Science Letters, v. 67, p. 70–78.

Tribovillard, N., Algeo, T. J., Lyons, T., & Riboulleau, A., 2006. Trace metals as paleoredox and paleoproductivity proxies: An update. Chemical Geology, 232(1-2), 12–32.

Tucker, M.E., 2001. Sedimentary Petrology: An introduction to the origin of sedimentary rocks, 3rd edition edition, Blackwell Science Ltd.

Tyson, R.V. and Pearson, T.H., 1991. Modern and ancient continental shelf anoxia: an overview. In: R.V. Tyson and T.H. Pearson (Editors), Modern and Ancient Continental Shelf Anoxia. Geol. Society of London, Special Publication, No. 58, pp. 1-24.

Wardle, R.J., 1979. Geology of the eastern margin of the Labrador Trough, Newfoundland and Labrador. Mineral Development Division, Newfoundland Department of Mines and Energy, Report 78-9.

Wardle, R.J., Wilton, D.H.C., James, D.T., Swinden, S., Kerr, A., Ryan, B., Miller, R.R., Gower C.F., Nunn, G.A.G., 1995. A field workshop on the geology and mineral deposits of Labrador, Memorial University of Newfoundland, internal document.

Wardle, R. J., & Van Kranendonk, M. J., 1996. The Palaeoproterozoic Southeastern Churchill Province of Labrador–Quebec, Canada: orogenic development as a consequence of oblique collision and indentation. Geological Society, London, Special Publications, 112(1), 137–153.

Wardle, R.J., James, D. T., Scott, D. J., & Hall, J., 2002. The southeastern Churchill Province: synthesis of a Paleoproterozoic transpressional orogen. Canadian Journal of Earth Sciences, 39(5), 639–663.

Li, Y.-L, 1991. Distribution patterns of the elements in the ocean: A synthesis., Geochimica Et Cosmochimica Acta 55(11), 3223–3240.

Li, Y.-L., Konhauser, K. O., Kappler, A., and Hao, X.-L., 2013. Experimental low-grade alteration of biogenic magnetite indicates microbial involvement in generation of banded iron formations. Earth and Planetary Science Letters, *361*(C), 229–237.

Zajac, I.S., 1974. The stratigraphy and mineralogy of the Sokoman Formation in the Knob Lake area, Quebec and Newfoundland, Geological Survey of Canada Bulletin 220, v. Bulletin 220, 159 p.

Appendix 1: Petrography

A1. Table of samples included in this study. Information include location, unit, lithology, and lithological description.

Sample	Easting	Northing	Unit	Lithology	Analyses	Thin Section	Lithological descriptions
nl11-01-01	312542	6061842	Lower Sokoman	IF	yes	yes	Dark grey tuffacious magnetite IF, moderately magnetic.
nl11-01-02	312541	6062153	Middle Sokoman	Syngenetic IF	yes	yes	Laminated oolithic quartz-jasper dominated, hematite magnetite IF.
nl11-01-03	313671	6062226	Montagnais Intrusive	Gabbro	yes	yes	Green fine grained gabbro with 1% dessiminated pyrite.
nl11-02-01	315891	6064550	Middle Sokoman	Syngenetic IF	yes	yes	Laminated, oolithic (magnetite) in quartz matrix.
nl11-02-02	315879	6064589	Middle Sokoman	Syngenetic IF	yes	yes	Laminated, oolithic magnetite-iron silicate quartz IF.
nl11-02-03	315818	6064605	Middle Sokoman	Epigenetic IF	yes	yes	Homogeneous hematite-magnetite (70%) quartz jasper IF.
nl11-02-04	315875	6064631	Lower Sokoman	IF	yes	yes	Dark grey massive to weakly laminated tuffaceous fine grained magnetite rich quartz IF.
nl11-02-05	315927	6064685	Lower Sokoman	IF	yes	yes	Dark grey massive to weakly laminated tuffaceous fine grained magnetite-hematite rich quartz IF.
nl11-02-06	315948	6064741	Middle Sokoman	Syngenetic IF	yes	yes	Grey to grey-bluish oolithic hematite-magnetite alternating in inhomogeneous shapes (replacement? with remnant bedding) with jasper-quartz Fe-poor areas.
nl11-02-07	315115	6064584	Menihek	Shale	yes	yes	Limonitic oxidized reddish laminated shale.
nl11-02-08	315118	6064544	Middle Sokoman	Fault Rock IF	yes	yes	Leached? clastic hematite-magnetite alternating in inhomogeneous shapes (replacement? with remnant bedding) with jasper-quartz Fe-poor areas.
nl11-02-09 (a)	315507	6064513	Middle Sokoman	Epigenetic IF	yes	yes	Grey to grey-bluish hematite-magnetite massive bed (5cm) alternating with jasper- quartz Fe-poor band.
nl11-02-09 (b)	315507	6064513	Middle Sokoman	Syngenetic IF	yes	yes	Homogeneous magnetite (dominant)and hematite IF.
nl11-02-10	315475	6064373	Wishart	Sandstone	yes	yes	Fine grained iron silicate rich laminated sandstone.
nl11-02-11	315389	6064293	Wishart	Sandstone	yes	yes	Laminated light grey medium fine to grained quartz sandstone.
nl11-02-12 (a)	315001	6063482	Middle Sokoman	Epigenetic IF	yes	yes	Grey to grey-bluish oolithic hematite-magnetite alternating in inhomogeneous shapes (replacement? with remnant bedding) with jasper-quartz Fe-poor areas.
nl11-02-12 (b)	315001	6063482	Middle Sokoman	Epigenetic IF	yes	yes	Grey to grey-bluish oolithic hematite-magnetite alternating in inhomogeneous shapes (replacement? with remnant bedding) with jasper-quartz Fe-poor areas.
nl11-02-13	314999	6063444	Middle Sokoman	Epigenetic IF	yes	yes	Layered to laminated, patchy magnetite and hematite IF with jasper ooliths. Strongly magnetic and partly oxidized.
nl11-03-01	314996	6063382	Lower Sokoman	IF	yes	yes	Dark grey laminated tuffaceous fine grained magnetite-hematite rich quartz IF.
nl11-03-02	314944	6063287	Lower Sokoman	IF	yes	yes	Dark grey laminated tuffaceous fine grained magnetite-hematite rich quartz IF.
nl11-03-03	314962	6062971	Wishart	Sandstone	yes	yes	Fine to medium grained medium grey weakly laminated quartz sandstone.
nl11-03-05	314489	6062824	Middle Sokoman	Syngenetic IF	yes	yes	Laminated and clastic If containing Jasper clasts (up too 1cm) in a hematite-magnetite quartz matrix.
nl11-03-06	314453	6062840	Middle Sokoman	Syngenetic IF	yes	yes	Laminated and clastic IF containing Jasper clasts (up too 1cm) in a hematite-magnetite quartz matrix.
nl11-03-07	314397	6062875	Middle Sokoman	Epigenetic IF	yes	yes	Homogeneous bluish grey hematite magnetite quartz jasper IF.
nl11-03-08	314385	6062816	Middle Sokoman	Epigenetic IF	yes	yes	Banded to laminated blue magnetite hematite quartz riebeckite IF. Contains bands of quartz jasper rich material alternating with oolithic facies.
nl11-03-09	314303	6062994	Middle Sokoman	Epigenetic IF	yes	yes	Laminated and clastic IF containing jasper or hematite-magnetite clasts (up too 2cm) in a hematite-magnetite quartz matrix. Presence of riebeckite rich laminations.
nl11-03-10	314278	6063079	Middle Sokoman	Epigenetic IF	yes	yes	Grey to grey-bluish hematite-magnetite alternating in bands (1-2cm) with jasper- quartz Fe-poor bands.
nl11-03-11	314219	6063073	Middle Sokoman	Epigenetic IF	yes	yes	Grey to grey-bluish hematite-magnetite alternating in bands (1-2cm) with jasper- quartz Fe-poor bands.
nl11-03-12	314052	6062764	Middle Sokoman	Fault Rock/Proximal	no	no	Leached, mostly quartz and goethite-limonite IF, with 20% 0.5 mm dissolution cavities.
nl11-03-13	314210	6062343	Middle Sokoman	Epigenetic IF	yes	yes	Layered to laminated and patchy magnetite and hematite chert with jasper ooliths. Weak to moderately magnetic and partly limonitic.
nl11-03-14	314169	6062325	Middle Sokoman	Epigenetic IF	yes	yes	Laminated and clastic IF containing jasper or hematite-magnetite clasts (up too 2cm) in a hematite-magnetite quartz matrix. Presence of riebeckite rich laminations.

A1., continued.

Sample	Easting	Northing	Unit	Lithology	Analyses	Thin Section	Lithological descriptions
nl11-03-16	314080	6062107	Wishart	Sandstone	yes	yes	Fine grained grey-green quartz iron silicate sandstone.
nl11-03-17	313869	6062348	Middle Sokoman	Syngenetic IF	yes	yes	Bluish grey, hematite and magnetite rich oolithic IF. Moderately banded (10cm). Weakly magnetic.
nl11-03-18	313882	6062388	Middle Sokoman	Epigenetic IF	yes	yes	Clastic, bluish grey hematite rich IF with clasts from 1- 50 mm, of red jasper or mix of hematite and jasper. Weak limonite.
nl11-03-19	313099	6061709	Wishart	Sandstone	yes	yes	Fine grained grey-green slaty quartz iron silicate sandstone.
nl11-03-20	313111	6061804	Wishart	Sandstone	yes	yes	Fine grained grey massive quartz sandstone.
nl11-03-21	312823	6061995	Ruth Shale	Shale IF	yes	yes	Green slaty magnetite-iron silicate tuffaceous IF. Moderately to strongly magnetic.
nl11-04-01	312561	6062053	Ruth Shale	Shale IF	yes	yes	Laminated green slaty magnetite-iron silicate tuffaceous IF. Moderately to strongly magnetic.
nl11-04-02	312591	6062108	Ruth Shale	Shale IF	yes	yes	Dark grey magnetite-hematite IF. Moderate strongly magnetic.
nl11-04-03	312594	6062156	Middle Sokoman	Epigenetic IF	yes	yes	Banded (2-3 cm) magnetite, hematite and jasper oolithic IF. Alternation of iron rich bands and jasper rich bands. Jasper rich bands are weakly limonitic and appear partly leached.
nl11-04-04	312545	6062183	Middle Sokoman	Epigenetic IF	yes	yes	Banded (2-3 cm) magnetite, hematite and jasper oolithic IF. Alternation of iron and jasper rich bands. Jasper bands are weakly limonitic and appear partly leached from their whiter color.
nl11-04-05	312268	6062240	Middle Sokoman	Fault Rock IF	yes	yes	Leached white and light grey chert/quartzite, with dissolution cavities (1-3mm) occasionally filled with limonite. 2 % of the rock is goethite amygdules.
nl11-04-06	312215	6062116	Middle Sokoman	Epigenetic IF	yes	yes	Banded (2-3 cm) magnetite, hematite and jasper oolithic IF. Alternation of iron and jasper rich bands. Jasper rich bands are weakly limonitic and appear partly leached from their whiter color.
nl11-04-07 (a)	312268	6062072	Middle Sokoman	Epigenetic IF	yes	yes	Laminated magnetite, hematite and jasper oolithic IF. Weakly limonitic with 1% void cavities.
nl11-04-07 (b)	312268	6062072	Middle Sokoman	Syngenetic IF	yes	yes	Laminated magnetite, hematite and jasper oolithic chert. Weakly limonitic with 1% void cavities.
nl11-04-08	312431	6062071	Middle Sokoman	Syngenetic IF	yes	yes	Clastic conglomeratic (clasts ≈ 1- 10 mm) quartz IF with clasts composed of red jasper or mix of hematite and jasper. Weakly limonitic.
nl11-04-09	312449	6062029	Ruth Shale	Shale IF	yes	yes	Laminated green slaty magnetite-iron silicate tuffaceous IF. Moderately to strongly magnetic.
nl11-04-11	313416	6059544	Middle Sokoman	Epigenetic IF	yes	yes	Grey to grey-bluish hematite-magnetite alternating (1-2cm) with jasper- quartz in both bands and as inhomogeneous shapes (replacement? Remnant bedding).
nl11-04-12	313403	6059537	Middle Sokoman	Epigenetic IF	yes	yes	Grey to grey-bluish hematite-magnetite 20% alternating in inhomogeneous shapes (replacement? with remnant bedding) with jasper-quartz Fe-poor areas.
nl11-04-13	313485	6059586	Middle Sokoman	Epigenetic IF	yes	yes	Grey to grey-bluish hematite-magnetite alternating (1-2cm) with jasper- quartz in both bands and as inhomogeneous shapes (replacement? Remnant bedding).
nl11-04-14	313512	6059682	Middle Sokoman	Epigenetic IF	yes	yes	Grey to grey-bluish hematite-magnetite (90%) alternating in inhomogeneous shapes (replacement? with remnant bedding) with jasper-quartz Fe-poor areas.
nl11-04-15	313477	6059697	Middle Sokoman	Epigenetic IF	yes	yes	Banded (2-3 cm) magnetite, hematite and jasper oolithic IF. Alternation of iron and jasper rich bands. Jasper rich bands appear partly leached. Weakly magnetic.
nl11-04-16	313564	6059542	Middle Sokoman	Syngenetic IF	yes	yes	Bluish-grey hematite rich IF (65%) containing jasper-rich remnant beddings.
nl11-04-17	313620	6059501	Middle Sokoman	Syngenetic IF	yes	yes	Homogeneous oolithic hematite- magnetite jasper quartz IF.
nl11-04-18	313784	6059398	Lower Sokoman	IF	yes	yes	Dark grey massive tuffaceous fine grained magnetite-hematite rich quartz IF.
nl11-05-02	314256	6058363	Upper Sokoman ?	Silicate IF	yes	yes	Iron silicate-magnetite and quartz IF.
nl11-05-03	314139	6058249	Upper Sokoman ?	Silicate IF	yes	yes	Iron silicate-magnetite and quartz IF.
nl11-05-04	314444	6058398	Upper Sokoman ?	Silicate IF	yes	no	Iron silicate-magnetite and quartz IF.
nl11-05-05	314432	6058442	Upper Sokoman ?	Silicate IF	yes	yes	Iron silicate-magnetite and quartz IF (limonitic).
nl11-05-08	314305	6058616	Upper Sokoman ?	Silicate IF	yes	yes	Iron silicate-magnetite and quartz IF.
nl11-05-09	314485	6058775	Upper Sokoman ?	Silicate IF	yes	yes	Oolithic iron silicate-magnetite and quartz IF.

A1., continued.

Sample	Easting	Northing	Unit	Lithology	Analyses	Thin Section	Lithological descriptions
nl11-05-10	313961	6059108	Montagnais Intrusive	Gabbro	yes	yes	Green fine grained gabbro with 1% disseminated pyrite.
nl11-05-11	313891	6059198	Montagnais Intrusive	Gabbro	yes	yes	Green fine grained gabbro with 1% disseminated pyrite.
nl11-05-12	313780	6059337	Lower Sokoman	IF	yes	yes	Dark grey laminated and oolithic tuffaceous fine grained magnetite-hematite rich quartz IF.
nl11-05-13	313741	6059418	Middle Sokoman	Syngenetic IF	yes	yes	Laminated, oolithic (magnetite) in quartz matrix.
nl11-05-14	313681	6059396	Middle Sokoman	Syngenetic IF	yes	yes	Grey to grey-bluish hematite-magnetite alternating in bands (1-2cm) with jasper- quartz Fe-poor bands.
nl11-05-15	313658	6059387	Middle Sokoman	Syngenetic IF	yes	yes	Grey to grey-bluish hematite-magnetite alternating in inhomogeneous shapes (replacement? with remnant bedding) with jasper-quartz Fe-poor areas.
nl11-05-16 (a)	313478	6059466	Middle Sokoman	Syngenetic IF	yes	yes	Clastic, grey to grey-bluish hematite-magnetite alternating in inhomogeneous shapes (replacement? with remnant bedding) with jasper-quartz Fe-poor areas. Part of sample has iron silicate filled tension gashes.
nl11-05-16 (b)	313478	6059466	Middle Sokoman	Epigenetic IF	yes	yes	Homogeneous jasperous oolithic with mixed jasper, hematite quartz matrix.
nl11-05-17	313401	6059498	Middle Sokoman	Epigenetic IF	yes	yes	Grey to grey-bluish hematite-magnetite alternating in inhomogeneous shapes (replacement? with remnant bedding) with jasper-quartz Fe-poor areas.
nl11-05-18a	313366	6059542	Middle Sokoman	Syngenetic IF	yes	yes	Homogeneous jasperous oolithic with mixed jasper, hematite and quartz matrix.
nl11-05-18b	313366	6059542	Middle Sokoman	Syngenetic IF	yes	yes	Homogeneous jasperous oolithic with mixed jasper, hematite, magnetite and quartz matrix.
nl11-06-01	312448	6060723	Wishart	Sandstone	no	no	Medium grained light grey weakly laminated quartz sandstone.
nl11-06-02	312347	6060894	Middle Sokoman	Syngenetic IF	yes	yes	Grey to grey-bluish hematite-magnetite alternating in bands (1-2cm) with jasper- quartz Fe-poor bands. Presence of white-quartz bands resembling leaching?
nl11-06-03	312195	6060572	Wishart	Sandstone	yes	yes	Grey, fine grained weakly schistose quartz sandstone.
nl11-06-04	312162	6060556	Wishart	Sandstone	yes	yes	Medium grained, light to medium grey-greenish quartz iron silicate sandstone.
nl11-06-05	311976	6060648	Lower Sokoman	IF	yes	yes	Dark grey laminated tuffaceous fine grained magnetite-hematite iron silicate quartz IF.
nl11-06-06	311915	6060701	Middle Sokoman	Epigenetic IF	yes	yes	Grey to grey-bluish hematite-magnetite alternating (1-2cm) with jasper- quartz in both bands and as inhomogeneous shapes (replacement? Remnant bedding).
nl11-06-07	311727	6060692	Middle Sokoman	Epigenetic IF	yes	yes	Grey to grey-bluish hematite-magnetite (70%) alternating with lenticular remnant bedding bands of jasper- quartz. 2% dissolution cavities ≈ 2-3 mm.
nl11-06-08	311542	6060793	Menihek	Shale	yes	yes	Limonitic oxidized reddish laminated shale.
nl12-01-01	314281	6062850	Middle Sokoman	Epigenetic IF	no	no	Grey to grey-bluish hematite-magnetite alternating in bands (1-2cm) with jasper- quartz Fe-poor bands.
nl12-01-02	314048	6062787	Middle Sokoman	Fault Rock/Proximal	no	no	Grey to grey-bluish hematite-magnetite alternating in inhomogeneous shapes (replacement? with remnant bedding) with jasper-quartz Fe-poor areas.
nl12-01-03	314048	6062787	Middle Sokoman	Fault Rock/Proximal	no	no	Leached white and light grey chert/quartzite and iron silicates, with dissolution cavities (1-3mm) occasionally filled with limonite.
nl12-01-04	314068	6062746	Middle Sokoman	Fault Rock/Proximal	no	no	Leached white and light grey chert/quartzite and iron silicates, with dissolution cavities (1-3mm) occasionally filled with limonite.
nl12-01-05	313965	6062359	Middle Sokoman	Syngenetic IF	no	no	-
nl12-01-06	315422	6064514	Middle Sokoman	Fault Rock/Distal	no	no	-
nl12-01-07	315350	6064520	Middle Sokoman	Fault Rock/Distal	no	no	Heterogeneous leached goethite iron-silicate-quartz IF.
nl12-01-08	315120	6064549	Middle Sokoman	Fault Rock/Distal	no	no	Heterogeneous leached goethite iron-silicate-quartz IF.
nl12-01-09	312268	6062245	Middle Sokoman	Fault Rock/Distal	no	no	Heterogeneous leached goethite iron-silicate-quartz IF.

Appendix 2: Lithogeochemical Data

A2. Bulk rock lithogeochemical data for Snelgrove Lake samples arranged by method of analysis: FUS-XRF = fusion X-ray fluorescence, FUS-MS = fusion inductively coupled mass spectrometer, AR-MS = aqua regia inductively coupled mass spectrometer.

Sample	nl11-01-01	nl11-01-02	nl11-01-03	nl11-02-01	nl11-02-02	nl11-02-03	nl11-02-04	nl11-02-05	nl11-02-06	nl11-02-07	nl11-02-08	nl11-02-09 (a)
Easting	312542	312541	313671	315891	315879	315818	315875	315927	315948	315115	315118	315507
Northing	6061842	6062153	6062226	6064550	6064589	6064605	6064631	6064685	6064741	6064584	6064544	6064513
Unit	Lower Sokoman	Middle Sokoman	Montagnais Intrusive	Middle Sokoman	Middle Sokoman	Middle Sokoman	Lower Sokoman	Lower Sokoman	Middle Sokoman	Menihek	Middle Sokoman	Middle Sokoman
FUS-XRF (wt %)												
SiO2	45.69	46.6	47.2	51.15	41.38	44.14	38.46	45.48	51.95	57.55	74.03	75.63
Al2O3	4.83	0.05	14.84	0.31	0.09	0.13	4.76	3.14	0.21	8.6	0.32	0.2
Fe2O3(T)	43.33	51.92	13.93	49.23	59.03	54.3	49.26	43.1	44.33	25.66	23.75	23
MnO	0.011	0.013	0.185	0.016	0.066	0.01	0.205	0.269	0.051	0.035	0.014	0.014
MgO	0.69	0.07	5.47	0.3	0.11	0.96	1.63	1.7	2.11	1.56	0.02	0.03
CaO	0.06	0.26	5.35	0.23	0.03	0.15	0.28	0.48	0.29	0.05	0.1	0.04
Na2O	0.1	0.07	2.21	0.16	0.05	0.12	1.65	0.62	0.17	0.04	0.14	0.35
K2O	3.95	0.04	2.06	0.11	0.03	0.04	2.52	1.97	0.1	0.08	0.13	0.04
TiO2	0.7	0.03	1.24	0.05	0.03	0.03	0.62	0.37	0.03	0.46	0.03	0.02
P2O5	0.11	0.03	0.3	0.04	0.03	0.04	0.11	0.14	0.01	0.07	0.04	0.03
Cr2O3	0.01	0.01	0.01	< 0.01	0.01	< 0.01	0.01	0.01	< 0.01	0.01	0.01	< 0.01
V2O5	0.013	< 0.003	0.046	< 0.003	< 0.003	< 0.003	0.011	0.007	< 0.003	0.026	< 0.003	< 0.003
LOI	0.27	0.18	7.77	-0.83	-0.75	0.33	0.65	2.26	0.8	5.31	1.01	0.65
Total	99.76	99.28	100.6	100.8	100.1	100.3	100.2	99.54	100.1	99.45	99.6	100
FUS-MS (ppm)												
V	78	6	330	9	15	10	45	36	6	165	< 5	6
Cr	40	< 20	60	< 20	< 20	< 20	30	20	< 20	70	< 20	< 20
Co	15	2	60	2	8	3	13	11	2	4	7	2
Ni	< 20	< 20	100	< 20	< 20	< 20	< 20	< 20	< 20	< 20	< 20	< 20
Cu	< 10	< 10	80	< 10	< 10	< 10	10	< 10	< 10	10	< 10	< 10
Zn	50	< 30	130	< 30	< 30	< 30	40	< 30	< 30	60	< 30	< 30
Ga	8	< 1	20	1	1	< 1	9	5	< 1	14	< 1	1
Ge	10.5	5.4	2.2	9.5	6.7	9.9	9.7	8.1	8.6	8.9	4.7	6.5
As	8	18	51	6	10	13	< 5	7	13	23	< 5	6
Rb	117	< 1	47	2	3	< 1	59	49	1	1	< 1	< 1
Sr	18	15	251	14	< 2	12	19	17	12	20	5	< 2
Y	8.1	2.5	22.8	2.6	4.7	3.2	8.6	7.5	1.9	9.8	1.2	1
Zr	82	4	105	4	5	3	60	45	< 1	133	1	2
Nb	16.9	2.3	8.5	1.8	0.9	1.7	12.4	8.5	0.6	22.7	0.4	1
Mo	< 2	< 2	< 2	< 2	< 2	< 2	< 2	< 2	< 2	< 2	< 2	< 2
Ag	< 0.5	< 0.5	< 0.5	< 0.5	< 0.5	< 0.5	< 0.5	< 0.5	< 0.5	< 0.5	< 0.5	< 0.5
In	< 0.1	< 0.1	< 0.1	< 0.1	< 0.1	< 0.1	< 0.1	< 0.1	< 0.1	< 0.1	< 0.1	< 0.1
Sn	1	< 1	1	< 1	< 1	< 1	< 1	< 1	< 1	1	< 1	< 1
Sb	< 0.2	0.3	0.4	< 0.2	< 0.2	< 0.2	< 0.2	< 0.2	< 0.2	1.2	< 0.2	< 0.2
Cs	3	< 0.1	0.6	0.1	0.4	< 0.1	0.7	0.7	< 0.1	0.1	< 0.1	< 0.1
Ba	328	9	630	11	14	16	228	166	6	23	< 3	6
La	13.8	10.1	20.2	6.57	3.72	4.69	12.5	11.9	2.29	11.6	1.98	1.91
Ce	28.6	21.5	45.3	14.5	10	10.9	26.2	24.9	5.05	24.6	4.78	3.47
Pr	3.44	2.54	5.87	1.74	0.77	1.29	3.15	2.91	0.61	2.73	0.56	0.4
Nd	11.9	9.13	25.5	6.17	2.91	4.77	11.6	10.6	2.14	10.5	2.02	1.31
Sm	2.03	1.26	5.42	0.8	0.53	0.73	2.06	1.81	0.33	2.05	0.3	0.18
Eu	0.514	0.319	1.52	0.242	0.189	0.23	0.615	0.504	0.099	0.443	0.095	0.054
Gd	1.6	0.79	4.74	0.61	0.68	0.57	1.83	1.53	0.28	1.74	0.29	0.19
Tb	0.24	0.1	0.77	0.08	0.11	0.08	0.28	0.23	0.05	0.3	0.05	0.04
Dy	1.53	0.51	4.23	0.45	0.73	0.53	1.58	1.34	0.3	1.8	0.22	0.21
Ho	0.32	0.09	0.83	0.09	0.18	0.11	0.31	0.26	0.06	0.37	0.04	0.04
Er	0.98	0.24	2.37	0.24	0.52	0.31	0.9	0.75	0.18	1.1	0.11	0.13
Tm	0.155	0.035	0.342	0.033	0.076	0.042	0.13	0.105	0.026	0.168	0.015	0.019
Yb	1.02	0.19	2.25	0.2	0.51	0.25	0.82	0.65	0.16	1.09	0.1	0.12
Lu	0.154	0.027	0.359	0.031	0.08	0.036	0.13	0.102	0.024	0.173	0.016	0.02
Hf	1.8	< 0.1	2.6	< 0.1	< 0.1	< 0.1	1.4	1.1	< 0.1	3	< 0.1	< 0.1
Ta	0.88	< 0.01	0.49	< 0.01	< 0.01	< 0.01	0.68	0.47	< 0.01	1.81	< 0.01	0.01
W	0.7	1	< 0.5	< 0.5	0.6	0.8	< 0.5	0.6	1.3	< 0.5	0.8	0.8
Tl	< 0.05	< 0.05	0.21	< 0.05	< 0.05	< 0.05	< 0.05	< 0.05	< 0.05	< 0.05	< 0.05	< 0.05
Pb	< 5	< 5	6	< 5	< 5	< 5	< 5	< 5	< 5	6	< 5	< 5
Bi	< 0.1	< 0.1	< 0.1	< 0.1	< 0.1	< 0.1	< 0.1	< 0.1	< 0.1	< 0.1	< 0.1	< 0.1
Th	1.29	0.59	1.1	0.45	0.07	0.34	1.1	0.84	0.16	7.51	0.17	0.11
U	0.23	0.03	0.25	0.03	0.06	0.03	0.24	0.19	0.04	2.87	0.13	0.05
AR-MS (ppm)												
Li	13.1	1.8	42.1	2.9	4	1.6	22.8	13.6	2.3	20.2	0.3	0.5
Be	0.9	1.1	0.6	0.8	2.8	1	1.1	1.1	0.9	1.3	0.5	0.4
Na	0.03	0.03	0.04	0.04	0.03	0.04	0.09	0.05	0.02	0.02	0.03	0.02
Mg	0.41	0.07	3.07	0.19	0.09	0.36	0.74	1.09	0.77	0.98	0.03	0.02
Al	0.48	0.06	3.99	0.12	0.09	0.07	0.33	0.25	0.05	3.82	0.05	0.06
K	0.43	0.02	0.25	0.03	0.02	0.02	0.31	0.26	0.02	0.02	0.01	0.01
Bi	< 0.02	0.11	0.03	0.04	0.04	0.05	0.04	< 0.02	0.04	0.12	0.03	< 0.02
Ca	0.04	0.16	3.57	0.13	0.02	0.12	0.2	0.33	0.19	0.03	0.04	0.02

A2., continued.

Sample	nl11-01-01	nl11-01-02	nl11-01-03	nl11-02-01	nl11-02-02	nl11-02-03	nl11-02-04	nl11-02-05	nl11-02-06	nl11-02-07	nl11-02-08	nl11-02-09 (a)
Easting	312542	312541	313671	315891	315879	315818	315875	315927	315948	315115	315118	315507
Northing	6061842	6062153	6062226	6064550	6064589	6064605	6064631	6064685	6064741	6064584	6064544	6064513
Unit	Lower Sokoman	Middle Sokoman	Montagnais Intrusive	Middle Sokoman	Middle Sokoman	Middle Sokoman	Lower Sokoman	Lower Sokoman	Middle Sokoman	Menihek	Middle Sokoman	Middle Sokoman
AR-MS (ppm)												
Sc	6.8	0.5	14.1	0.3	0.6	0.3	0.5	4.2	< 0.1	6.8	0.1	< 0.1
V	64	8	176	11	20	12	38	39	7	125	7	7
Cr	22.8	7.8	29.6	2.4	5.5	8.5	19.4	14.9	0.9	52.1	10.3	4.4
Mn	125	144	1030	135	613	146	1610	2090	411	213	112	94
Fe	26.5	29.6	8.67	31.7	40	27.8	31.4	27.4	25.9	17	16	15.2
Co	13.5	2.2	51.3	1.8	9	3	13.8	11.8	2.3	4.1	7.8	2
Ni	13.6	2.3	85.6	2.1	2.2	1.9	10.5	7.9	1.4	12.9	1.7	3.1
Cu	2.54	3.82	72	3.91	2.58	1	5.96	7.45	1.59	9.9	0.7	3.01
Zn	27.1	6.4	105	1.3	9.9	3.4	27.2	24.9	< 0.1	49.6	4.7	1.8
Ga	4.1	0.33	13.8	0.69	0.72	0.48	4.18	3.07	0.25	13.4	0.38	0.51
Ge	1.1	1.6	0.3	2.3	1.8	1.7	1	1.1	1.6	1	1.3	1.1
As	2.3	27.4	41.8	7.5	6.8	10.5	0.5	3.3	15	23.2	3	4.4
Se	< 0.1	3.1	0.2	1.4	< 0.1	3.1	< 0.1	< 0.1	0.6	< 0.1	0.5	< 0.1
Rb	55.6	2.3	13.3	3.1	3.6	1.9	34.7	26.7	1.9	1.5	1.1	0.9
Sr	5.2	15.1	150	12.7	2	13.1	17.2	16	10.8	8.5	4.9	2.1
Y	1.67	1.63	12.1	1.31	1.43	1.61	3.62	3.98	0.58	2.95	0.93	0.71
Zr	0.1	< 0.1	< 0.1	< 0.1	< 0.1	< 0.1	0.9	3.5	< 0.1	13.4	< 0.1	< 0.1
Nb	< 0.1	0.2	< 0.1	< 0.1	< 0.1	< 0.1	< 0.1	< 0.1	< 0.1	< 0.1	< 0.1	< 0.1
Mo	0.09	1.98	0.25	0.81	< 0.01	0.54	0.1	< 0.01	0.26	0.57	0.28	1.21
Ag	0.08	1.27	0.42	0.78	0.11	0.69	0.08	0.08	0.53	0.37	0.46	0.06
Cd	< 0.01	< 0.01	0.03	< 0.01	< 0.01	< 0.01	< 0.01	< 0.01	< 0.01	< 0.01	< 0.01	< 0.01
In	0.03	< 0.02	0.04	< 0.02	< 0.02	< 0.02	< 0.02	0.02	< 0.02	0.03	< 0.02	< 0.02
Sn	0.36	0.16	0.44	0.13	< 0.05	0.05	< 0.05	0.14	0.05	0.85	0.08	0.08
Sb	< 0.02	0.6	0.22	0.34	0.08	0.29	< 0.02	< 0.02	0.18	0.32	0.19	0.09
Te	< 0.02	0.61	0.04	0.29	< 0.02	0.5	< 0.02	0.17	0.57	0.06	0.71	< 0.02
Cs	2.14	0.06	0.13	0.12	0.33	0.06	0.61	0.62	0.09	0.07	< 0.02	0.02
Ba	29.5	4.9	47.3	7.2	10.8	7.5	17.8	18.1	2.7	5.1	< 0.5	< 0.5
La	8.9	8.6	18.4	5.8	3.4	4.6	10.9	10.5	2	8.9	1.8	1.6
Ce	18.4	18.1	41.9	11.9	8.68	10.2	22.7	22.7	3.61	19.4	3.73	2.26
Pr	2.2	2.1	5.6	1.4	0.8	1.3	2.7	2.8	0.5	2.2	0.5	0.4
Nd	8.38	7.25	23	5.46	2.83	4.63	10.4	10.3	1.76	8	1.75	1.18
Sm	1.4	1.1	4.1	0.8	0.6	0.7	1.9	1.8	0.3	1.4	0.3	0.2
Eu	0.4	0.3	1.1	0.3	0.2	0.2	0.5	0.5	< 0.1	0.2	< 0.1	< 0.1
Gd	1	0.8	3.7	0.5	0.4	0.5	1.6	1.5	0.2	1	0.3	0.1
Tb	0.1	< 0.1	0.5	< 0.1	< 0.1	< 0.1	0.2	0.2	< 0.1	0.1	< 0.1	< 0.1
Dy	0.58	0.44	2.67	0.35	0.27	0.33	0.91	0.89	0.15	0.67	0.16	0.14
Ho	< 0.1	< 0.1	0.5	< 0.1	< 0.1	< 0.1	0.1	0.1	< 0.1	0.1	< 0.1	< 0.1
Er	0.2	0.2	1.1	0.2	0.1	0.2	0.3	0.3	< 0.1	0.3	< 0.1	< 0.1
Tm	< 0.1	< 0.1	0.2	< 0.1	< 0.1	< 0.1	< 0.1	< 0.1	< 0.1	< 0.1	< 0.1	< 0.1
Yb	0.1	0.1	0.9	0.1	0.1	0.1	0.2	0.2	< 0.1	0.3	< 0.1	< 0.1
Lu	< 0.1	< 0.1	0.1	< 0.1	< 0.1	< 0.1	< 0.1	< 0.1	< 0.1	< 0.1	< 0.1	< 0.1
Hf	< 0.1	< 0.1	< 0.1	< 0.1	< 0.1	< 0.1	< 0.1	< 0.1	< 0.1	< 0.1	< 0.1	< 0.1
Ta	< 0.05	< 0.05	< 0.05	0.21	< 0.05	< 0.05	< 0.05	< 0.05	< 0.05	< 0.05	< 0.05	< 0.05
W	< 0.1	0.6	< 0.1	1.1	< 0.1	< 0.1	< 0.1	< 0.1	0.5	< 0.1	< 0.1	< 0.1
Re	< 0.001	< 0.001	< 0.001	< 0.001	< 0.001	< 0.001	0.01	0.01	0.01	0.01	0.01	< 0.001
Au	< 5	< 5	< 5	< 5	< 5	< 5	< 5	< 5	< 5	< 5	< 5	< 5
Tl	< 0.02	0.13	0.1	0.09	< 0.02	0.08	< 0.02	0.02	0.05	0.06	0.06	< 0.02
Pb	2.82	2.66	4.38	1.19	0.92	0.64	1.64	1.49	0.62	5.13	0.66	0.65
Th	0.8	1.2	0.7	0.8	< 0.1	0.5	0.8	0.7	0.3	4.8	0.2	< 0.1
U	0.1	< 0.1	< 0.1	< 0.1	< 0.1	< 0.1	0.1	0.1	< 0.1	1.4	0.1	< 0.1

A2., continued.

Sample	nl11-02-09 (b)	nl11-02-10	nl11-02-11	nl11-02-12 (a)	nl11-02-12 (b)	nl11-02-13	nl11-03-01	nl11-03-02	nl11-03-03	nl11-03-05	nl11-03-06	nl11-03-07
Easting	315507	315475	315389	315001	315001	314999	314996	314944	314962	314489	314453	314397
Northing	6064513	6064373	6064293	6063482	6063482	6063444	6063382	6063287	6062971	6062824	6062840	6062875
Unit	Middle Sokoman	Wishart	Wishart	Middle Sokoman	Middle Sokoman	Middle Sokoman	Lower Sokoman	Lower Sokoman	Wishart	Middle Sokoman	Middle Sokoman	Middle Sokoman
FUS-XRF (wt %)												
SiO2	33.47	87.83	89.5	49.92	70.45	60.89	50.51	46.1	76.03	47.4	55.42	51.73
Al2O3	0.57	3.73	4.22	0.19	0.43	0.25	2.26	4.96	10.6	0.48	0.38	0.06
Fe2O3(T)	63.95	4.81	1.28	46.29	26.55	36.58	43.74	40.24	4.3	48.25	36.21	45.13
MnO	0.017	0.017	0.011	0.223	0.05	0.115	0.283	0.241	0.016	0.008	0.081	0.063
MgO	0.09	0.75	0.18	0.22	0.43	1.07	0.11	1.01	1.19	2.33	3.48	0.88
CaO	0.13	0.05	0.04	0.62	0.11	0.04	0.19	1.25	0.11	0.1	1.03	1
Na2O	0.08	0.02	0.14	0.06	0.13	0.12	0.3	0.08	0.67	1.09	1.83	0.34
K2O	0.03	1.02	2.76	0.07	0.15	0.06	1.64	3.53	4.47	0.17	0.11	0.03
TiO2	0.06	0.13	0.08	0.02	0.03	0.03	0.24	0.6	0.39	0.05	0.02	0.03
P2O5	0.06	0.02	0.04	0.03	0.04	0.04	0.1	0.11	0.04	0.01	0.02	0.01
Cr2O3	< 0.01	0.01	0.01	< 0.01	0.01	0.01	0.01	0.01	0.01	0.01	< 0.01	0.01
V2O5	< 0.003	< 0.003	< 0.003	0.004	< 0.003	< 0.003	0.005	0.011	0.007	< 0.003	< 0.003	< 0.003
LOI	0.88	1.29	0.49	0.94	0.44	0.2	-0.33	1.22	1.78	-0.43	1.29	1.09
Total	99.34	99.68	98.75	98.59	98.83	99.41	99.06	99.36	99.61	99.47	99.87	100.4
FUS-MS (ppm)												
V	19	20	18	12	9	6	27	54	52	6	5	< 5
Cr	< 20	50	40	< 20	< 20	< 20	20	40	130	< 20	< 20	< 20
Co	2	5	1	7	3	2	7	11	7	1	4	4
Ni	< 20	< 20	< 20	< 20	< 20	< 20	< 20	< 20	< 20	< 20	< 20	< 20
Cu	< 10	10	< 10	< 10	< 10	< 10	< 10	< 10	10	< 10	< 10	< 10
Zn	< 30	50	< 30	< 30	< 30	30	< 30	< 30	50	< 30	< 30	< 30
Ga	2	6	5	< 1	1	1	3	8	14	< 1	< 1	< 1
Ge	8.6	2.9	1.2	8.1	6.1	12.1	6.6	9.3	3	17.8	19	9.3
As	11	< 5	< 5	38	17	5	< 5	5	< 5	< 5	< 5	12
Rb	< 1	19	59	1	1	4	26	83	167	8	< 1	< 1
Sr	13	18	41	9	5	2	15	32	82	3	40	25
Y	2.7	5.2	4.9	2.7	2.2	2.1	6.2	6.8	10.5	4.3	2.7	1.7
Zr	12	118	92	2	4	4	23	52	176	4	1	4
Nb	3.8	1.8	0.8	0.8	0.8	0.6	4.1	9.6	5.1	0.9	1	0.2
Mo	< 2	< 2	< 2	< 2	< 2	< 2	< 2	< 2	< 2	< 2	< 2	< 2
Ag	< 0.5	< 0.5	< 0.5	< 0.5	< 0.5	< 0.5	< 0.5	< 0.5	0.6	< 0.5	< 0.5	< 0.5
In	< 0.1	< 0.1	< 0.1	< 0.1	< 0.1	< 0.1	< 0.1	< 0.1	< 0.1	< 0.1	< 0.1	< 0.1
Sn	< 1	< 1	< 1	< 1	< 1	< 1	< 1	< 1	1	< 1	< 1	< 1
Sb	0.3	< 0.2	< 0.2	0.3	< 0.2	0.2	< 0.2	< 0.2	< 0.2	< 0.2	0.3	< 0.2
Cs	< 0.1	0.3	0.9	0.2	0.2	0.3	0.1	1.1	6.9	0.4	< 0.1	< 0.1
Ba	10	263	472	25	17	4	184	321	618	8	10	24
La	6.91	7.5	6.77	2.35	2.31	2.33	7.81	10.5	26.6	4.42	5.19	1.82
Ce	14.6	16.6	16	6.55	6.34	5.04	14.7	21.4	52.5	8.68	11.3	4.23
Pr	1.73	1.93	1.66	0.57	0.58	0.56	1.71	2.58	5.66	1	1.31	0.48
Nd	6.15	7.34	6.3	2.12	2.05	2.12	6.36	9.73	19.8	3.74	4.41	1.65
Sm	0.84	1.4	1.18	0.36	0.33	0.34	1.1	1.71	3.41	0.59	0.7	0.28
Eu	0.245	0.29	0.303	0.111	0.111	0.121	0.35	0.513	0.709	0.247	0.22	0.104
Gd	0.61	1.09	1.15	0.37	0.33	0.33	1.04	1.59	2.48	0.57	0.56	0.32
Tb	0.09	0.15	0.16	0.06	0.05	0.05	0.16	0.23	0.36	0.09	0.09	0.04
Dy	0.51	0.77	0.78	0.37	0.32	0.34	0.93	1.34	1.93	0.53	0.44	0.28
Ho	0.1	0.14	0.14	0.08	0.07	0.07	0.2	0.26	0.37	0.12	0.09	0.06
Er	0.27	0.4	0.4	0.23	0.2	0.23	0.56	0.75	1.07	0.33	0.24	0.18
Tm	0.039	0.059	0.058	0.033	0.029	0.035	0.077	0.109	0.162	0.045	0.036	0.028
Yb	0.26	0.39	0.38	0.21	0.19	0.24	0.46	0.69	1.08	0.26	0.21	0.19
Lu	0.042	0.063	0.059	0.033	0.03	0.039	0.067	0.107	0.179	0.037	0.033	0.03
Hf	0.2	2.6	2.1	< 0.1	< 0.1	< 0.1	0.6	1.3	4.1	< 0.1	< 0.1	< 0.1
Ta	0.12	0.19	0.09	< 0.01	0.01	< 0.01	0.22	0.57	0.58	0.01	< 0.01	< 0.01
W	0.6	< 0.5	< 0.5	1	1.4	2	0.9	2.6	1.2	0.6	2.6	0.9
Tl	< 0.05	0.1	0.3	< 0.05	< 0.05	< 0.05	< 0.05	0.09	0.61	< 0.05	< 0.05	< 0.05
Pb	< 5	7	10	< 5	< 5	< 5	< 5	< 5	15	< 5	< 5	< 5
Bi	< 0.1	< 0.1	< 0.1	< 0.1	< 0.1	< 0.1	< 0.1	< 0.1	0.1	< 0.1	< 0.1	< 0.1
Th	0.62	3.27	2.93	0.13	0.17	0.11	0.45	0.98	9.27	0.17	0.25	< 0.05
U	0.12	0.61	0.6	0.07	0.05	0.05	0.13	0.22	2.14	0.04	0.04	0.03
AR-MS (ppm)												
Li	1.1	8.8	2.3	2	2.2	4.2	1.8	4.9	19.5	8.4	6.1	3
Be	1	0.3	0.4	1.3	1.3	1.3	0.4	0.8	0.6	0.5	1.4	0.9
Na	0.03	0.02	0.02	0.03	0.03	0.04	0.05	0.02	0.04	0.1	0.15	0.07
Mg	0.06	0.45	0.05	0.08	0.1	0.28	0.05	0.63	0.55	0.44	0.57	0.37
Al	0.16	1.18	0.38	0.05	0.06	0.09	0.17	0.64	1.75	0.08	0.03	0.03
K	0.01	0.07	0.26	0.02	0.02	0.04	0.14	0.33	0.93	0.06	0.01	0.01
Bi	0.04	0.06	0.03	0.04	< 0.02	< 0.02	< 0.02	< 0.02	0.09	< 0.02	0.09	< 0.02
Ca	0.09	0.02	0.02	0.44	0.06	0.02	0.13	0.87	0.03	0.03	0.69	0.73

A2., continued.

Sample	nl11-02-09 (b)	nl11-02-10	nl11-02-11	nl11-02-12 (a)	nl11-02-12 (b)	nl11-02-13	nl11-03-01	nl11-03-02	nl11-03-03	nl11-03-05	nl11-03-06	nl11-03-07
Easting	315507	315475	315389	315001	315001	314999	314996	314944	314962	314489	314453	314397
Northing	6064513	6064373	6064293	6063482	6063482	6063444	6063382	6063287	6062971	6062824	6062840	6062875
Unit	Middle Sokoman	Wishart	Wishart	Middle Sokoman	Middle Sokoman	Middle Sokoman	Lower Sokoman	Lower Sokoman	Wishart	Middle Sokoman	Middle Sokoman	Middle Sokoman
AR-MS (ppm)												
Sc	0.7	1.9	0.5	< 0.1	0.3	0.3	2.7	7.2	2.1	< 0.1	< 0.1	< 0.1
V	18	10	2	12	11	8	26	58	16	4	< 1	5
Cr	0.6	27.6	15	6	6.7	3	11.1	28.5	37.9	3.8	< 0.5	2.3
Mn	227	65	34	1710	410	952	2180	1800	39	83	591	523
Fe	33.5	3.06	0.59	22.1	16.4	25.2	27.7	26.5	1.84	29.4	19.4	25.4
Co	2.1	4.9	0.9	7.6	3.2	2.6	7.6	11.7	5.7	1.3	2.7	4.8
Ni	2.2	6.3	4	1.8	2.5	2.1	8.2	14	15.1	1.8	1.7	2.1
Cu	2.34	2.65	2.26	1.08	6.07	1.52	4.11	6.72	2.92	1.55	3.61	0.53
Zn	2.6	25.3	0.2	11.9	29.6	5.9	9.3	14.6	97.8	4.2	1.5	6.7
Ga	1.18	4.07	1.38	0.6	0.73	0.76	1.42	5.5	5.83	0.39	0.21	0.21
Ge	2	0.4	0.2	2	0.9	1.5	1	1.9	0.4	1.4	0.9	1.5
As	5.9	2.2	2.2	20.9	13.2	4.5	1.1	1.3	< 0.1	3.1	1.5	5.8
Se	1	< 0.1	< 0.1	0.7	< 0.1	0.4	< 0.1	< 0.1	0.7	< 0.1	< 0.1	0.8
Rb	1.1	3.3	11.9	1.7	1.8	4.7	5.6	32.1	74.7	7.2	1	1.2
Sr	12.1	4	6.9	8.6	4.9	3.1	15.7	28.4	7	3.1	35.3	30.7
Y	1.66	2.81	3.66	2.42	1.17	1.12	2.77	3.33	7.62	0.64	1.64	1.78
Zr	< 0.1	11.9	8.3	< 0.1	< 0.1	< 0.1	< 0.1	< 0.1	38.5	< 0.1	< 0.1	< 0.1
Nb	< 0.1	< 0.1	< 0.1	< 0.1	< 0.1	< 0.1	< 0.1	< 0.1	< 0.1	< 0.1	< 0.1	< 0.1
Mo	0.41	< 0.01	< 0.01	0.34	0.42	< 0.01	< 0.01	< 0.01	< 0.01	0.07	0.5	< 0.01
Ag	0.44	0.38	0.33	0.38	0.35	0.1	0.13	0.05	0.37	0.32	0.5	0.07
Cd	< 0.01	< 0.01	< 0.01	0.12	< 0.01	< 0.01	< 0.01	< 0.01	< 0.01	< 0.01	< 0.01	< 0.01
In	< 0.02	< 0.02	< 0.02	< 0.02	< 0.02	< 0.02	< 0.02	0.02	< 0.02	< 0.02	< 0.02	< 0.02
Sn	0.12	< 0.05	0.15	0.38	0.14	< 0.05	0.13	0.18	0.28	< 0.05	< 0.05	< 0.05
Sb	0.18	0.05	0.09	0.22	0.11	0.08	0.02	< 0.02	0.05	0.05	< 0.02	< 0.02
Te	0.23	0.13	0.04	0.5	< 0.02	0.36	< 0.02	< 0.02	0.15	0.04	0.38	0.08
Cs	0.04	0.04	0.16	0.15	0.21	0.33	0.08	0.91	3.08	0.42	0.09	0.06
Ba	3.3	29.3	54.6	14.1	10.6	< 0.5	18.8	23.1	93.4	5	5.3	13.2
La	5.3	7.4	5.9	2.3	1.9	2.1	6.3	8.9	27	3.6	4.5	1.9
Ce	10.9	16.3	14.6	5.62	4.37	3.88	11.3	17.8	54.6	6.52	8.81	3.56
Pr	1.4	2	1.6	0.5	0.4	0.5	1.5	2.2	6.1	0.8	1.1	0.4
Nd	4.76	7.4	6.1	2.06	1.76	1.74	5.54	8.75	19.9	3.15	3.67	1.75
Sm	0.7	1.2	1.1	0.3	0.3	0.3	1	1.6	3.3	0.5	0.6	0.3
Eu	0.2	0.2	0.2	0.1	< 0.1	0.1	0.3	0.4	0.6	0.2	0.2	0.1
Gd	0.6	0.9	1	0.4	0.3	0.2	0.9	1.5	2.2	0.3	0.5	0.3
Tb	< 0.1	0.1	0.1	< 0.1	< 0.1	< 0.1	0.1	0.2	0.3	< 0.1	< 0.1	< 0.1
Dy	0.36	0.58	0.6	0.37	0.21	0.22	0.54	0.87	1.54	0.15	0.33	0.23
Ho	< 0.1	0.1	0.1	< 0.1	< 0.1	< 0.1	< 0.1	0.1	0.3	< 0.1	< 0.1	< 0.1
Er	0.2	0.2	0.3	0.3	0.1	0.1	0.2	0.3	0.7	< 0.1	0.2	0.2
Tm	< 0.1	< 0.1	< 0.1	< 0.1	< 0.1	< 0.1	< 0.1	< 0.1	< 0.1	< 0.1	< 0.1	< 0.1
Yb	< 0.1	0.2	0.2	0.2	< 0.1	< 0.1	0.1	0.2	0.6	< 0.1	0.1	0.1
Lu	< 0.1	< 0.1	< 0.1	< 0.1	< 0.1	< 0.1	< 0.1	< 0.1	< 0.1	< 0.1	< 0.1	< 0.1
Hf	< 0.1	0.1	< 0.1	< 0.1	< 0.1	< 0.1	< 0.1	< 0.1	0.6	< 0.1	< 0.1	< 0.1
Ta	< 0.05	< 0.05	< 0.05	< 0.05	< 0.05	< 0.05	< 0.05	< 0.05	< 0.05	< 0.05	< 0.05	< 0.05
W	0.2	< 0.1	< 0.1	< 0.1	< 0.1	< 0.1	< 0.1	5.3	< 0.1	< 0.1	< 0.1	0.7
Re	< 0.001	< 0.001	< 0.001	0.01	0.01	< 0.001	< 0.001	< 0.001	< 0.001	0.01	< 0.001	< 0.001
Au	< 5	< 5	< 5	< 5	< 5	< 5	< 5	< 5	< 5	< 5	< 5	< 5
Tl	0.03	0.04	0.07	0.05	0.04	< 0.02	< 0.02	0.05	0.24	0.03	0.02	< 0.02
Pb	1.11	4.37	5.61	1.45	1.03	0.88	1.21	0.76	10.1	1.08	1.52	0.47
Th	0.5	2.5	1.9	0.2	0.1	< 0.1	0.3	0.6	5.4	0.2	0.2	< 0.1
U	< 0.1	0.3	0.3	< 0.1	< 0.1	< 0.1	< 0.1	< 0.1	1.3	< 0.1	< 0.1	< 0.1

A2., continued.

Sample	nl11-03-08	nl11-03-09	nl11-03-10	nl11-03-11	nl11-03-13	nl11-03-14	nl11-03-16	nl11-03-17	nl11-03-18	nl11-03-19	nl11-03-20	nl11-03-21
Easting	314385	314303	314278	314219	314210	314169	314080	313869	313882	313099	313111	312823
Northing	6062816	6062994	6063079	6063073	6062343	6062325	6062107	6062348	6062388	6061709	6061804	6061995
Unit	Middle Sokoman	Middle Sokoman	Middle Sokoman	Middle Sokoman	Middle Sokoman	Middle Sokoman	Wishart	Middle Sokoman	Middle Sokoman	Wishart	Wishart	Ruth Shale
FUS-XRF (wt %)												
SiO2	41.22	50.57	54.71	39.54	63.82	56.66	71.94	47.5	36.25	66.67	61.52	45.27
Al2O3	0.31	0.2	0.36	0.18	0.2	0.26	14.34	0.26	0.22	15.44	19.93	10.25
Fe2O3(T)	56.83	47.33	42.55	58.64	33.92	41.4	2.64	48.3	60.51	6.05	4.26	29.81
MnO	0.008	0.006	0.03	0.01	0.015	0.006	0.007	0.066	0.022	0.009	0.007	0.146
MgO	0.96	0.58	0.81	0.41	0.31	0.37	1.62	0.57	1.85	1.44	1.5	1.33
CaO	0.04	0.09	0.09	0.02	0.07	0.11	0.13	0.91	0.06	0.09	0.08	0.3
Na2O	0.83	0.48	0.18	0.06	0.07	0.32	4.12	0.32	0.08	1.64	1	0.47
K2O	0.05	0.04	0.11	0.02	0.04	0.09	2.55	0.06	0.08	5.42	7.4	8.27
TiO2	0.03	0.03	0.03	0.06	0.01	0.02	0.54	0.03	0.03	0.56	0.74	2.22
P2O5	0.02	0.01	0.03	0.05	0.05	0.06	0.06	0.01	0.04	0.06	0.07	0.19
Cr2O3	0.02	0.01	< 0.01	0.01	< 0.01	0.01	0.02	0.01	< 0.01	0.02	0.02	0.01
V2O5	< 0.003	< 0.003	< 0.003	< 0.003	< 0.003	< 0.003	0.014	< 0.003	0.004	0.01	0.02	0.035
LOI	-0.34	0.33	-0.34	0.89	0.7	0.11	1.52	1.04	0.77	2.65	3.1	0.86
Total	99.97	99.67	98.56	99.89	99.2	99.42	99.5	99.07	99.91	100.1	99.65	99.16
FUS-MS (ppm)												
V	< 5	10	7	11	7	7	119	9	19	62	120	204
Cr	< 20	30	< 20	< 20	< 20	< 20	180	< 20	< 20	90	160	110
Co	2	3	1	4	1	2	9	2	6	14	21	21
Ni	< 20	< 20	< 20	< 20	< 20	< 20	40	< 20	< 20	30	40	40
Cu	< 10	< 10	< 10	< 10	< 10	< 10	10	< 10	< 10	10	30	10
Zn	< 30	< 30	< 30	< 30	< 30	< 30	50	< 30	< 30	50	60	130
Ga	< 1	< 1	< 1	< 1	< 1	< 1	26	< 1	1	21	29	15
Ge	11.3	10	6.6	6.9	6.2	9.4	3.6	7.7	7.8	2.7	2.9	12.7
As	12	14	< 5	10	17	12	< 5	13	38	10	6	< 5
Rb	< 1	< 1	2	< 1	< 1	< 1	134	< 1	5	149	232	289
Sr	< 2	3	3	< 2	4	4	97	14	2	110	103	47
Y	2.7	1.7	2.4	3.3	1.4	1.8	16.8	2.8	2.7	17.4	15	13.7
Zr	3	7	1	4	1	2	236	4	8	361	173	170
Nb	0.6	0.4	0.5	1.6	0.8	0.7	9.5	0.9	1.4	14	13	34.4
Mo	< 2	< 2	< 2	< 2	< 2	< 2	< 2	< 2	< 2	< 2	< 2	< 2
Ag	< 0.5	< 0.5	< 0.5	< 0.5	< 0.5	< 0.5	0.8	< 0.5	< 0.5	1	< 0.5	0.7
In	< 0.1	< 0.1	< 0.1	< 0.1	< 0.1	< 0.1	< 0.1	< 0.1	< 0.1	< 0.1	< 0.1	< 0.1
Sn	< 1	< 1	< 1	< 1	< 1	< 1	2	< 1	< 1	2	3	2
Sb	< 0.2	< 0.2	< 0.2	0.8	0.4	0.3	0.4	< 0.2	0.3	< 0.2	< 0.2	< 0.2
Cs	< 0.1	0.1	0.1	< 0.1	< 0.1	< 0.1	3.8	< 0.1	0.8	6.7	8.2	5.3
Ba	14	26	6	8	18	15	336	19	16	666	601	675
La	3.82	1.55	2.01	2.31	2.41	1.9	35.3	3.2	2.76	49	48.8	20.8
Ce	7.86	3.7	4.62	4.33	5.11	4.24	67	7.24	6.04	95.9	96.7	42.5
Pr	0.88	0.37	0.53	0.47	0.55	0.49	7.54	0.85	0.68	11	10.7	5.21
Nd	3.2	1.48	1.98	2.06	1.96	1.75	26.8	3.18	2.51	36.4	39.3	20.6
Sm	0.46	0.25	0.36	0.44	0.35	0.38	4.64	0.51	0.43	5.78	6.62	4.08
Eu	0.173	0.091	0.129	0.172	0.097	0.117	0.788	0.191	0.119	1.1	1.35	1.09
Gd	0.44	0.25	0.36	0.4	0.27	0.33	3.47	0.47	0.39	4.23	4.45	3.28
Tb	0.06	0.04	0.07	0.07	0.04	0.05	0.52	0.07	0.06	0.6	0.59	0.46
Dy	0.4	0.26	0.4	0.46	0.25	0.29	2.9	0.41	0.39	3.16	3.06	2.72
Ho	0.09	0.06	0.08	0.1	0.05	0.06	0.56	0.09	0.09	0.61	0.54	0.53
Er	0.25	0.17	0.24	0.32	0.14	0.17	1.59	0.25	0.28	1.61	1.48	1.55
Tm	0.034	0.025	0.034	0.047	0.022	0.025	0.237	0.036	0.042	0.242	0.222	0.235
Yb	0.2	0.17	0.21	0.31	0.15	0.16	1.54	0.22	0.28	1.53	1.44	1.56
Lu	0.029	0.027	0.033	0.05	0.025	0.027	0.251	0.034	0.044	0.247	0.225	0.258
Hf	< 0.1	0.1	< 0.1	< 0.1	< 0.1	< 0.1	5.5	< 0.1	0.1	8.2	4.1	3.5
Ta	< 0.01	0.03	< 0.01	0.06	< 0.01	< 0.01	0.92	< 0.01	0.01	0.9	1.01	2.05
W	1	< 0.5	0.6	2.8	1.1	4.6	< 0.5	0.8	1.3	0.9	< 0.5	< 0.5
Tl	< 0.05	< 0.05	< 0.05	< 0.05	< 0.05	< 0.05	0.43	< 0.05	< 0.05	0.72	0.96	0.1
Pb	< 5	< 5	< 5	6	< 5	< 5	< 5	< 5	< 5	10	6	7
Bi	< 0.1	< 0.1	< 0.1	< 0.1	< 0.1	< 0.1	< 0.1	< 0.1	< 0.1	< 0.1	0.2	< 0.1
Th	0.1	0.14	0.1	0.17	0.14	0.11	14.7	0.19	0.16	16.6	15.6	1.98
U	0.04	0.06	0.05	0.08	0.06	0.02	2.72	0.06	0.1	2.13	2.7	0.72
AR-MS (ppm)												
Li	5.5	2.7	3.5	1.9	0.7	2.3	6.1	2130	7.8	17.1	4	31
Be	0.6	0.5	0.7	1	1.3	0.9	0.8	0.8	1.4	0.9	1.2	1.9
Na	0.12	0.06	0.03	0.03	0.035	0.05	0.095	1.62	0.02	0.05	0.04	0.04
Mg	0.1	0.08	0.18	0.11	0.07	0.08	0.72	0.17	0.31	0.57	0.29	0.82
Al	0.03	0.03	0.06	0.09	0.04	0.03	1.51	0.07	0.09	2.07	1.67	0.88
K	0.01	0.01	0.03	0.01	0.01	0.01	0.56	0.03	0.05	0.86	0.91	0.99
Bi	< 0.02	0.03	0.03	< 0.02	< 0.02	< 0.02	< 0.02	0.22	< 0.02	0.07	0.36	< 0.02
Ca	0.05	0.06	0.04	0.02	0.05	0.06	0.05	0.71	0.04	0.06	0.05	0.18

A2., continued.

Sample	nl11-03-08	nl11-03-09	nl11-03-10	nl11-03-11	nl11-03-13	nl11-03-14	nl11-03-16	nl11-03-17	nl11-03-18	nl11-03-19	nl11-03-20	nl11-03-21
Easting	314385	314303	314278	314219	314210	314169	314080	313869	313882	313099	313111	312823
Northing	6062816	6062994	6063079	6063073	6062343	6062325	6062107	6062348	6062388	6061709	6061804	6061995
Unit	Middle Sokoman	Middle Sokoman	Middle Sokoman	Middle Sokoman	Middle Sokoman	Middle Sokoman	Wishart	Middle Sokoman	Middle Sokoman	Wishart	Wishart	Ruth Shale
AR-MS (ppm)												
Sc	< 0.1	< 0.1	0.2	0.2	< 0.1	< 0.1	3	0.6	0.1	2.5	2	12.1
V	1	< 1	10	9	6	6	26	8	17	19	13	153
Cr	< 0.5	7.8	9.7	< 0.5	< 0.5	6.6	50.2	7.7	7.3	34	26	62
Mn	64	65	279	140	120	48	26	557	144	55	18	1090
Fe	30.3	20.3	28.4	33.7	18.1	22.8	1.45	25.9	28.5	2.66	1.41	20.2
Co	1.9	1.6	1.7	4.2	1.4	1.4	5	4	3.9	12.1	14	20.9
Ni	1.3	1.2	1.8	2	1.3	1.5	23.3	6.1	1.7	28.5	28.6	26.5
Cu	0.49	0.41	0.77	0.78	1.04	1.5	0.9	6.4	0.32	8.79	19.8	11.8
Zn	7.8	3.8	7.8	4.2	18.2	1.9	11.2	4460	8.7	35	10.4	109
Ga	0.24	0.18	0.67	0.65	0.32	0.4	6.95	0.39	0.75	6.32	5.08	9.23
Ge	1.1	1	1.7	1.6	1.1	1.3	0.3	1.3	1.3	0.4	0.3	1.1
As	5.2	6.3	3.9	6	9.6	5.6	0.7	8	20.5	7.9	4.2	1.1
Se	< 0.1	< 0.1	0.1	< 0.1	< 0.1	1.4	< 0.1	< 0.1	0.7	0.3	< 0.1	< 0.1
Rb	0.6	1.2	2.1	0.5	0.8	0.6	33.3	2.5	5.3	36	46.8	160
Sr	1.9	2.7	2.8	1.2	4.1	4.4	4.6	16.7	2.8	16.4	13.2	11.6
Y	0.55	0.6	1.06	1.65	1.14	1.46	6.28	1.57	1.36	7.21	7.61	7.98
Zr	9.2	< 0.1	< 0.1	< 0.1	< 0.1	< 0.1	4.9	125	< 0.1	2.3	< 0.1	8
Nb	< 0.1	< 0.1	< 0.1	< 0.1	< 0.1	< 0.1	< 0.1	< 0.1	< 0.1	< 0.1	< 0.1	< 0.1
Mo	< 0.01	< 0.01	0.11	< 0.01	< 0.01	< 0.01	< 0.01	< 0.01	0.02	< 0.01	< 0.01	0.35
Ag	0.08	0.28	0.42	0.05	0.34	0.29	0.19	0.3	0.28	0.21	0.19	0.08
Cd	0.01	< 0.01	< 0.01	< 0.01	< 0.01	< 0.01	< 0.01	10.2	0.02	< 0.01	< 0.01	< 0.01
In	< 0.02	< 0.02	< 0.02	< 0.02	< 0.02	< 0.02	< 0.02	< 0.02	< 0.02	< 0.02	< 0.02	0.05
Sn	< 0.05	< 0.05	< 0.05	< 0.05	< 0.05	< 0.05	0.2	1.02	< 0.05	0.21	0.19	0.17
Sb	< 0.02	0.02	0.03	0.02	0.08	0.03	< 0.02	0.11	0.04	< 0.02	< 0.02	< 0.02
Te	< 0.02	0.31	< 0.02	0.17	0.25	< 0.02	0.11	0.15	0.42	0.4	< 0.02	< 0.02
Cs	0.05	0.06	0.13	0.03	0.06	0.06	0.63	0.16	0.77	0.72	1.18	4.36
Ba	5.4	8.5	2.3	< 0.5	9.3	6.9	68.3	13	4.2	93.2	73.1	54.3
La	2.9	1.7	1.7	1.5	2.1	1.8	25.8	4.3	2.4	43.6	48.7	19.7
Ce	5.67	3.32	3.5	2.75	3.76	3.21	50.9	8.73	4.61	85.7	98.2	40.7
Pr	0.7	0.4	0.5	0.4	0.5	0.4	5.9	1	0.6	9.3	11.3	5.2
Nd	2.71	1.27	1.88	1.67	1.77	1.48	20.2	3.83	2.18	31.7	38.3	19.3
Sm	0.4	0.2	0.3	0.3	0.3	0.3	3.2	0.7	0.4	5.3	6.1	3.5
Eu	0.1	< 0.1	0.1	0.1	< 0.1	0.1	0.5	0.2	0.1	1	1.2	0.9
Gd	0.3	0.2	0.3	0.3	0.3	0.3	2.3	0.5	0.3	4	4.1	2.8
Tb	< 0.1	< 0.1	< 0.1	< 0.1	< 0.1	< 0.1	0.3	< 0.1	< 0.1	0.4	0.4	0.3
Dy	0.13	0.14	0.21	0.3	0.245	0.26	1.26	0.36	0.23	1.75	1.95	1.93
Ho	< 0.1	< 0.1	< 0.1	< 0.1	< 0.1	< 0.1	0.2	< 0.1	< 0.1	0.3	0.3	0.3
Er	< 0.1	< 0.1	0.1	0.1	0.1	0.1	0.6	0.1	0.1	0.8	0.7	0.8
Tm	< 0.1	< 0.1	< 0.1	< 0.1	< 0.1	< 0.1	< 0.1	< 0.1	< 0.1	0.1	0.1	0.1
Yb	< 0.1	< 0.1	< 0.1	0.1	< 0.1	< 0.1	0.5	0.2	0.1	0.5	0.6	0.6
Lu	< 0.1	< 0.1	< 0.1	< 0.1	< 0.1	< 0.1	< 0.1	2	< 0.1	< 0.1	< 0.1	< 0.1
Hf	< 0.1	< 0.1	< 0.1	< 0.1	< 0.1	< 0.1	< 0.1	< 0.1	< 0.1	< 0.1	< 0.1	< 0.1
Ta	< 0.05	< 0.05	< 0.05	< 0.05	< 0.05	< 0.05	< 0.05	< 0.05	< 0.05	< 0.05	< 0.05	< 0.05
W	0.2	< 0.1	< 0.1	< 0.1	< 0.1	< 0.1	< 0.1	0.1	< 0.1	< 0.1	< 0.1	< 0.1
Re	< 0.001	< 0.001	< 0.001	< 0.001	< 0.001	< 0.001	< 0.001	< 0.001	0.01	< 0.001	0.01	< 0.001
Au	< 5	< 5	< 5	< 5	< 5	< 5	< 5	< 5	62	< 5	< 5	< 5
Tl	< 0.02	0.04	0.02	< 0.02	< 0.02	< 0.02	0.1	0.11	0.02	0.14	0.13	0.03
Pb	0.49	0.56	1.09	1.44	1	0.87	1.24	3.07	2.94	6.56	2.06	2.23
Th	< 0.1	1.3	< 0.1	< 0.1	0.1	< 0.1	7.3	0.7	0.1	11.8	9.9	1.2
U	< 0.1	< 0.1	< 0.1	< 0.1	< 0.1	< 0.1	1.1	< 0.1	< 0.1	1.1	1.4	0.2

A2., continued.

Sample	nl11-04-01	nl11-04-02	nl11-04-03	nl11-04-04	nl11-04-05	nl11-04-06	nl11-04-07 (a)	nl11-04-07 (b)	nl11-04-08	nl11-04-09	nl11-04-11	nl11-04-12
Easting	312561	312591	312594	312545	312268	312215	312268	312268	312431	312449	313416	313403
Northing	6062053	6062108	6062156	6062183	6062240	6062116	6062072	6062072	6062071	6062029	6059544	6059537
Unit	Ruth Shale	Ruth Shale	Middle Sokoman	Middle Sokoman	Middle Sokoman	Middle Sokoman	Middle Sokoman	Middle Sokoman	Middle Sokoman	Ruth Shale	Middle Sokoman	Middle Sokoman
FUS-XRF (wt %)												
SiO2	48.73	47.42	53.23	46.94	89.97	49.09	51.85	41.58	51.04	47.37	67.13	76.89
Al2O3	8.54	8.38	0.22	0.15	0.1	0.28	0.26	0.01	0.32	8.15	0.16	0.13
Fe2O3(T)	30.03	33.96	43.76	49.83	7.51	49.32	45.69	57.89	46.6	32.23	31.01	21.23
MnO	0.258	0.159	0.015	0.027	0.02	0.004	0.013	0.037	0.014	0.313	0.044	0.073
MgO	1.44	0.9	1.94	2.09	0.03	0.19	0.62	< 0.01	0.22	1.07	0.17	0.12
CaO	0.33	0.24	0.06	0.02	0.02	0.05	0.05	0.02	0.1	0.25	0.1	0.26
Na2O	0.33	0.92	0.09	0.1	< 0.01	0.05	0.08	0.07	0.08	0.7	0.09	0.05
K2O	6.68	6.12	0.04	0.06	0.03	0.03	0.08	0.03	0.05	6.12	0.1	0.03
TiO2	1.09	1.48	0.03	0.04	0.02	0.04	0.03	0.03	0.04	1.01	0.03	0.02
P2O5	0.17	0.16	0.07	0.02	0.08	0.04	0.02	0.02	0.03	0.16	0.04	0.02
Cr2O3	0.01	0.01	0.05	< 0.01	< 0.01	< 0.01	< 0.01	< 0.01	< 0.01	0.01	< 0.01	< 0.01
V2O5	0.019	0.021	< 0.003	0.003	< 0.003	< 0.003	< 0.003	0.003	0.003	0.018	0.003	< 0.003
LOI	2.01	0.13	0.77	0.69	0.82	0.79	0.64	0.49	0.73	2.83	0.34	0.63
Total	99.63	99.9	100.3	99.97	98.61	99.89	99.33	100.2	99.23	100.2	99.21	99.46
FUS-MS (ppm)												
V	115	141	7	10	7	11	7	10	29	115	14	7
Cr	70	90	< 20	< 20	< 20	< 20	< 20	< 20	< 20	60	< 20	< 20
Co	19	21	4	4	1	4	8	2	2	20	2	2
Ni	30	40	< 20	< 20	< 20	< 20	< 20	< 20	< 20	30	< 20	< 20
Cu	20	10	< 10	< 10	< 10	< 10	< 10	< 10	< 10	20	< 10	< 10
Zn	70	90	< 30	< 30	60	< 30	< 30	< 30	< 30	70	< 30	< 30
Ga	11	12	1	1	< 1	1	< 1	< 1	1	11	1	< 1
Ge	10.2	11.8	10.4	9.9	1.5	6.8	9.7	6	13.4	10.1	5.1	5.2
As	< 5	< 5	13	18	6	23	18	24	10	6	11	11
Rb	206	213	1	8	< 1	< 1	< 1	< 1	5	184	1	< 1
Sr	46	39	2	< 2	< 2	3	< 2	2	3	34	3	4
Y	11.3	11.2	3.8	2.7	1	2.4	2.8	1.1	3	10.5	2.6	1.7
Zr	108	124	12	4	1	10	3	4	5	95	6	4
Nb	19.8	22.3	0.8	0.5	0.7	1.2	0.6	0.5	1.6	16.8	0.8	0.4
Mo	< 2	< 2	< 2	< 2	< 2	< 2	< 2	< 2	< 2	< 2	< 2	< 2
Ag	< 0.5	< 0.5	< 0.5	< 0.5	< 0.5	< 0.5	< 0.5	< 0.5	< 0.5	< 0.5	< 0.5	< 0.5
In	< 0.1	< 0.1	< 0.1	< 0.1	< 0.1	< 0.1	< 0.1	< 0.1	< 0.1	< 0.1	< 0.1	< 0.1
Sn	1	1	< 1	< 1	< 1	< 1	< 1	< 1	< 1	1	< 1	< 1
Sb	< 0.2	< 0.2	2.2	< 0.2	0.7	< 0.2	0.2	0.3	0.8	< 0.2	< 0.2	< 0.2
Cs	3.8	3.4	< 0.1	0.8	< 0.1	0.2	< 0.1	< 0.1	0.4	2.5	0.3	0.1
Ba	459	461	8	13	3	10	13	14	21	392	65	42
La	17	16.4	3.74	2.88	1.14	2.56	2.09	1.25	1.87	15.6	1.52	1.48
Ce	34.2	33	7.47	6.06	1.42	6.02	4.95	2.88	4.04	31.6	4.59	3.66
Pr	4.19	4.03	0.84	0.58	0.14	0.7	0.5	0.29	0.49	3.86	0.39	0.33
Nd	16.9	16	3.06	2.16	0.55	2.53	1.84	1.19	1.93	15.9	1.56	1.03
Sm	3.12	3.07	0.49	0.36	0.1	0.45	0.34	0.2	0.33	2.93	0.34	0.17
Eu	0.909	0.903	0.196	0.125	0.033	0.157	0.141	0.081	0.192	0.878	0.109	0.063
Gd	2.65	2.5	0.51	0.36	0.14	0.45	0.4	0.2	0.39	2.46	0.4	0.23
Tb	0.37	0.38	0.08	0.07	0.02	0.07	0.07	0.03	0.06	0.35	0.06	0.04
Dy	2.13	2.1	0.5	0.45	0.14	0.43	0.42	0.19	0.41	1.99	0.38	0.23
Ho	0.41	0.41	0.11	0.1	0.04	0.08	0.1	0.04	0.09	0.39	0.08	0.05
Er	1.12	1.14	0.35	0.29	0.12	0.24	0.3	0.13	0.29	1.07	0.23	0.15
Tm	0.162	0.171	0.052	0.044	0.017	0.036	0.045	0.019	0.044	0.152	0.034	0.023
Yb	1.05	1.14	0.32	0.27	0.11	0.24	0.28	0.13	0.28	0.94	0.22	0.15
Lu	0.167	0.182	0.047	0.043	0.017	0.037	0.043	0.02	0.041	0.146	0.034	0.023
Hf	2.4	2.7	0.2	< 0.1	< 0.1	0.2	< 0.1	< 0.1	< 0.1	2.2	< 0.1	< 0.1
Ta	1.14	1.36	0.02	0.01	0.02	0.02	< 0.01	0.03	0.02	1.01	0.02	< 0.01
W	< 0.5	< 0.5	0.6	0.9	< 0.5	1	0.7	< 0.5	1.5	< 0.5	0.9	0.9
Tl	0.1	< 0.05	< 0.05	< 0.05	< 0.05	< 0.05	< 0.05	< 0.05	< 0.05	< 0.05	< 0.05	< 0.05
Pb	< 5	5	< 5	< 5	5	< 5	< 5	< 5	< 5	< 5	< 5	< 5
Bi	< 0.1	< 0.1	< 0.1	< 0.1	< 0.1	< 0.1	< 0.1	< 0.1	< 0.1	< 0.1	< 0.1	< 0.1
Th	1.59	1.5	0.26	0.13	0.15	0.18	0.09	0.06	0.14	1.38	0.18	0.09
U	0.48	0.44	0.07	0.05	1.63	0.06	0.04	0.05	0.05	0.4	0.05	0.03
AR-MS (ppm)												
Li	13.5	26.4	3	5.5	0.3	1.8	0.7	0.6	7	8.5	0.7	0.5
Be	1.5	1.9	1.2	1.1	0.2	0.9	0.9	0.9	1.7	0.9	0.9	0.6
Na	0.04	0.07	0.03	0.03	0.02	0.05	0.03	0.02	0.03	0.06	0.03	0.02
Mg	0.89	0.59	0.33	0.45	0.01	0.06	0.14	0.01	0.15	0.7	0.09	0.06
Al	1.04	0.68	0.1	0.09	0.05	0.15	0.08	0.03	0.12	0.59	0.08	0.04
K	1.02	0.72	0.02	0.04	0.01	0.02	0.01	0.01	0.04	0.59	0.02	0.01
Bi	< 0.02	< 0.02	< 0.02	< 0.02	0.03	0.12	0.04	< 0.02	< 0.02	< 0.02	< 0.02	0.06
Ca	0.22	0.17	0.03	0.02	0.02	0.04	0.02	0.01	0.08	0.18	0.08	0.19

A2., continued.

Sample	nl11-04-01	nl11-04-02	nl11-04-03	nl11-04-04	nl11-04-05	nl11-04-06	nl11-04-07 (a)	nl11-04-07 (b)	nl11-04-08	nl11-04-09	nl11-04-11	nl11-04-12
Easting	312561	312591	312594	312545	312268	312215	312268	312268	312431	312449	313416	313403
Northing	6062053	6062108	6062156	6062183	6062240	6062116	6062072	6062072	6062071	6062029	6059544	6059537
Unit	Ruth Shale	Ruth Shale	Middle Sokoman	Middle Sokoman	Middle Sokoman	Middle Sokoman	Middle Sokoman	Middle Sokoman	Middle Sokoman	Ruth Shale	Middle Sokoman	Middle Sokoman
AR-MS (ppm)												
Sc	11.3	12	0.5	0.3	< 0.1	0.6	0.4	0.2	0.4	11.2	< 0.1	< 0.1
V	93	116	10	9	4	12	6	3	30	99	6	5
Cr	40.3	57.9	9.2	< 0.5	28.6	7.4	1.4	< 0.5	12.2	44.1	< 0.5	2
Mn	1830	1240	104	262	130	79	137	378	162	2370	336	568
Fe	19	22.7	28.4	27.1	5.02	27.4	24.5	26.7	26.6	20.5	15.7	11.4
Co	18.1	21.6	3	3.2	1.3	3.4	6.4	2	2	20	2	1.9
Ni	20.6	25.9	2.3	1.6	10.7	2.5	2	1.6	2.4	24.4	1.3	1.7
Cu	15.1	12.2	2.03	< 0.01	4.24	2.08	2.56	1.42	1.34	17.7	1.07	2.01
Zn	54.9	73.7	27.5	2.3	57.6	14.3	1.7	28.4	13.9	83.2	7	1
Ga	8.32	7.53	0.78	0.7	0.24	0.9	0.45	0.19	0.74	6.89	0.52	0.39
Ge	1	1.3	1.1	1.4	0.2	1.5	1.6	1.2	2.8	1.3	0.7	0.9
As	2.2	0.9	10.2	13.2	5.6	14.1	8.6	13.9	6.9	3.2	6.7	5.6
Se	< 0.1	1.1	0.1	< 0.1	< 0.1	< 0.1	< 0.1	< 0.1	< 0.1	< 0.1	< 0.1	< 0.1
Rb	141	119	1.1	7.4	1.2	1.9	1	2.3	5.2	84.6	2.7	1.1
Sr	11.2	13.7	2.4	1.7	0.6	3.1	1.8	1.9	3.6	10.1	2.2	4
Y	6.14	5.89	1.32	0.81	1.03	1.2	1.39	0.81	2.14	5.86	2.27	1.5
Zr	11.5	9.8	< 0.1	< 0.1	< 0.1	84.3	< 0.1	< 0.1	< 0.1	9	< 0.1	< 0.1
Nb	< 0.1	< 0.1	< 0.1	< 0.1	< 0.1	< 0.1	< 0.1	< 0.1	< 0.1	< 0.1	< 0.1	< 0.1
Mo	0.13	0.88	< 0.01	0.1	0.87	0.08	< 0.01	< 0.01	0.04	0.34	< 0.01	0.05
Ag	0.03	0.03	0.26	0.23	0.18	0.27	0.17	0.06	0.16	0.05	0.04	0.12
Cd	0.03	0.04	0.02	< 0.01	< 0.01	< 0.01	< 0.01	< 0.01	< 0.01	0.04	< 0.01	< 0.01
In	0.04	0.04	< 0.02	< 0.02	< 0.02	< 0.02	< 0.02	< 0.02	< 0.02	0.05	< 0.02	< 0.02
Sn	0.76	0.13	0.11	< 0.05	0.07	0.17	< 0.05	< 0.05	< 0.05	0.51	< 0.05	0.07
Sb	< 0.02	< 0.02	0.47	0.02	0.11	0.05	0.02	< 0.02	0.45	< 0.02	0.02	< 0.02
Te	< 0.02	< 0.02	0.48	0.36	0.17	0.13	0.15	< 0.02	0.38	0.08	< 0.02	< 0.02
Cs	3.2	2.8	0.06	0.74	0.02	0.18	0.07	0.04	0.33	2	0.18	0.1
Ba	33.2	42	3	5.5	< 0.5	3.1	6	4.3	14	36.8	42	32.3
La	15.9	15.9	3.8	2	0.9	2.7	1.7	1.1	1.8	15.6	1.4	1.3
Ce	33.1	32.9	6.89	3.97	1.04	5.45	3.31	1.79	3.6	32.7	3.48	2.53
Pr	4.3	4.2	0.8	0.5	0.2	0.6	0.4	0.3	0.5	4.2	0.3	0.3
Nd	16.8	15.5	3.02	1.91	0.49	2.57	1.54	0.91	1.81	15.8	1.49	1
Sm	3.1	2.8	0.5	0.3	0.1	0.5	0.3	0.2	0.4	2.9	0.3	0.2
Eu	0.8	0.8	0.2	< 0.1	< 0.1	0.1	0.1	< 0.1	0.2	0.8	0.1	< 0.1
Gd	2.4	2.2	0.4	0.2	0.1	0.4	0.3	0.2	0.3	2.2	0.3	0.2
Tb	0.3	0.3	< 0.1	< 0.1	< 0.1	< 0.1	< 0.1	< 0.1	< 0.1	0.3	< 0.1	< 0.1
Dy	1.43	1.45	0.27	0.16	0.14	0.25	0.21	0.17	0.3	1.33	0.34	0.23
Ho	0.2	0.2	< 0.1	< 0.1	< 0.1	< 0.1	< 0.1	< 0.1	< 0.1	0.2	< 0.1	< 0.1
Er	0.6	0.5	0.2	0.1	< 0.1	0.1	0.2	0.1	0.2	0.5	0.2	0.1
Tm	< 0.1	< 0.1	< 0.1	< 0.1	< 0.1	< 0.1	< 0.1	< 0.1	< 0.1	< 0.1	< 0.1	< 0.1
Yb	0.5	0.3	< 0.1	< 0.1	< 0.1	0.1	0.2	< 0.1	0.2	0.4	0.2	< 0.1
Lu	< 0.1	< 0.1	< 0.1	< 0.1	< 0.1	1	< 0.1	< 0.1	< 0.1	< 0.1	< 0.1	< 0.1
Hf	< 0.1	< 0.1	< 0.1	< 0.1	< 0.1	< 0.1	< 0.1	< 0.1	< 0.1	< 0.1	< 0.1	< 0.1
Ta	< 0.05	< 0.05	< 0.05	< 0.05	< 0.05	< 0.05	< 0.05	< 0.05	< 0.05	< 0.05	< 0.05	< 0.05
W	< 0.1	< 0.1	< 0.1	< 0.1	< 0.1	< 0.1	< 0.1	< 0.1	< 0.1	< 0.1	< 0.1	< 0.1
Re	0.01	< 0.001	< 0.001	< 0.001	0.01	0.01	< 0.001	< 0.001	< 0.001	< 0.001	< 0.001	< 0.001
Au	< 5	< 5	< 5	< 5	< 5	< 5	< 5	< 5	< 5	< 5	< 5	< 5
Tl	0.06	0.02	0.02	0.03	0.03	0.02	0.02	< 0.02	0.02	0.02	< 0.02	< 0.02
Pb	1.35	1.67	1.21	1.59	0.35	1.42	0.72	0.73	0.5	1.54	0.8	0.58
Th	1.1	1	1.4	0.4	1.6	0.3	0.2	< 0.1	0.2	1	0.1	< 0.1
U	0.2	0.2	< 0.1	< 0.1	1.5	< 0.1	< 0.1	< 0.1	< 0.1	0.2	< 0.1	< 0.1

A2., continued.

Sample	nl11-04-13	nl11-04-14	nl11-04-15	nl11-04-16	nl11-04-17	nl11-04-18	nl11-05-02	nl11-05-03	nl11-05-04	nl11-05-05	nl11-05-08	nl11-05-09
Easting	313485	313512	313477	313564	313620	313784	314256	314139	314444	314432	314305	314485
Northing	6059586	6059682	6059697	6059542	6059501	6059398	6058363	6058249	6058398	6058442	6058616	6058775
Unit	Middle Sokoman	Middle Sokoman	Middle Sokoman	Middle Sokoman	Middle Sokoman	Lower Sokoman	Silicate	IF Silicate	IF Silicate	IF Silicate	IF Silicate	IF SIlicate	IF
FUS-XRF (wt %)												
SiO2	47.71	53.64	39.36	37.3	29.15	44.54	64.3	56.13	72.52	61.84	75.55	76.57
Al2O3	0.22	0.38	0.23	0.55	0.95	6.52	0.32	0.57	0.42	0.15	0.28	0.17
Fe2O3(T)	49.65	42.51	58.71	58.91	63.94	41.17	33.41	39	24.15	28.3	22.62	21.99
MnO	0.11	0.137	0.035	0.024	0.039	0.026	0.127	0.327	0.039	0.067	0.053	0.029
MgO	0.3	0.26	0.24	1.51	3.48	1.63	0.21	1.5	0.92	1.17	0.56	0.2
CaO	0.7	0.63	0.07	0.04	0.08	0.12	0.15	0.24	0.09	3.83	0.14	0.09
Na2O	0.1	0.18	0.14	0.23	0.43	0.82	0.09	0.05	0.01	0.06	0.02	0.11
K2O	0.07	0.04	0.08	0.05	0.08	4.54	0.08	0.3	0.29	0.16	0.14	0.06
TiO2	0.02	0.02	0.03	0.05	0.07	0.71	0.03	0.04	0.04	0.04	0.02	0.02
P2O5	0.01	0.02	0.04	0.01	0.05	0.07	0.06	0.04	0.01	0.02	0.01	0.06
Cr2O3	< 0.01	< 0.01	< 0.01	< 0.01	0.01	0.01	< 0.01	0.05	0.01	0.01	0.01	< 0.01
V2O5	0.004	0.003	0.003	< 0.003	0.003	0.019	< 0.003	< 0.003	< 0.003	< 0.003	< 0.003	< 0.003
LOI	0.87	1.15	0.37	0.95	1.1	-0.48	0.59	0.85	1.22	4.39	0.24	-0.22
Total	99.76	98.97	99.31	99.63	99.38	99.69	99.36	99.1	99.72	100	99.64	99.08
FUS-MS (ppm)												
V	28	18	28	11	21	125	24	16	14	7	< 5	6
Cr	< 20	< 20	< 20	< 20	< 20	70	< 20	< 20	40	< 20	< 20	< 20
Co	8	4	5	7	6	16	4	4	1	5	2	2
Ni	< 20	< 20	< 20	< 20	< 20	30	< 20	< 20	< 20	< 20	< 20	< 20
Cu	< 10	< 10	< 10	< 10	< 10	10	< 10	10	10	< 10	< 10	< 10
Zn	< 30	< 30	< 30	< 30	< 30	< 30	< 30	< 30	< 30	30	< 30	< 30
Ga	1	1	1	1	1	9	2	2	1	< 1	< 1	< 1
Ge	6.4	5.2	5.9	6.3	11.2	9.4	4.5	6.9	10.6	10.1	3.9	3.4
As	26	23	27	25	25	< 5	20	22	< 5	< 5	32	6
Rb	1	< 1	< 1	2	5	158	3	5	1	< 1	< 1	< 1
Sr	6	9	4	3	5	26	7	5	5	222	3	< 2
Y	3.5	3.4	3.5	2.8	4.2	6.3	4.7	3.2	0.9	2.3	0.6	0.9
Zr	6	7	7	7	12	43	7	7	4	4	2	3
Nb	1	1.2	1.4	1.6	2.5	7.2	1.5	0.7	0.2	< 0.2	0.8	0.4
Mo	< 2	< 2	< 2	< 2	< 2	< 2	< 2	< 2	< 2	< 2	< 2	< 2
Ag	< 0.5	< 0.5	< 0.5	< 0.5	< 0.5	< 0.5	< 0.5	< 0.5	< 0.5	< 0.5	< 0.5	< 0.5
In	< 0.1	< 0.1	< 0.1	< 0.1	< 0.1	< 0.1	< 0.1	< 0.1	< 0.1	< 0.1	< 0.1	< 0.1
Sn	< 1	< 1	< 1	< 1	< 1	< 1	< 1	< 1	< 1	< 1	< 1	< 1
Sb	0.3	0.3	0.6	< 0.2	0.3	< 0.2	< 0.2	< 0.2	< 0.2	< 0.2	< 0.2	< 0.2
Cs	0.4	0.1	0.3	0.4	0.6	4.6	0.4	0.3	< 0.1	< 0.1	< 0.1	< 0.1
Ba	70	44	58	23	23	408	10	7	4	5	< 3	< 3
La	2.16	2.52	3.06	2.51	3.42	7.96	5.62	2.69	0.63	1.1	1.69	1.57
Ce	5.85	7.8	8.92	6.98	7.69	15.6	15.7	7.33	1.32	2.33	3.53	4.27
Pr	0.49	0.56	0.72	0.64	0.9	1.87	1.06	0.63	0.15	0.26	0.37	0.37
Nd	1.83	1.97	2.87	2.16	3.37	7.71	4.07	2.49	0.58	0.98	1.44	1.27
Sm	0.36	0.35	0.5	0.42	0.6	1.44	0.73	0.5	0.14	0.21	0.24	0.16
Eu	0.12	0.135	0.158	0.16	0.259	0.479	0.208	0.196	0.041	0.108	0.048	0.047
Gd	0.47	0.41	0.56	0.42	0.63	1.33	0.83	0.5	0.14	0.26	0.19	0.17
Tb	0.08	0.08	0.09	0.07	0.11	0.21	0.13	0.08	0.02	0.05	0.03	0.03
Dy	0.52	0.55	0.56	0.47	0.67	1.22	0.73	0.51	0.15	0.32	0.15	0.17
Ho	0.11	0.12	0.12	0.1	0.14	0.24	0.15	0.1	0.03	0.07	0.03	0.04
Er	0.36	0.39	0.37	0.32	0.44	0.7	0.45	0.32	0.09	0.2	0.1	0.11
Tm	0.057	0.061	0.056	0.05	0.064	0.103	0.07	0.048	0.015	0.028	0.016	0.017
Yb	0.39	0.39	0.36	0.34	0.42	0.67	0.48	0.31	0.1	0.16	0.1	0.12
Lu	0.064	0.062	0.056	0.052	0.064	0.11	0.081	0.049	0.015	0.022	0.016	0.019
Hf	< 0.1	0.1	< 0.1	0.1	0.2	1.1	< 0.1	0.1	< 0.1	< 0.1	< 0.1	< 0.1
Ta	0.01	0.01	0.02	0.05	0.08	0.45	0.01	0.03	0.01	< 0.01	< 0.01	< 0.01
W	< 0.5	1.4	< 0.5	4.1	3.6	< 0.5	< 0.5	< 0.5	< 0.5	< 0.5	< 0.5	< 0.5
Tl	< 0.05	< 0.05	< 0.05	< 0.05	< 0.05	< 0.05	< 0.05	< 0.05	< 0.05	< 0.05	< 0.05	< 0.05
Pb	10	< 5	< 5	< 5	< 5	< 5	< 5	< 5	< 5	< 5	5	< 5
Bi	< 0.1	< 0.1	< 0.1	< 0.1	< 0.1	< 0.1	< 0.1	< 0.1	< 0.1	< 0.1	< 0.1	< 0.1
Th	0.25	0.16	0.18	0.2	0.23	0.81	0.17	0.16	0.07	< 0.05	0.17	0.12
U	0.07	0.04	0.09	0.04	0.05	0.19	0.09	0.07	0.04	0.02	0.02	0.03
AR-MS (ppm)												
Li	1.1	0.8	1.2	2	24.2	19.8	0.9	0.9	0.9	0.2	0.6	0.5
Be	1.3	1.5	1.9	0.7	0.8	1.8	1.5	1.1	0.5	0.4	0.5	0.6
Na	0.03	0.04	0.04	0.05	0.03	0.06	0.03	0.02	0.04	0.02	0.03	0.03
Mg	0.12	0.19	0.11	0.41	0.71	1.02	0.15	0.16	0.09	0.1	0.08	0.05
Al	0.06	0.06	0.05	0.11	0.15	0.98	0.12	0.07	0.04	0.02	0.03	0.03
K	0.02	0.02	0.02	0.03	0.04	0.95	0.06	0.05	0.04	0.01	0.02	0.02
Bi	0.09	< 0.02	0.03	0.18	< 0.02	0.03	< 0.02	< 0.02	< 0.02	< 0.02	< 0.02	< 0.02
Ca	0.47	0.5	0.05	0.03	0.06	0.07	0.11	0.15	0.04	2.52	0.04	0.02

A2., continued.

Sample	nl11-04-13	nl11-04-14	nl11-04-15	nl11-04-16	nl11-04-17	nl11-04-18	nl11-05-02	nl11-05-03	nl11-05-04	nl11-05-05	nl11-05-08	nl11-05-09
Easting	313485	313512	313477	313564	313620	313784	314256	314139	314444	314432	314305	314485
Northing	6059586	6059682	6059697	6059542	6059501	6059398	6058363	6058249	6058398	6058442	6058616	6058775
Unit	Middle Sokoman	Middle Sokoman	Middle Sokoman	Middle Sokoman	Middle Sokoman	Lower Sokoman	Silicate	IF Silicate	IF Silicate	IF Silicate	IF Silicate	IF SIlicate	IF
AR-MS (ppm)													
Sc	< 0.1	0.4	< 0.1	0.7	1.4	10.7	0.5	0.1	< 0.1	< 0.1	< 0.1	< 0.1	
V	14	17	16	10	14	99	20	8	< 1	< 1	2	7	
Cr	< 0.5	7.7	< 0.5	5.6	3.5	38.5	7.8	< 0.5	9.7	6.1	< 0.5	3.8	
Mn	725	1070	225	212	338	247	1000	1390	129	331	122	99	
Fe	21.1	21	26.5	31.1	27.6	27.2	22.4	16.1	3.1	2.87	9.52	12.6	
Co	5.8	4.4	4.5	5.1	2.9	15.9	4	2.2	0.4	0.3	0.8	1.4	
Ni	1.7	5.4	2.6	2.5	1.6	21.5	2.5	1	1.1	0.8	1	1.5	
Cu	0.48	1.14	2.87	1.85	0.92	12.2	3	3.79	3.78	< 0.01	0.7	0.18	
Zn	21.1	3.8	142	10.1	3.6	47.1	7.3	2.1	3.2	6.3	< 0.1	< 0.1	
Ga	0.42	0.49	0.45	0.52	0.74	7.15	1.04	0.55	0.28	0.16	0.27	0.44	
Ge	1.2	1	1.2	1	1.2	1.4	1.1	0.9	0.5	0.5	0.6	0.6	
As	10.1	13.4	12.6	13.9	15.4	< 0.1	18.9	19	1.5	< 0.1	31.4	6.1	
Se	< 0.1	1	< 0.1	< 0.1	< 0.1	< 0.1	< 0.1	< 0.1	< 0.1	< 0.1	< 0.1	< 0.1	
Rb	1.6	0.9	1.4	1.9	4.9	123	5.8	3.2	1.6	0.7	1.2	0.9	
Sr	4.3	9.9	3.4	2.8	4.7	14.1	8.2	5.2	3.1	230	3.4	1.9	
Y	2.64	3.55	3.11	0.93	1.4	1.76	4.84	2.7	0.73	2.29	0.55	0.74	
Zr	< 0.1	< 0.1	< 0.1	< 0.1	< 0.1	< 0.1	< 0.1	< 0.1	< 0.1	< 0.1	< 0.1	< 0.1	
Nb	< 0.1	< 0.1	< 0.1	< 0.1	< 0.1	< 0.1	< 0.1	< 0.1	< 0.1	< 0.1	< 0.1	< 0.1	
Mo	< 0.01	0.01	0.02	< 0.01	< 0.01	< 0.01	0.08	< 0.01	< 0.01	< 0.01	< 0.01	< 0.01	
Ag	0.46	0.17	0.38	0.19	0.13	0.28	0.28	0.2	0.2	0.17	0.21	0.1	
Cd	< 0.01	< 0.01	< 0.01	0.04	< 0.01	0.03	< 0.01	0.03	< 0.01	< 0.01	< 0.01	< 0.01	
In	< 0.02	< 0.02	< 0.02	< 0.02	< 0.02	0.03	< 0.02	< 0.02	< 0.02	< 0.02	< 0.02	< 0.02	
Sn	0.08	< 0.05	< 0.05	< 0.05	< 0.05	0.21	0.05	< 0.05	< 0.05	< 0.05	< 0.05	< 0.05	
Sb	0.05	0.19	0.09	0.06	< 0.02	< 0.02	0.04	< 0.02	< 0.02	< 0.02	< 0.02	< 0.02	
Te	< 0.02	0.08	< 0.02	0.46	0.22	0.06	0.08	< 0.02	< 0.02	< 0.02	< 0.02	0.06	
Cs	0.22	0.06	0.21	0.3	0.52	3.95	0.34	0.16	0.04	0.04	0.03	0.02	
Ba	32.3	27.7	25.3	12.7	9	29.4	4.2	2.9	1.2	3.2	< 0.5	< 0.5	
La	1.5	2.2	3	2.1	2.7	7.1	5.7	2.5	0.8	1.2	1.6	1.4	
Ce	3.73	6.59	7.65	5.05	5.57	14.3	16	6.14	1.08	2.21	2.83	3.04	
Pr	0.4	0.5	0.8	0.5	0.7	1.8	1.2	0.6	0.2	0.3	0.3	0.3	
Nd	1.32	1.93	2.66	1.88	2.89	7.08	4.45	2.12	0.56	1.13	1.32	1.16	
Sm	0.3	0.3	0.4	0.3	0.5	1.3	0.8	0.4	0.1	0.2	0.2	0.2	
Eu	0.1	0.1	0.1	0.1	0.2	0.4	0.2	0.2	< 0.1	0.1	< 0.1	< 0.1	
Gd	0.3	0.5	0.5	0.3	0.6	1	0.8	0.4	0.1	0.3	0.2	0.2	
Tb	< 0.1	< 0.1	< 0.1	< 0.1	< 0.1	0.1	0.1	< 0.1	< 0.1	< 0.1	< 0.1	< 0.1	
Dy	0.38	0.57	0.53	0.28	0.375	0.52	0.73	0.43	0.12	0.27	0.12	0.18	
Ho	< 0.1	0.1	0.1	< 0.1	< 0.1	< 0.1	0.2	0.1	< 0.1	< 0.1	< 0.1	< 0.1	
Er	0.3	0.4	0.3	0.1	0.2	0.2	0.5	0.3	< 0.1	0.2	< 0.1	< 0.1	
Tm	< 0.1	< 0.1	< 0.1	< 0.1	< 0.1	< 0.1	< 0.1	< 0.1	< 0.1	< 0.1	< 0.1	< 0.1	
Yb	0.3	0.3	0.2	0.1	< 0.1	< 0.1	0.4	0.2	< 0.1	0.2	< 0.1	< 0.1	
Lu	< 0.1	< 0.1	< 0.1	< 0.1	< 0.1	< 0.1	< 0.1	< 0.1	< 0.1	< 0.1	< 0.1	< 0.1	
Hf	< 0.1	< 0.1	< 0.1	< 0.1	< 0.1	< 0.1	< 0.1	< 0.1	< 0.1	< 0.1	< 0.1	< 0.1	
Ta	< 0.05	< 0.05	< 0.05	< 0.05	< 0.05	< 0.05	< 0.05	< 0.05	< 0.05	< 0.05	< 0.05	< 0.05	
W	< 0.1	< 0.1	< 0.1	< 0.1	< 0.1	< 0.1	< 0.1	< 0.1	< 0.1	< 0.1	< 0.1	< 0.1	
Re	< 0.001	< 0.001	< 0.001	< 0.001	< 0.001	< 0.001	< 0.001	< 0.001	< 0.001	< 0.001	< 0.001	< 0.001	
Au	< 5	< 5	< 5	< 5	< 5	< 5	< 5	< 5	< 5	< 5	< 5	< 5	
Tl	< 0.02	< 0.02	< 0.02	< 0.02	< 0.02	0.04	< 0.02	< 0.02	0.02	< 0.02	< 0.02	< 0.02	
Pb	1.5	0.85	0.95	1.72	1.1	1.3	2.84	0.38	0.17	0.57	0.42	0.52	
Th	< 0.1	0.1	0.1	0.1	0.2	0.6	0.1	< 0.1	0.7	0.5	< 0.1	< 0.1	
U	< 0.1	< 0.1	< 0.1	< 0.1	< 0.1	< 0.1	< 0.1	< 0.1	< 0.1	< 0.1	< 0.1	< 0.1	

A2., continued.

Sample	nl11-05-10	nl11-05-11	nl11-05-12	nl11-05-13	nl11-05-14	nl11-05-15	nl11-05-16 (a)	nl11-05-16 (b)	nl11-05-17	nl11-05-18(a)	nl11-05-18(b)	nl11-06-02
Easting	313961	313891	313780	313741	313681	313658	313478	313478	313401	313366	313366	312347
Northing	6059108	6059198	6059337	6059418	6059396	6059387	6059466	6059466	6059498	6059542	6059542	6060894
Unit	Montagnais Intrusive	Montagnais Intrusive	Lower Sokoman	Middle Sokoman	Middle Sokoman	Middle Sokoman	Middle Sokoman	Middle Sokoman	Middle Sokoman	Middle Sokoman	Middle Sokoman	Middle Sokoman
FUS-XRF (wt %)												
SiO2	47.42	46.16	42.63	40.26	51.15	30.98	54.73	66.04	36.82	71.17	41.82	34.12
Al2O3	15.66	16.29	5.89	1.03	0.24	1.07	0.77	0.49	0.08	0.28	0.84	0.16
Fe2O3(T)	15.58	14.25	44.38	51.2	43.27	63.28	41.22	31.78	61.17	27.6	54.66	63.74
MnO	0.205	0.209	0.048	0.096	0.155	0.009	0.138	0.086	0.054	0.095	0.578	0.014
MgO	5.53	5.7	0.82	0.97	0.83	2.59	1.14	0.3	0.28	0.07	0.52	0.59
CaO	8.72	9.3	0.08	2.42	1.62	0.04	0.05	0.05	0.23	0.08	0.06	0.02
Na2O	2.94	2.56	0.36	0.39	0.23	0.6	0.21	0.06	0.07	0.1	0.23	0.03
K2O	0.52	1.25	4.63	0.26	0.04	0.12	0.13	0.26	0.03	0.11	0.23	0.11
TiO2	1.13	1.01	0.56	0.09	0.03	0.08	0.05	0.08	0.03	0.04	0.09	0.05
P2O5	0.2	0.19	0.06	0.07	0.02	0.02	0.02	0.02	0.01	0.02	0.03	0.04
Cr2O3	0.01	0.01	0.01	0.01	0.01	< 0.01	< 0.01	0.01	< 0.01	< 0.01	0.01	< 0.01
V2O5	0.048	0.043	0.02	0.004	< 0.003	< 0.003	< 0.003	< 0.003	0.006	0.004	0.011	< 0.003
LOI	2.65	3.09	-0.12	2.79	2.61	0.72	0.9	0.06	0.28	0.13	0.49	0.55
Total	100.6	100.1	99.37	99.59	100.2	99.5	99.36	99.24	99.06	99.7	99.57	99.43
FUS-MS (ppm)												
V	360	314	118	33	12	18	16	24	23	22	54	17
Cr	80	70	60	< 20	< 20	< 20	< 20	< 20	< 20	< 20	< 20	< 20
Co	97	111	15	3	3	8	9	3	6	3	9	3
Ni	120	140	30	< 20	< 20	< 20	< 20	< 20	< 20	< 20	< 20	< 20
Cu	130	170	20	< 10	< 10	< 10	< 10	< 10	< 10	10	< 10	< 10
Zn	150	130	40	< 30	< 30	< 30	< 30	< 30	< 30	< 30	< 30	< 30
Ga	21	20	7	2	< 1	< 1	2	1	1	1	3	< 1
Ge	2.1	1.7	8.2	7	7.9	6.4	3.9	5	5.2	6.7	6.7	8.6
As	< 5	< 5	< 5	5	14	21	11	16	29	25	67	22
Rb	6	17	179	6	< 1	3	4	1	1	< 1	3	< 1
Sr	547	483	21	63	27	3	< 2	3	4	3	7	< 2
Y	24.1	21.2	5.9	3.7	2.2	2.3	2.6	3.5	1.9	6	10.2	3
Zr	74	65	81	18	4	16	25	6	9	8	24	7
Nb	4.9	4.5	4.7	2.8	1	3.7	1.4	0.7	1.5	1.1	5.5	0.9
Mo	< 2	< 2	< 2	< 2	< 2	< 2	< 2	< 2	< 2	< 2	< 2	< 2
Ag	< 0.5	< 0.5	< 0.5	< 0.5	< 0.5	< 0.5	< 0.5	< 0.5	< 0.5	< 0.5	< 0.5	< 0.5
In	< 0.1	< 0.1	< 0.1	< 0.1	< 0.1	< 0.1	< 0.1	< 0.1	< 0.1	< 0.1	< 0.1	< 0.1
Sn	1	< 1	< 1	< 1	< 1	< 1	< 1	< 1	< 1	< 1	< 1	< 1
Sb	< 0.2	< 0.2	< 0.2	0.3	0.2	0.7	< 0.2	< 0.2	0.3	< 0.2	0.8	< 0.2
Cs	0.1	0.1	5	0.3	0.1	0.3	0.8	0.3	0.2	0.1	0.9	< 0.1
Ba	329	792	298	55	56	27	23	15	64	13	31	10
La	13.8	12.4	6.28	3.73	2.78	2.98	2.42	2.69	1.73	4.55	5.98	2.42
Ce	32.4	28.7	12.9	8.23	6.44	7.98	6.93	6.64	5.06	16	19.8	5.91
Pr	4.51	4.02	1.57	0.95	0.72	0.68	0.56	0.55	0.39	1.19	1.54	0.62
Nd	20	17.5	6.29	3.88	2.72	2.56	2.05	2.22	1.49	4.97	6.2	2.48
Sm	4.62	4.14	1.24	0.75	0.45	0.55	0.31	0.37	0.25	1.09	1.44	0.44
Eu	1.43	1.4	0.357	0.222	0.168	0.197	0.117	0.112	0.083	0.379	0.496	0.145
Gd	4.53	4.07	0.97	0.69	0.46	0.39	0.41	0.45	0.27	1.16	1.53	0.41
Tb	0.77	0.66	0.17	0.11	0.07	0.07	0.06	0.09	0.05	0.2	0.29	0.07
Dy	4.42	3.83	1.01	0.63	0.43	0.41	0.42	0.59	0.32	1.17	1.84	0.41
Ho	0.86	0.78	0.2	0.13	0.09	0.09	0.09	0.14	0.07	0.24	0.39	0.09
Er	2.54	2.24	0.61	0.36	0.24	0.27	0.28	0.44	0.22	0.67	1.17	0.28
Tm	0.381	0.327	0.095	0.048	0.034	0.045	0.042	0.069	0.034	0.094	0.17	0.045
Yb	2.51	2.21	0.65	0.29	0.22	0.33	0.27	0.46	0.23	0.56	1.06	0.3
Lu	0.405	0.37	0.105	0.046	0.033	0.056	0.043	0.076	0.036	0.082	0.164	0.047
Hf	2	1.7	1.7	0.3	< 0.1	0.4	0.5	< 0.1	0.1	< 0.1	0.3	0.1
Ta	0.3	0.26	0.39	0.08	0.02	0.16	0.04	< 0.01	0.03	0.02	0.11	0.02
W	< 0.5	< 0.5	0.9	< 0.5	0.5	0.7	2	< 0.5	1.4	1.6	3.3	< 0.5
Tl	< 0.05	0.11	< 0.05	< 0.05	< 0.05	< 0.05	< 0.05	< 0.05	< 0.05	< 0.05	< 0.05	< 0.05
Pb	< 5	< 5	< 5	< 5	< 5	6	< 5	< 5	< 5	< 5	< 5	< 5
Bi	< 0.1	< 0.1	< 0.1	< 0.1	< 0.1	< 0.1	< 0.1	< 0.1	< 0.1	< 0.1	< 0.1	< 0.1
Th	0.88	0.66	0.79	0.27	0.16	0.4	0.14	0.13	0.18	0.15	0.44	0.28
U	0.17	0.15	0.2	0.08	0.04	0.08	0.06	0.08	0.07	0.08	0.17	0.07
AR-MS (ppm)												
Li	20	20.3	24.1	0.7	1.5	1.6	2.8	2.9	0.9	2.5	0.9	1.6
Be	0.2	0.3	0.6	0.6	1	0.9	0.9	0.6	2	1	0.9	1.1
Na	0.06	0.06	0.04	0.03	0.04	0.03	0.05	0.04	0.03	0.16	0.04	0.03
Mg	1.9	1.81	0.51	0.18	0.54	0.48	0.65	0.19	0.13	0.05	0.34	0.15
Al	2.99	2.94	0.54	0.08	0.05	0.1	0.25	0.09	0.04	0.05	0.17	0.05
K	0.03	0.05	0.54	0.02	0.02	0.02	0.09	0.03	0.01	0.02	0.05	0.01
Bi	< 0.02	< 0.02	< 0.02	< 0.02	< 0.02	0.03	0.06	< 0.02	< 0.02	0.05	0.07	0.03
Ca	1.38	1.32	0.04	0.02	1.24	0.03	0.04	0.04	0.17	0.06	0.05	0.02

A2., continued.

Sample	nl11-05-10	nl11-05-11	nl11-05-12	nl11-05-13	nl11-05-14	nl11-05-15	nl11-05-16 (a)	nl11-05-16 (b)	nl11-05-17	nl11-05-18(a)	nl11-05-18(b)	nl11-06-02
Easting	313961	313891	313780	313741	313681	313658	313478	313478	313401	313366	313366	312347
Northing	6059108	6059198	6059337	6059418	6059396	6059387	6059466	6059466	6059498	6059542	6059542	6060894
Unit	Montagnais Intrusive	Montagnais Intrusive	Lower Sokoman	Middle Sokoman	Middle Sokoman	Middle Sokoman	Middle Sokoman	Middle Sokoman	Middle Sokoman	Middle Sokoman	Middle Sokoman	Middle Sokoman
AR-MS (ppm)												
Sc	4.1	3.4	7.7	0.3	0.7	1.1	1.2	0.5	0.1	0.3	1.4	0.2
V	106	89	91	16	12	12	17	16	17	15	30	10
Cr	30.7	21.9	29.8	< 0.5	12.9	1.9	5.2	< 0.5	< 0.5	2.7	3.8	7.6
Mn	901	874	400	664	1210	118	1110	660	403	707	4400	140
Fe	6.34	5.96	29	19.5	23.9	31.1	24.4	19.9	28.1	17.9	29.5	35.1
Co	43.3	56.3	15.3	3.2	3.6	3.8	9	3.4	5.4	2.8	8.5	3.1
Ni	83.2	98	20.3	2	2.9	1.9	2.7	3	2.1	2.7	4.4	1.5
Cu	121	152	16.5	2.34	3.48	0.19	2.81	2.96	0.35	7.4	4.29	0.31
Zn	71.3	69.7	29.7	0.8	35.1	2	23.4	14.2	6.2	5.8	16.7	10.3
Ga	7.71	7.39	4.48	0.72	0.44	0.58	1.42	0.69	0.51	0.6	1.8	0.44
Ge	0.3	0.3	1	0.6	1.6	0.9	0.8	0.7	1.2	0.8	0.8	1.8
As	< 0.1	< 0.1	1.5	11.1	8.3	14.7	7	10.7	15.8	29.3	47.9	12.6
Se	< 0.1	0.3	< 0.1	< 0.1	< 0.1	0.4	< 0.1	< 0.1	0.9	< 0.1	1.1	0.3
Rb	0.9	1.8	90.2	3.1	1.2	2	5.3	2.8	1	1.4	5.2	1.3
Sr	104	95.3	6.9	2.3	31.9	1.9	2.5	2.9	3.3	3.5	6.3	1.5
Y	17.2	12.8	1.41	0.96	2.26	0.96	1.1	1.05	1.41	3.35	4.13	0.9
Zr	5.7	4.5	< 0.1	< 0.1	< 0.1	< 0.1	< 0.1	< 0.1	< 0.1	< 0.1	< 0.1	< 0.1
Nb	< 0.1	< 0.1	< 0.1	< 0.1	< 0.1	< 0.1	< 0.1	< 0.1	< 0.1	< 0.1	< 0.1	< 0.1
Mo	< 0.01	< 0.01	0.14	< 0.01	< 0.01	< 0.01	< 0.01	< 0.01	0.58	1.57	0.84	0.32
Ag	0.2	0.18	0.21	0.15	0.12	0.1	0.08	0.15	0.15	0.21	0.78	0.74
Cd	0.1	0.09	< 0.01	< 0.01	0.02	< 0.01	0.03	0.02	< 0.01	< 0.01	< 0.01	< 0.01
In	0.02	0.02	0.02	< 0.02	< 0.02	< 0.02	< 0.02	< 0.02	< 0.02	< 0.02	< 0.02	< 0.02
Sn	0.27	0.16	0.26	< 0.05	< 0.05	< 0.05	0.11	0.05	< 0.05	0.1	0.18	0.1
Sb	< 0.02	< 0.02	0.03	0.16	0.06	< 0.02	0.05	0.14	0.05	0.12	0.46	0.25
Te	< 0.02	0.21	0.19	0.17	0.5	0.36	< 0.02	< 0.02	< 0.02	0.02	0.1	0.74
Cs	0.08	0.08	4.1	0.27	0.1	0.23	0.72	0.3	0.15	0.12	0.8	0.03
Ba	9.6	23.6	37	7	47.3	11.1	14.6	8	34.4	9.2	21.1	4.2
La	11	9.2	4.6	2.5	2.9	1.9	2.8	3.7	1.4	4.4	5.1	1.6
Ce	26.4	21.8	9.19	5.71	6.12	4.82	6.24	6.84	3.28	15.4	17.2	3.86
Pr	3.7	3.1	1.2	0.6	0.7	0.5	0.5	0.6	0.3	1.2	1.4	0.4
Nd	15.8	13.2	4.53	1.98	2.51	1.85	1.77	1.98	0.98	4.95	5.74	1.58
Sm	3.4	2.8	0.9	0.4	0.5	0.4	0.4	0.4	0.2	1	1.3	0.3
Eu	0.6	0.6	0.3	0.1	0.2	0.1	0.1	< 0.1	< 0.1	0.3	0.4	0.1
Gd	3.4	2.8	0.7	0.3	0.4	0.4	0.3	0.3	0.2	0.9	1.3	0.2
Tb	0.5	0.4	< 0.1	< 0.1	< 0.1	< 0.1	< 0.1	< 0.1	< 0.1	0.1	0.2	< 0.1
Dy	3.12	2.47	0.45	0.22	0.39	0.31	0.24	0.24	0.28	0.77	1.11	0.16
Ho	0.6	0.5	< 0.1	< 0.1	< 0.1	< 0.1	< 0.1	< 0.1	< 0.1	0.1	0.2	< 0.1
Er	1.6	1.3	0.1	0.1	0.2	0.1	0.1	0.1	0.2	0.4	0.6	< 0.1
Tm	0.2	0.2	< 0.1	< 0.1	< 0.1	< 0.1	< 0.1	< 0.1	< 0.1	< 0.1	< 0.1	< 0.1
Yb	1.2	0.9	< 0.1	0.1	0.2	0.1	< 0.1	0.1	0.1	0.2	0.4	< 0.1
Lu	0.2	0.1	< 0.1	< 0.1	< 0.1	< 0.1	< 0.1	< 0.1	< 0.1	< 0.1	< 0.1	< 0.1
Hf	< 0.1	< 0.1	< 0.1	< 0.1	< 0.1	< 0.1	< 0.1	< 0.1	< 0.1	< 0.1	< 0.1	< 0.1
Ta	< 0.05	< 0.05	< 0.05	< 0.05	< 0.05	< 0.05	< 0.05	< 0.05	< 0.05	< 0.05	< 0.05	< 0.05
W	< 0.1	< 0.1	< 0.1	< 0.1	< 0.1	< 0.1	< 0.1	< 0.1	< 0.1	0.8	1.6	0.8
Re	< 0.001	< 0.001	< 0.001	< 0.001	0.01	< 0.001	< 0.001	< 0.001	< 0.001	< 0.001	< 0.001	< 0.001
Au	< 5	< 5	< 5	< 5	9	< 5	< 5	< 5	< 5	< 5	< 5	< 5
Tl	0.02	0.04	< 0.02	< 0.02	< 0.02	< 0.02	< 0.02	< 0.02	0.02	0.02	0.1	0.09
Pb	0.87	1.24	2.31	0.71	0.7	1.23	1.25	1.33	0.65	2.04	3.3	0.78
Th	0.6	0.5	0.4	< 0.1	0.1	0.2	< 0.1	< 0.1	0.2	0.2	0.8	0.3
U	< 0.1	< 0.1	0.1	< 0.1	< 0.1	< 0.1	< 0.1	< 0.1	< 0.1	< 0.1	0.1	< 0.1

A2., continued.

Sample	nl11-06-03	nl11-06-04	nl11-06-05	nl11-06-06	nl11-06-07	nl11-06-08
Easting	312195	312162	311976	311915	311727	311542
Northing	6060572	6060556	6060648	6060701	6060692	6060793
Unit	Wishart	Wishart	Lower Sokoman	Middle Sokoman	Middle Sokoman	Menihek
FUS-XRF (wt %)						
SiO2	74.34	86.64	49.51	50.55	48.57	75.59
Al2O3	12.7	3.74	5.39	0.21	0.16	3.55
Fe2O3(T)	2.72	5.89	35.39	47.04	50.37	16.24
MnO	0.011	0.017	0.459	< 0.001	0.01	0.008
MgO	1.08	0.87	1.22	1.17	0.02	0.44
CaO	0.14	0.15	0.26	0.03	0.04	0.04
Na2O	0.68	0.37	0.4	0.16	0.1	0.06
K2O	5.3	0.92	4.13	0.03	0.03	0.27
TiO2	0.52	0.1	0.58	0.03	0.03	0.19
P2O5	0.04	0.07	0.18	0.02	0.02	0.21
Cr2O3	0.01	0.01	0.01	< 0.01	< 0.01	0.01
V2O5	0.009	0.004	0.016	< 0.003	0.005	0.014
LOI	1.98	1.21	1.31	0.51	0.6	3.45
Total	99.53	99.99	98.86	99.75	99.95	100.1
FUS-MS (ppm)						
V	72	13	103	6	17	111
Cr	120	40	80	< 20	< 20	30
Co	5	6	15	4	1	< 1
Ni	< 20	< 20	30	< 20	< 20	< 20
Cu	20	10	20	< 10	< 10	10
Zn	50	40	50	< 30	< 30	40
Ga	17	6	7	1	< 1	7
Ge	3.2	2.8	9.6	11	5.7	7
As	5	< 5	< 5	14	26	17
Rb	183	19	127	< 1	< 1	6
Sr	80	23	29	7	3	39
Y	14.3	6.1	8.3	4.8	1.9	8.3
Zr	230	168	61	10	7	67
Nb	7.4	0.6	9.5	4.1	1.4	9.9
Mo	< 2	< 2	< 2	< 2	< 2	5
Ag	0.8	0.6	< 0.5	< 0.5	< 0.5	< 0.5
In	< 0.1	< 0.1	< 0.1	< 0.1	< 0.1	< 0.1
Sn	2	< 1	< 1	< 1	< 1	1
Sb	< 0.2	< 0.2	< 0.2	< 0.2	0.7	0.4
Cs	5.4	0.3	0.9	< 0.1	< 0.1	0.5
Ba	716	203	238	14	19	183
La	28	11.5	13.9	6.09	3.42	14.1
Ce	54	24.8	25	9.52	7.95	29.8
Pr	6.03	2.73	2.92	1.6	0.78	3.31
Nd	21.8	10.2	11.7	6.01	2.78	12.9
Sm	3.82	1.77	2.11	1.23	0.4	2.34
Eu	0.765	0.291	0.573	0.334	0.14	0.478
Gd	3.01	1.27	1.83	1.14	0.39	1.99
Tb	0.46	0.18	0.26	0.16	0.07	0.28
Dy	2.65	0.92	1.41	0.86	0.38	1.45
Ho	0.51	0.18	0.27	0.17	0.08	0.28
Er	1.47	0.47	0.78	0.47	0.24	0.83
Tm	0.212	0.067	0.118	0.066	0.038	0.125
Yb	1.4	0.45	0.76	0.41	0.26	0.82
Lu	0.232	0.076	0.116	0.061	0.039	0.13
Hf	5.6	3.7	1.3	0.3	< 0.1	1.3
Ta	0.71	0.09	0.56	0.23	0.01	1.06
W	< 0.5	< 0.5	< 0.5	4	1.4	< 0.5
Tl	0.7	0.09	< 0.05	< 0.05	< 0.05	0.11
Pb	17	5	< 5	< 5	< 5	8
Bi	0.1	< 0.1	< 0.1	< 0.1	< 0.1	< 0.1
Th	11.9	6.15	0.89	0.58	0.18	2.67
U	2.32	0.59	0.23	0.05	0.05	7.21
AR-MS (ppm)						
Li	9	6.6	2.3	0.6	1.1	4.3
Be	0.6	0.2	0.5	1	1.6	0.7
Na	0.04	0.02	0.04	0.02	0.05	0.03
Mg	0.33	0.53	0.73	0.24	0.02	0.29
Al	1.58	1.29	0.32	0.12	0.08	1.45
K	0.8	0.07	0.26	0.01	0.01	0.04
Bi	0.11	0.06	0.03	< 0.02	< 0.02	0.05
Ca	0.02	0.09	0.17	0.02	0.03	0.02

A2., continued.

Sample	nl11-06-03	nl11-06-04	nl11-06-05	nl11-06-06	nl11-06-07	nl11-06-08
Easting	312195	312162	311976	311915	311727	311542
Northing	6060572	6060556	6060648	6060701	6060692	6060793
Unit	Wishart	Wishart	Lower Sokoman	Middle Sokoman	Middle Sokoman	Menihek
AR-MS (ppm)						
Sc	2.2	1.4	4.2	0.1	0.3	3.6
V	15	5	72	4	17	84
Cr	34.4	17.8	46.8	< 0.5	5.8	23.3
Mn	32	96	3380	45	105	68
Fe	1.15	3.74	23.8	25.5	25.8	10.8
Co	2.9	5.5	14.6	2.9	1.9	0.8
Ni	7.6	3.7	18.7	1.5	2.1	4.1
Cu	3.34	1.57	10.5	1.06	3.86	8.65
Zn	10.8	10.2	33.6	< 0.1	11	19.9
Ga	4.7	3.88	3.45	0.71	0.58	7.15
Ge	0.2	0.3	1.2	1.5	1.1	0.6
As	4.9	< 0.1	1.2	9.1	15.1	18.7
Se	< 0.1	< 0.1	0.6	0.4	1.5	0.8
Rb	52.4	3.3	26	0.4	0.4	4.3
Sr	7.7	6.8	16.2	6.9	3.9	37
Y	9.42	2.83	4.58	3.32	1.9	5.19
Zr	28.5	6.1	1.3	< 0.1	< 0.1	< 0.1
Nb	< 0.1	< 0.1	< 0.1	< 0.1	< 0.1	< 0.1
Mo	< 0.01	< 0.01	0.2	0.05	0.06	5.07
Ag	0.15	0.15	0.58	0.09	0.12	0.49
Cd	< 0.01	< 0.01	0.01	< 0.01	< 0.01	< 0.01
In	< 0.02	< 0.02	0.02	< 0.02	< 0.02	0.03
Sn	0.22	< 0.05	0.06	0.25	0.05	0.69
Sb	< 0.02	< 0.02	0.19	< 0.02	0.41	0.33
Te	< 0.02	< 0.02	0.1	0.04	0.02	0.29
Cs	1.28	0.06	0.56	0.05	0.05	0.42
Ba	89.1	13.4	15.7	5.3	10	139
La	27.7	11.5	12.8	4.7	3.2	13.5
Ce	55.5	25	24	6.96	6.81	29.9
Pr	6.5	2.8	2.9	1.3	0.7	3.5
Nd	21.8	9.79	10.9	5.05	2.61	12.7
Sm	3.7	1.6	1.9	1	0.4	2.3
Eu	0.7	0.2	0.6	0.3	0.1	0.5
Gd	2.6	1.1	1.6	0.9	0.4	1.7
Tb	0.3	0.1	0.2	0.1	< 0.1	0.2
Dy	1.83	0.53	1.05	0.62	0.38	1.11
Ho	0.3	< 0.1	0.2	0.1	< 0.1	0.2
Er	0.9	0.2	0.4	0.3	0.2	0.5
Tm	0.1	< 0.1	< 0.1	< 0.1	< 0.1	< 0.1
Yb	0.8	0.2	0.2	0.2	0.2	0.4
Lu	0.1	< 0.1	< 0.1	< 0.1	< 0.1	< 0.1
Hf	0.3	< 0.1	< 0.1	< 0.1	< 0.1	< 0.1
Ta	< 0.05	< 0.05	< 0.05	< 0.05	< 0.05	< 0.05
W	< 0.1	< 0.1	0.2	< 0.1	< 0.1	< 0.1
Re	< 0.001	< 0.001	< 0.001	< 0.001	0.01	< 0.001
Au	< 5	< 5	< 5	< 5	< 5	< 5
Tl	0.17	0.03	0.06	< 0.02	< 0.02	0.13
Pb	9.85	1.9	1.49	0.85	0.8	6.52
Th	7.1	4.8	0.9	0.4	0.1	1.9
U	1.4	0.3	0.1	< 0.1	< 0.1	5.5